Pacific Northwest
NATIONAL LABORATORY

PNNL-37964, Rev. 0
EWG-RPT-055, Rev. 0

K-3 Refractory Corrosion Test Results, HAL24M2

July 2025

T Jin, L Le, NL Canfield, K Bryce, E Nienhuis-Marcial, X Lu, JD Vienna

U.S. DEPARTMENT of ENERGY

Prepared for the U.S. Department of Energy
under Contract DE-AC05-76RL01830

DISCLAIMER

This report was prepared as an account of work sponsored by an agency of the United States Government. Neither the United States Government nor any agency thereof, nor Battelle Memorial Institute, nor any of their employees, makes **any warranty, express or implied, or assumes any legal liability or responsibility for the accuracy, completeness, or usefulness of any information, apparatus, product, or process disclosed, or represents that its use would not infringe privately owned rights**. Reference herein to any specific commercial product, process, or service by trade name, trademark, manufacturer, or otherwise does not necessarily constitute or imply its endorsement, recommendation, or favoring by the United States Government or any agency thereof, or Battelle Memorial Institute. The views and opinions of authors expressed herein do not necessarily state or reflect those of the United States Government or any agency thereof.

PACIFIC NORTHWEST NATIONAL LABORATORY
operated by
BATTELLE
for the
UNITED STATES DEPARTMENT OF ENERGY
under Contract DE-AC05-76RL01830

Printed in the United States of America

Available to DOE and DOE contractors from
the Office of Scientific and Technical Information,
P.O. Box 62, Oak Ridge, TN 37831-0062
www.osti.gov
ph: (865) 576-8401
fox: (865) 576-5728
email: reports@osti.gov

Available to the public from the National Technical Information Service
5301 Shawnee Rd., Alexandria, VA 22312
ph: (800) 553-NTIS (6847)
or (703) 605-6000
email: info@ntis.gov
Online ordering: http://www.ntis.gov

PNNL-37964, Rev. 0
EWG-RPT-055, Rev. 0

K-3 Refractory Corrosion Test Results, HAL24M2

July 2025

T Jin, L Le, NL Canfield, K Bryce, E Nienhuis-Marcial, X Lu, JD Vienna

Prepared for
the U.S. Department of Energy
under Contract DE-AC05-76RL01830

Pacific Northwest National Laboratory
Richland, Washington 99354

Abstract

This report summarizes the refractory corrosion data of the high-Al matrix of Direct Feed High-Level Waste (DFHLW) glasses generated to expand glass compositional ranges. Design of a 20 high-Al glass matrix, HAL24M2, was reported in Russell et al. (2025, in progress). The HAL24M2 glasses were tested for K-3 corrosion and the results are presented in this report.

Corrosion of Monofrax K-3 refractory materials in the HAL24M2 glass melts was measured using a crucible-scale method. Two test conditions, 1150 °C/7days and 1200 °C/7days were applied. The melt-line neck corrosion depth of the test coupons was measured by micro-computed tomography (micro-CT). The measured K-3 neck corrosion values were compared to predicted values using the model in Vienna et al. (2024). The model slightly over-predicted the neck corrosion depth of these glasses.

Acknowledgments

The authors gratefully acknowledge the financial support provided by the U.S. Department of Energy Hanford Field Office Waste Treatment and Immobilization Plant Enhanced Waste Glass Project, with technical oversight by Albert Kruger. The following Pacific Northwest National Laboratory (PNNL) staff members are acknowledged for their contributions: Aaron Sachs and David MacPherson for quality assurance, Chrissy Charron and Cassie Martin for programmatic support during the conduct of this work, Saehwa Chong for technical review, and Will Eaton, Renee Russell, and Mark Hall for project management.

Acronyms, Abbreviations, and Symbols

ASTM	American Society for Testing Materials
DFHLW	Direct Feed High-Level Waste
DOE	U.S. Department of Energy
EWG	enhanced waste glass
HLW	high-level waste
K-3	Monofrax® K-3 refractory
LAW	low-activity waste
micro-CT	micro-computed tomography
NQAP	Nuclear Quality Assurance Program
PNNL	Pacific Northwest National Laboratory
Pt/Rh	platinum/rhodium
WTP	Waste Treatment and Immobilization Plant

Contents

Figures

Tables

1.0 Introduction

Baseline glass compositions have been developed and demonstrated for successful immobilization of Hanford high-level waste (HLW) (Vienna and Kim 2014). These formulations were developed to start up the Hanford Tank Waste Treatment and Immobilization Plant (WTP) and therefore were developed over a narrow range of waste compositions based on fully leached and washed tank sludges with modest waste loading (Peeler et al. 2015). Recent enhanced waste glass (EWG) formulations have shown promise in increasing the waste loading of pretreated sludge compositions from a broader range of HLW feeds (Vienna et al. 2016). Advancements in formulations through the EWG program have recently led to the possibility that the WTP HLW Facility can be efficiently started under a direct feed high-level waste (DFHLW) mode (Vienna et al. 2023). Minimal pretreatment and significant concentrations of tank supernate can decrease mission life by 5-10 years and reduce the cost of cleanup by $12.5B-$25.0B (Herman et al. 2022).

DFHLW feeds have several key compositional differences from those of leached and washed (e.g., pretreated) sludges that ultimately could limit waste loading:

1. DFHLW feeds will likely be retrieved with tank supernate to improve the ability to mobilize solids and deliver them from tank farms to the HLW Facility. The supernate is rich in sodium (typically up to 4 $mol \cdot L^{-1}$ [Na]), sulfate, and other components that are generally washed out of pretreated sludge and managed in the low-activity waste (LAW) treatment flowsheet (Britton 2023). This results in higher ranges of Na_2O and SO_3 in DFHLW feed, requiring expanded composition bounds to allow for increased waste loading in glass.

2. Aluminum leaching was a primary function of the pretreatment process. Caustic leaching removed a weighted average of 77% of the Al in tank waste sludge (Certa et al. 2005). The lack of leaching requires broader composition ranges for Al_2O_3 in DFHLW glasses.

3. The concentrations of other components (e.g., Cr_2O_3, F, P_2O_5, Cl, K_2O) are increased by the reduced washing and lack of leaching anticipated in the DFHLW flowsheet.

It was proposed to increase the loading of potential DFHLW feeds in glass by expanding the existing database (Lu et al. 2023) and glass property-composition models (Vienna et al. 2016) in the high Al, high S, and high Na compositional region.

- Al_2O_3: As concentrations of Al_2O_3 and Na_2O increase in glass, so does the probability of nepheline [$NaAlSiO_4$] formation (Lu et al. 2021). Nepheline formation during slow cooling in the HLW glass canister is likely to cause the glass to fail to meet chemical durability requirements (Vienna et al. 2017). Although some data in the higher Al_2O_3 and Na_2O composition region has been developed, much more is required to expand the composition region and reduce the prediction uncertainty for nepheline models. Early estimates suggest that Al_2O_3 concentrations in HLW glass limited by nepheline can be increased from the Vienna et al. (2013) limit of 23 wt% or the WTP baseline (Vienna and Kim 2014) of 13 wt% to over 30 wt% (Kroll et al. 2019).

- Na_2O: Increasing data and model validity for glasses with increased Na_2O content is paramount for minimizing impacts to the HLW flowsheet. At some point, increasing the concentration of Na_2O will decrease the chemical durability of glass, increase the corrosion rate of melter components, and the electrical conductivity of the melt, and will decrease the melt viscosity. Several data sets exist for LAW formulations that can augment the current HLW models (Vienna et al. 2022). However, the composition regions are not the same, so data on additional glasses is required to bridge the gap. Early estimates suggest that Na_2O concentration in HLW glass can be

increased from the Vienna et al. (2013) limit of 23 wt% or the WTP baseline (Vienna and Kim 2014) of 20 wt% to near 30 wt%.

- SO_3: As concentrations of SO_3, Cl, Cr_2O_3, F, and P_2O_5 increase, so does the propensity for molten salt accumulation in the melter (Vienna et al. 2014; Skidmore et al. 2019). As the concentrations of these components are higher in DFHLW feeds compared to pretreated feeds, the concentration ranges of these components need to be expanded and the solubility measured to improve loading of DFHLW in glass. Early estimates suggest that SO_3 concentration in HLW melter feed can be increased from the WTP baseline (Vienna and Kim 2014) of 0.44 wt% to 2 wt%.

This report documents the refractory corrosion data of a high-Al_2O_3 matrix to extend DFHLW glass compositional ranges. The refractory corrosion test was performed on Monofrax® K-3 (K-3 for short), a commercial high-Cr_2O_3 fused cast refractory material produced by Monofrax LLC, Falconer, NY, which has been widely used to build the liners of nuclear waste glass melters (Bingham et al. 2011; Selkregg 2018). For over two decades, crucible-scale test of K-3 corrosion in simulated waste glass melts has been conducted to develop empirical models. (Gan et al. 2001; Muller et al. 2018; Vienna et al. 2022, 2024).

1.1 Quality Assurance

This work was performed in accordance with the Pacific Northwest National Laboratory (PNNL) Nuclear Quality Assurance Program (NQAP). The NQAP complies with DOE Order 414.1D, *Quality Assurance*, and 10 CFR 830, *Nuclear Safety Management*, Subpart A, *Quality Assurance Requirements*. The NQAP uses NQA-1-2012, *Quality Assurance Requirements for Nuclear Facility Application*, as its consensus standard and NQA-1-2012, Subpart 4.2.1, as the basis for its graded approach to quality.

The NQAP works in conjunction with PNNL's laboratory-level Quality Management Program, which is based on the requirements as defined in DOE Order 414.1D and 10 CFR 830 Subpart A.

The work of this report was performed at a technology readiness level of 5.

2.0 Test Methods

This section describes the test methods of the high-Al 20 glass matrix (HAL24M2) (Russell et al. 2025). The descriptions include glass fabrication and K-3 corrosion test.

2.1 Glass Fabrication

The glasses were batched using appropriate masses of single-metal oxides, single-metal carbonates, sodium salts, and boric acid to form the target compositions. The batched powders were melted in platinum (Pt)-10% rhodium (Rh) crucibles. Laboratory crucible-scale fabrication of glasses is intended to fabricate a glass sample with a controlled composition for property testing, and it is not intended to mimic the actual melter process or feed processability.

The batched powders were thoroughly mixed in a plastic bag for at least 30 s until there was a uniform color of the mixture. The powders were transferred to an agate milling chamber and milled for 4 min in a vibratory mill (Angstrom TE110) and placed into a clean Pt-10% Rh crucible for melting. Glasses were melted using either the Deltech or tilt-pour furnace.

Glasses melted in the Deltech furnace (Deltech Model DT-31-RS, Denver, Colorado) were melted at least two times. First and second melts were performed at 1150 ± 10 ℃ for 1 h ± 10 min. After the first melt, the glass was air quenched on a stainless-steel pouring plate, ground to a fine powder for 5 min (+ 1 min if glass chunks were still present) in a tungsten carbide (WC) vibratory mill (AngstromTE110) and melted a second time. After each melt, the glass was observed under an optical microscope, and the presence of undissolved particles and/or salts was reported. When the glass contained a large amount of undissolved particles, a third melt was performed at 1200 ℃ for 1 h ± 10 min after the glass was reduced to powder as described above.

For the tilt-pour furnace (UltraMELT, TLT-2P, Ronkonkoma, NY), melting was performed by following the *Operating Procedure for the Tilt-Pour Furnace*, EWG-OP-086, Rev. 1.0.[1] Melting with a tilt-pour furnace took about 1 h for charging glass powders at 1150 ± 50 ℃, and the powder was melted for 1 to 1.5 h after charging. The melt was stirred every 10 to 15 min for < 1 min to obtain homogeneous distribution of the glass melt. After the first melt was air quenched on a pouring plate, the glass was observed under an optical microscope, and the presence of undissolved particles and/or salts was reported. A second melt was performed for the glasses with large amounts of undissolved particles and/or salts present.

2.2 Refractory Corrosion Test

The refractory corrosion test was performed using a crucible-scale test method based on ASTM-C621-09 with minor modifications of crucible size and coupon size. The setup is shown in Figure 2.1. K-3 test coupons were cut from K-3 refractory slabs (Monofrax LLC, Falconer, NY) into 1-cm × 1-cm × 11-cm coupons. A notch was cut on the top end of the coupons to denote face ‘A-A’. Each coupon was mounted with the crucible lid made by castable alumina (RESCOR™ CER- CAST CERAMIC 780, Cotronics Corp., Brooklyn, NY) with a 1-cm × 1-cm slot in the center. The test coupon was inserted into a Pt crucible with crushed glass. The loaded crucible was heated in a furnace and the K-3 test coupon was submerged into a static glass melt at 1150 °C or 1200 °C for 7 days. Following the 7-day test, the coupons were removed from the glass melt for characterization.

[1] Neeway, JJ. 2024. *Operating Procedure for Tilt-Pour Furnace*. EWG-OP-086, Rev. 1.0.

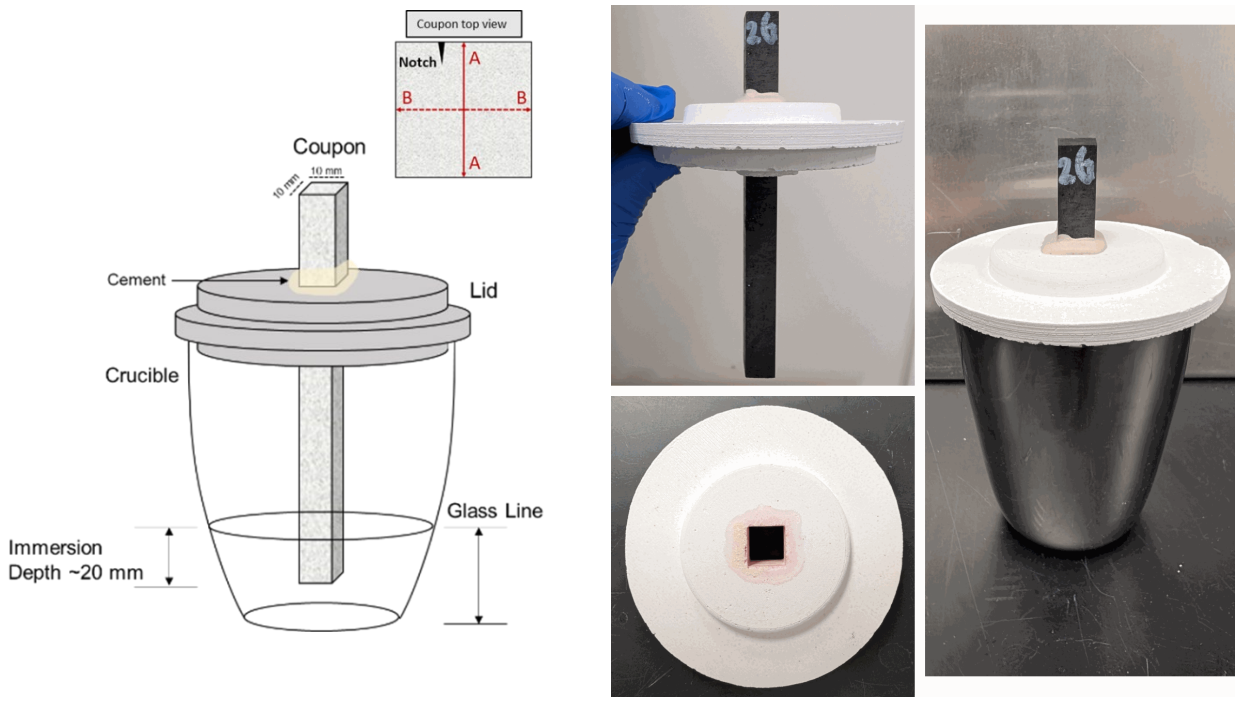

Figure 2.1. K-3 corrosion test setup in a static glass melt showing general measurements for coupon size and positioning, glass depth, and coupon immersion depth.

Both pre-test and post-test coupons were scanned by Zeiss Xradia Versa 610 micro-computed tomography (micro-CT) (Carl Zeiss Microscopy GmbH, Jena, Germany). As shown in Figure 2.2, the coupons were mounted in 3D printed plastic sample holders. Up to four coupons were bundled to fit in the scanning volume. Each single scan covers a cylindrical volume ~ 4-cm tall and 4-cm in diameter; three to five scans were conducted vertically to cover a 6-10 cm length. (Single scans must be partially overlapped for stitching.) Voxel size was set to 0.04 mm. A certified volume standard steel sphere was used to verify the voxel size of the micro-CT measurement.

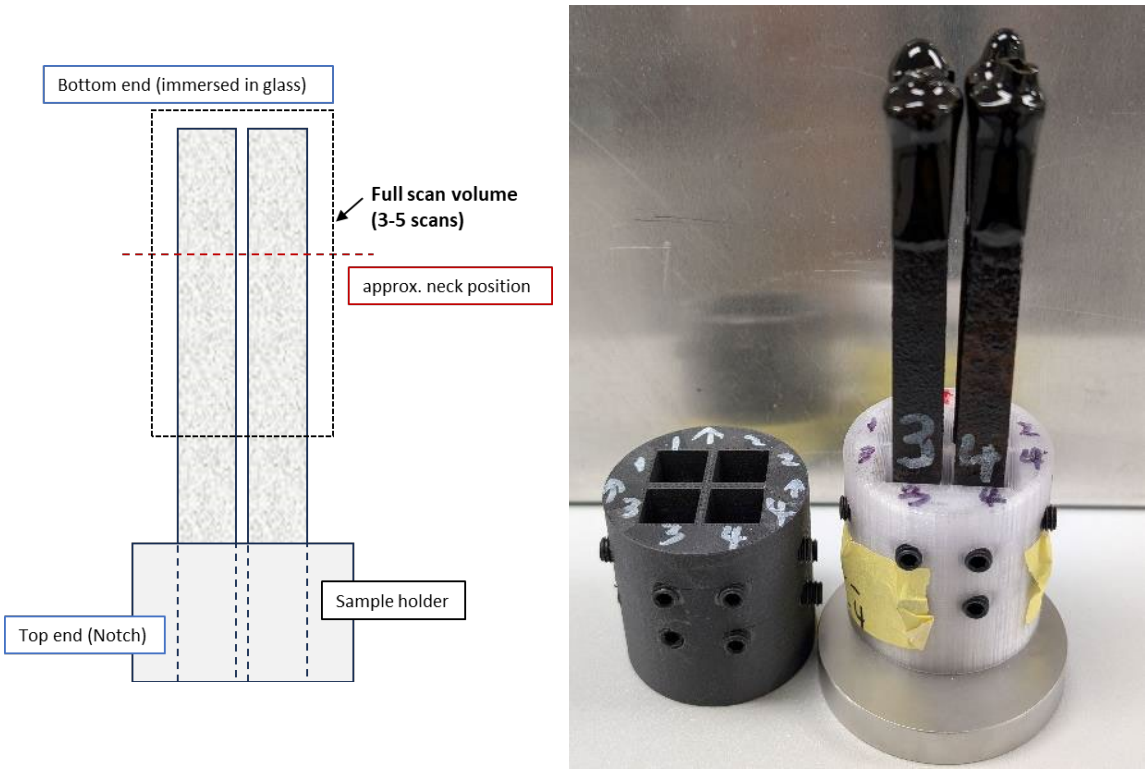

Figure 2.2. Samples for micro-CT scan.

The K-3 corrosion was calculated by dimension changes of the coupons after crucible tests in glass melts. As shown in Figure 2.3, the micro-CT scan produces a "stack" of x-ray images, which can be reconstructed into a 3D object for each sample. The 3D object can be sliced from different angles for analysis. Each coupon was scanned twice by micro-CT, pre-test and post-test. The data, two stacks of images, was adjusted and aligned for analysis. Each image stack contains a 50-mm-long section of coupon (1250 slices × 0.04 mm = 50 mm; each slice is one voxel thick, 0.04 mm), with each slice set to 12 mm × 12 mm (300 × 300 pixel, where pixel size is the same as voxel size for the 2D images). The pre-test and post-test image stacks of the same sample were aligned by matching the slices with visible features (grain sizes, pores, etc.), i.e., the same slice number in the pre- and post-test image stacks should have corresponded to the same position on the sample.

After adjusting and aligning, each slice was converted to a binary outline image and then a bounding rectangle of the outline. Adjustment of contrast of the x-ray images was necessary to draw the outline of the post-test coupons to separate the glass and the K-3, which are of different brightness in the x-ray images. After generating the stack of outlines from the x-ray image stack, a stack of bounding rectangles was generated from the stack of outlines (Figure 2.3). A data set was generated by measuring the dimensions of the A-A and B-B directions of the bounding rectangles: $G_A(i)$ and $G_B(i)$, the dimensions of the A-A and B-B directions of the *i*th slice of the pre-test stack; $g_A(i)$ and $g_B(i)$, the dimensions of the A-A and B-B directions of the *i*th slice of the post-test stack (i = 1–1250). The dimension change or corrosion depth (d_{corr}) of each slice was calculated by:

$$d_{corr,_A}(i) = \frac{G_A(i) - g_A(i)}{2} \quad (2.1)$$

$$d_{corr,_B}(i) = \frac{G_B(i) - g_B(i)}{2} \quad (2.2)$$

The maximum corrosion depth along the coupon is the neck corrosion depth ($d_{neck,A}$ and $d_{neck,B}$) and the average neck corrosion (d_{neck}) of the A and B side were calculated by:

$$d_{neck,_A} = MAX[d_{corr,_A}(i)] = MAX[\frac{G_A(i) - g_A(i)}{2}] \quad (2.3)$$

$$d_{neck,_B} = MAX[d_{corr,_B}(i)] = MAX[\frac{G_B(i) - g_B(i)}{2}] \quad (2.4)$$

$$d_{neck} = \frac{d_{neck,_A} + d_{neck,_B}}{2} \quad (2.5)$$

The results are discussed in Section 3.0.

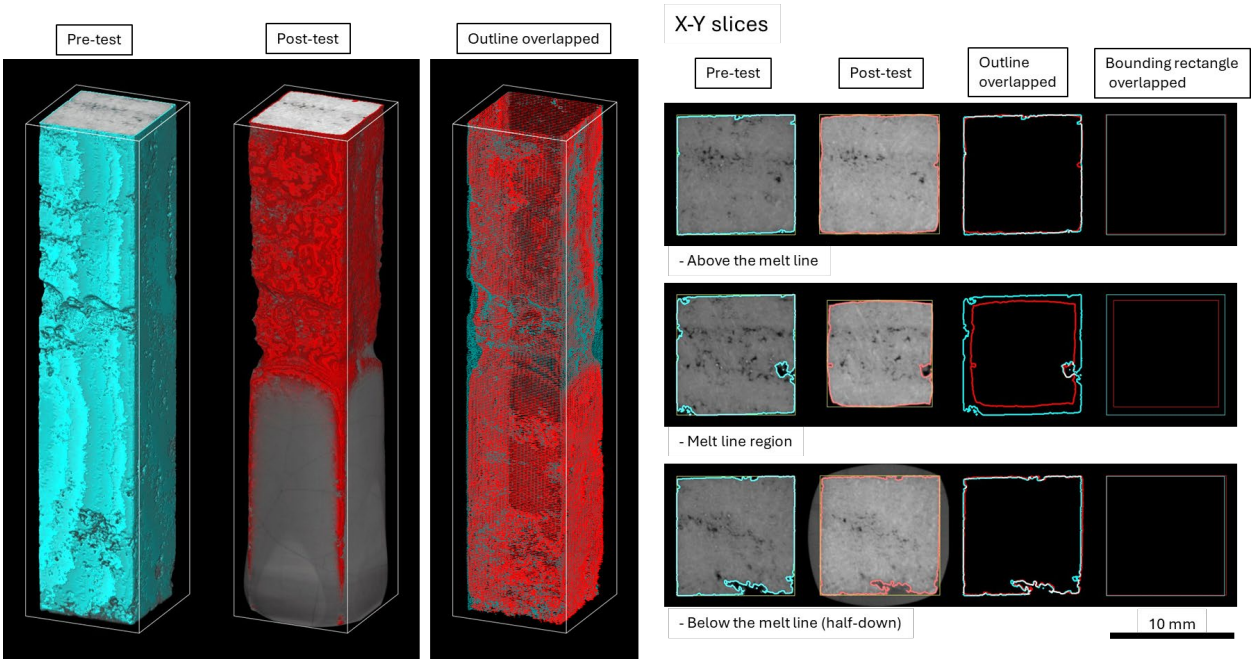

(a) (b)

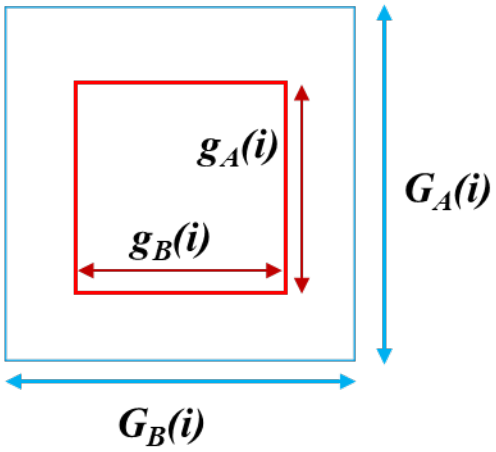

(c)

Figure 2.3. Procedure of measuring refractory corrosion using micro-CT scanning images. The brighter material is the K-3 phase, and the darker material is the glass remaining on the coupon surface after test. (a) 3D view of an example coupon HAL24M2-04 1200 °C 7 d. The outlines of the pre-test coupon (in cyan) and the post-test coupon (in red) are aligned and overlapped. The bounding box is 12 mm × 12 mm (x-y plane) × 50 mm (along z-axis). (b) Horizontal cross section (slices of x-y plane) from different locations; the bounding rectangles (on the right) are drawn based on the outlines for dimension measurement. (c) Dimension measured on the bounding rectangles.

3.0 Results and Discussion

Table 3.1 and Figure 3.1 summarize the measured neck corrosion depths of the HAL24M2 glasses. Each glass was tested under two different temperatures: 1150 °C for 7 days and 1200 °C for 7 days. Test coupon photos are shown in Appendix A and micro-CT scan images are shown in Appendix B. For each coupon, the neck corrosion depth was measured in two perpendicular directions as discussed in Section 2.2. The average values of the two measurements are reported with the standard deviation (SD).. During the micro-CT measurement, setting the threshold to outline the scanned materials can lead to a measurement uncertainty of ~1 to 3 voxels (0.04 to 0.12 mm). Therefore, a conservative estimated uncertainty is ~0.12 mm for the neck corrosion depth data. A pooled SD was used, which was calculated using duplicated data sets generated from different institutions, samples, and/or time (Vienna et al., 2022).

In this high-Al matrix, some glasses showed low corrosivity on the K-3 coupons without forming a visible neck. For one glass, HAL24M2-03, the corrosion neck was only observed on the coupons after the 1200 °C/7days test but not on the coupons after the 1150 °C/7days test. For five glasses, HAL24M2-06, -13, -17, -18, and -20, no corrosion neck was observed after tests at either of the two temperatures. (see the images in Appendix B).

The current K-3 neck corrosion upper limit is 0.04 in., which is based on a previous dataset of bubbling test data. There is an estimated offset for neck corrosion depth data from the static test in this report to be compared with those from the previous bubbling test (Vienna et al. 2025). Applying the offset of 0.5949 ln[in.] to the 1200 °C/7days measured data, only one glass, HAL24M2-01, has a neck corrosion depth on K-3 exceeding the 0.04-in. limit.

Figure 3.2 shows the measured neck corrosion depth of the 1200 °C for 7 days test samples plotted against model predictions for responses obtained under this test condition from Vienna et al. (2024). The y-axis error bars are uncertainty of predicted values calculated by the model; and the x-axis error bars are applied using a fixed value of 0.3311 ln[in.] which is a pooled standard deviation reported in Vienna et al. (2022). The model slightly over-predicted the neck corrosion depth of these glasses.

Table 3.1. K-3 refractory corrosion neck depth, d_{neck}, mm.

Glass ID	1150 °C-7 Days	1200 °C-7 Days
HAL24M2-01	2.37 ± 0.071	2.63 ± 0.014
HAL24M2-02	0.63 ± 0.014	0.78 ± 0.057
HAL24M2-03	0.03 ± 0.014	0.08 ± 0
HAL24M2-04	0.35 ± 0.014	0.59 ± 0.042
HAL24M2-05	0.22 ± 0	0.25 ± 0.014
HAL24M2-06	0.02 ± 0.028	0.02 ± 0.028
HAL24M2-07	0.18 ± 0.028	0.24 ± 0.028
HAL24M2-08	0.09 ± 0.014	0.08 ± 0
HAL24M2-09	0.1 ± 0.028	0.18 ± 0.057
HAL24M2-10	0.07 ± 0.014	0.1 ± 0.028
HAL24M2-11	0.05 ± 0.014	0.05 ± 0.014
HAL24M2-12	0.13 ± 0.042	0.16 ± 0.028
HAL24M2-13	0.01 ± 0.014	0 ± 0.028*
HAL24M2-14	0.24 ± 0.028	0.48 ± 0
HAL24M2-15	0.25 ± 0.014	0.40 ± 0.028
HAL24M2-16	0.03 ± 0.014	0.02 ± 0
HAL24M2-17	0 ± 0*	0.01 ± 0.014
HAL24M2-18	-0.02 ± 0*	-0.01 ± 0.014*
HAL24M2-19	0.50 ± 0.057	0.70 ± 0.028
HAL24M2-20	-0.02 ± 0*	0.02 ± 0.057

* Zero or negative values were measured from the post-test coupons without a visible neck, which indicated that the coupon size did not change or slightly expanded. The micro-CT images are shown in Appendix B.

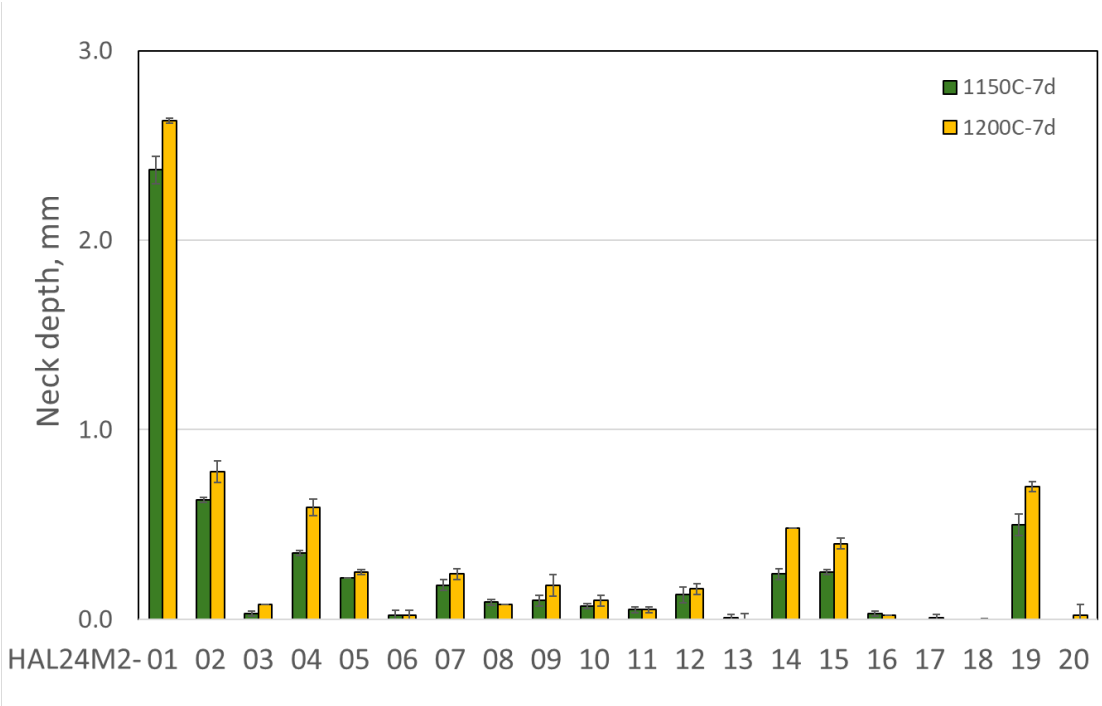

Figure 3.1. K-3 refractory corrosion neck depth.

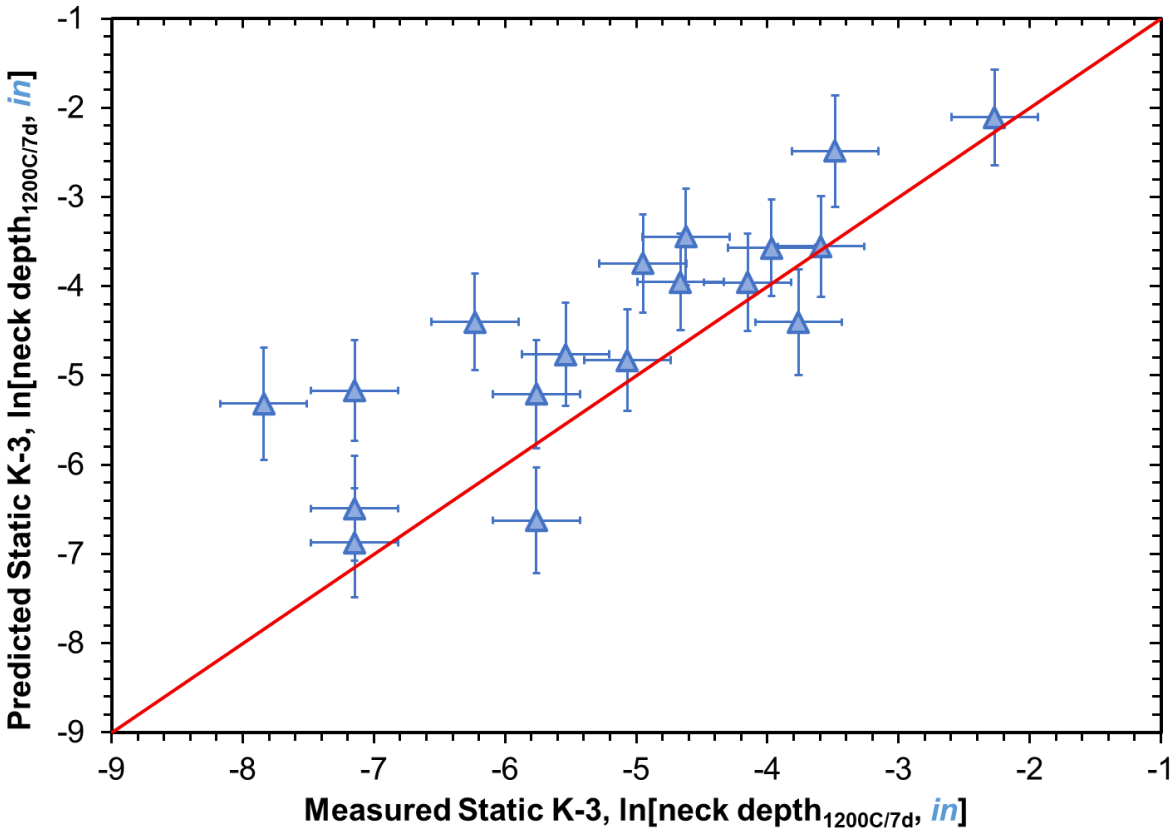

Figure 3.2. Measured and predicted (Vienna et al. 2024) K-3 refractory corrosion neck depth. Red line is the 1:1 line between the measured and predicted values. Uncertainties for measured values are represented by the pooled SD reported in Vienna et al. (2022).

4.0 Conclusions

This report documents the results of the refractory corrosion tests of a high-Al matrix of simulated DFHLW glasses, HAL24M2. Of the twenty glasses tested, after the 1200 °C for 7-days test, only one, HAL24M2-01, failed the nominal 0.04-in. K-3 neck corrosion limit assuming a 0.5949 ln[in.] offset, which is applied to static test data to be comparable with the limit for the previous bubbling test data.

5.0 Bibliography

10 CFR 830, *Nuclear Safety Management*. Code of Federal Regulations, as amended.

ASTM C621-09, *Standard Test Method for Isothermal Corrosion Resistance of Refractories to Molten Glass*. ASTM International, West Conshohocken, PA.

Bingham PA, AJ Connelly, NC Hyatt, and RJ Hand. 2011. "Corrosion of glass contact refractories for the vitrification of radioactive wastes: a review." *International Materials Reviews* 56(4):226–242.

Britton MD. 2023. *Revised DFHLW Washing and Blending Study Campaign Inventory*. WRPS-2300881, Washington River Protection Solutions, Richland, WA.

Certa, PJ, TM Hohl, AM Johnson, SL Orcutt, RS Wittman, and DS Kim. 2005. *Sensitivity of Hanford Immobilized High Level Waste Glass Mass to Chromium and Aluminum Partitioning Assumptions*, RPP-20003, Rev. 1, CH2MHill Hanford Group, Richland, WA.

DOE Order 414.1D, *Quality Assurance*. U.S. Department of Energy, Washington, D.C.

Dunst KP. 2020. *Process Inputs Basis of Design (PIBOD) for HLW*. 24590-DB-PET-19-001, Rev. 1, River Protection Project, Waste Treatment Plant, Richland, WA.

Gan H, X Lu, I Vidensky, P Catherine, IL Pegg, IS Muller, AC Buechele, P Branch, L Su, C Mooers, E Malone, G Bazemore, and M Ing. 2001. *Corrosion of K-3 Refractory and Metal Alloys in RPP-WTP LAW Glasses*, VSL-01R3540-1, Rev. 0. Vitreous State Laboratory, The Catholic University of America, Washington, DC.

Herman, CC, PR Dixon, TM Brouns, ME Stone, RT Jubin, KG Picha, MS Vassiliou, RP Miklos, SM Robinson, MJ Rigali, J Manna, S Venkatesh, and DM Tate. 2022. *R&D Roadmap for Hanford Tank Waste Mission Acceleration*, NNLEMS-2022-00005, Rev. 0, Network of National Laboratories for Environmental Management and Stewardship, Washington, D.C.

Kroll, JO, ZJ Nelson, CH Skidmore, DA Dixon and JD Vienna. 2019. "Formulation of High-Al_2O_3 Waste Glasses from Projected Hanford Waste Compositions and Assessment of Current Glass Property Models." *Journal of Non-Crystalline Solids* 517:17-25.

Lu X, I Sargin, and JD Vienna. 2021. "Predicting nepheline precipitation in waste glasses using ternary submixture model and machine learning." *Journal of American Ceramic Society* 104:5636-5647.

Lu X, T Jin, JD Vienna, and CL Trivelpiece. 2023. *Waste Glass Property Database and Data Qualification Plan*. PNNL-34447, Pacific Northwest National Laboratory, Richland, WA.

Muller IS, K Gilbo, M Chaudhuri, IL Pegg, and I Joseph. 2018. *K-3 Refractory corrosion and sulfate solubility model enhancement (Final Report)*, VSL-18R4360-1, Rev. 0, ORP-63490, Rev. 0. Vitreous State Laboratory, The Catholic University of America, Washington, DC.

NQA-1-2012, *Quality Assurance Requirements for Nuclear Facility Application*. American Society of Mechanical Engineers, New York, NY.

Peeler, DK, JD Vienna, MJ Schweiger, and KM Fox. 2015. *Advanced High-Level Waste Glass Research and Development Plan*, PNNL-24450, Pacific Northwest National Laboratory, Richland, WA.

Russell, RL, V Gervasio, X Lu, NA Lumetta, NL Canfield, LM Seymour, JT Reiser, JJ Neeway, S Chong, JL George, and JD Vienna. 2025 *Expansion of the Direct Feed High-Level Waste Glass Composion in the High Al Range*. PNNL-36304, Rev. 1, Pacific Northwest National Laboratory, Richland, WA. (in progress)

Selkregg K. 2018. "Fusion cast refractories: roles of containment." *American Ceramic Society Bulletin.* 97(2):21–28.

Skidmore CH, JD Vienna, T Jin, DS Kim, BA Stanfill, KM Fox, and AA Kruger. 2019. "Sulfur solubility in low activity waste glass and its correlation to melter tolerance." *International Journal of Applied Glass Science*, 10(4): 558-568.

Vienna, JD, DC Skorski, DS Kim, and J Matyáš. 2013. *Glass Property Models and Constraints for Estimating the Glass to be Produced at Hanford by Implementing Current Advanced Glass Formulation Efforts*. PNNL-22631, Pacific Northwest National Laboratory, Richland, WA.

Vienna, J.D, DS Kim, IS Muller, GF Piepel, and AA Kruger. 2014. "Toward Understanding the Effect of Low-Activity Waste Glass Composition on Sulfur Solubility". *Journal of the American Ceramic Society*, 97: 3135-3142.

Vienna JD and DS Kim. 2014. *Preliminary IHLW Formulation Algorithm Description*. 24590-RPT-RT-05-001, Rev. 1, River Protection Project, Waste Treatment Plant, Richland, WA.

Vienna JD, GF Piepel, DS Kim, JV Crum, CE Lonergan, BA Stanfill, BJ Riley, SK Cooley, and T Jin. 2016. *Update of Hanford Glass Property Models and Constraints for Use in Estimating the Glass Mass to be Produced at Hanford by Implementing Current Enhanced Glass Formulation Efforts*. PNNL-25835, Pacific Northwest National Laboratory, Richland, WA.

Vienna, JD, JO Kroll, PR Hrma, JB Lang, and JV Crum. 2017. "Submixture model to predict nepheline precipitation in waste glasses". *International Journal of Applied Glass Science*, 8(2):143-157.

Vienna JD, A Heredia-Langner, SK Cooley, AE Holmes, DS Kim, and NA Lumetta. 2022. *Glass Property-Composition Models for Support of Hanford WTP LAW Facility Operation*. PNNL-30932, Rev. 2, Pacific Northwest National Laboratory, Richland, WA.

Vienna JD, X Lu, P Ferkl, J Marcial, MS Fountain, M Trenidad, R Hanson, MD Britton, L Cree, and W Abdul. 2023. "High-Level Waste Glass Processing over Broad Range of Alternative Feed Compositions." In *Proceedings of the 2023 Waste Management Symposia*, Phoenix, AZ.

Vienna JD, X Lu, P Ferkl, LL Gunnell, A Heredia-Langner, NA Lumetta, T Jin, JT Reiser, and V Gervasio. 2024. *Glass Property-Composition Models Update for use in Direct Feed High-Level Waste Flowsheet Development*. PNNL-35884, Pacific Northwest National Laboratory, Richland, WA.

Vienna JD., X Lu, P Ferkl, D Kim, J Marcial, J Bai, and JV Crum. 2025. *Glass Property-Composition Models Update for use in Direct Feed High-Level Waste Flowsheet Development: EWG2.6*. PNNL-37762. Pacific Northwest National Laboratory, Richland, WA.

Appendix A – K-3 Coupons after Refractory Corrosion Test

The photographs in this appendix show the K-3 refractory coupons after corrosion testing with HAL24M2 glasses. Note that the coupons are upside down in the photos; the top of each coupon is the section immersed in the glass melt.

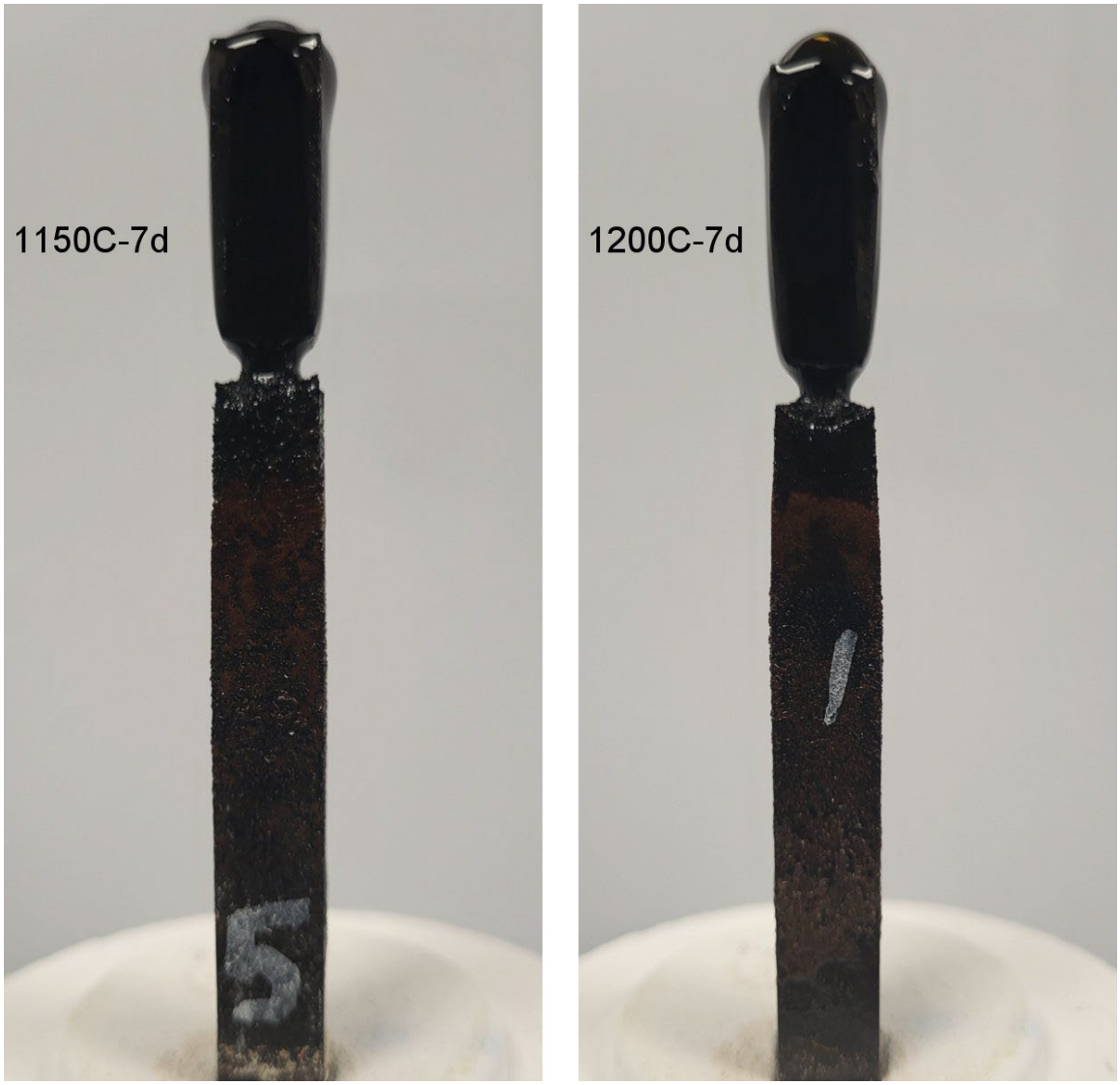

Figure A.1. K-3 coupons after refractory corrosion test, HAL24M2-01.

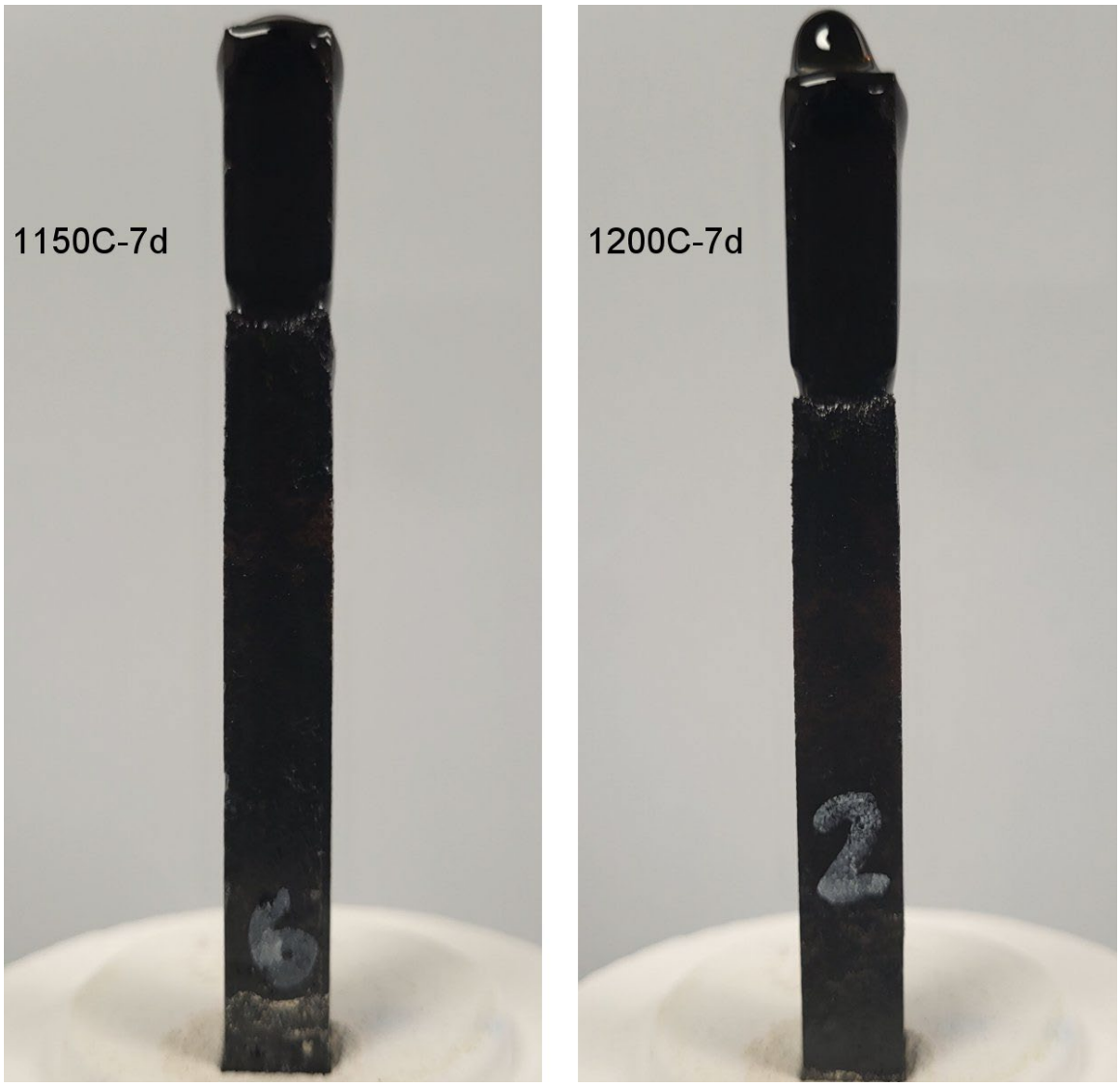

Figure A.2. K-3 coupons after refractory corrosion test, HAL24M2-02.

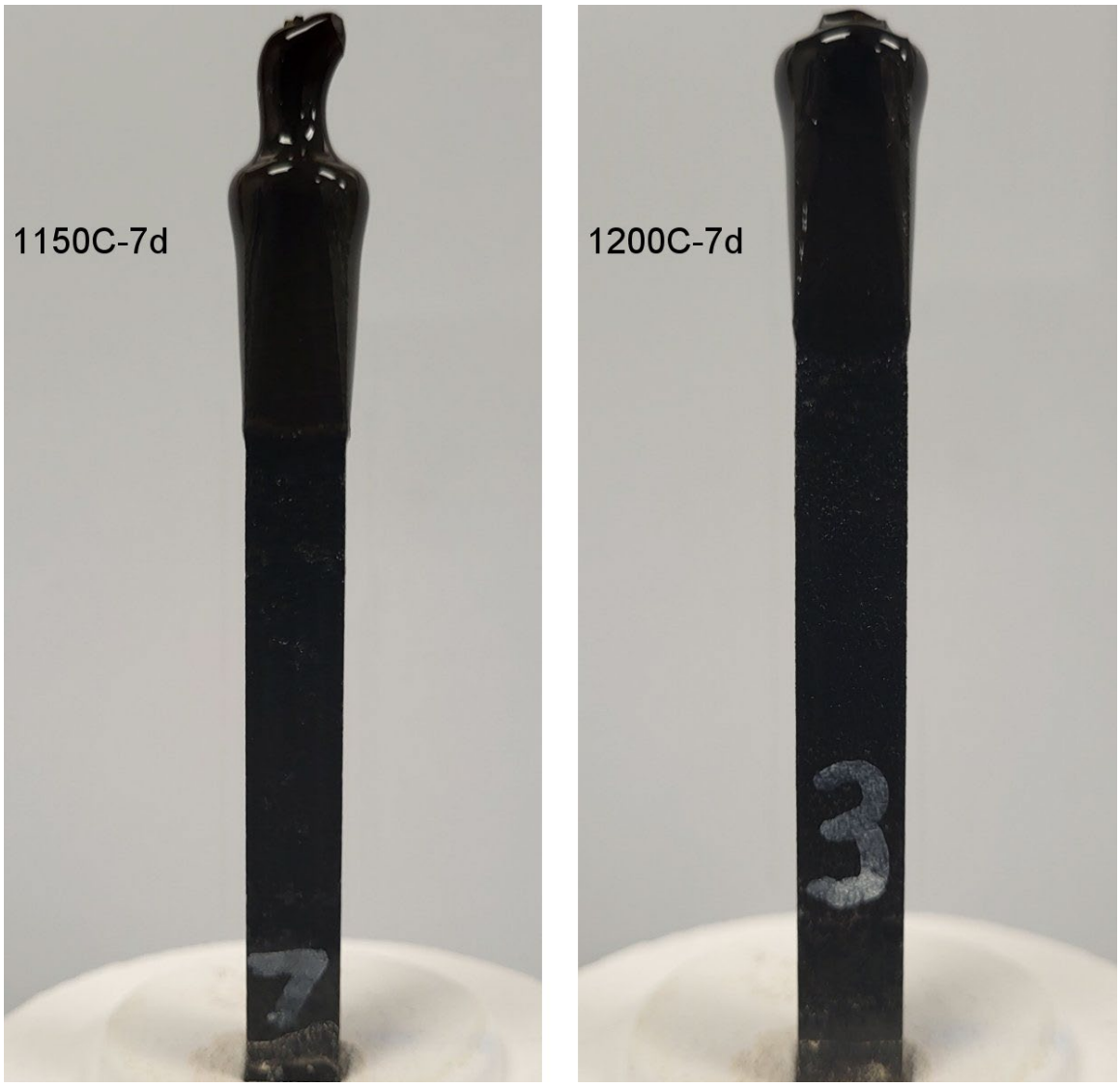

Figure A.3. K-3 coupons after refractory corrosion test, HAL24M2-03.

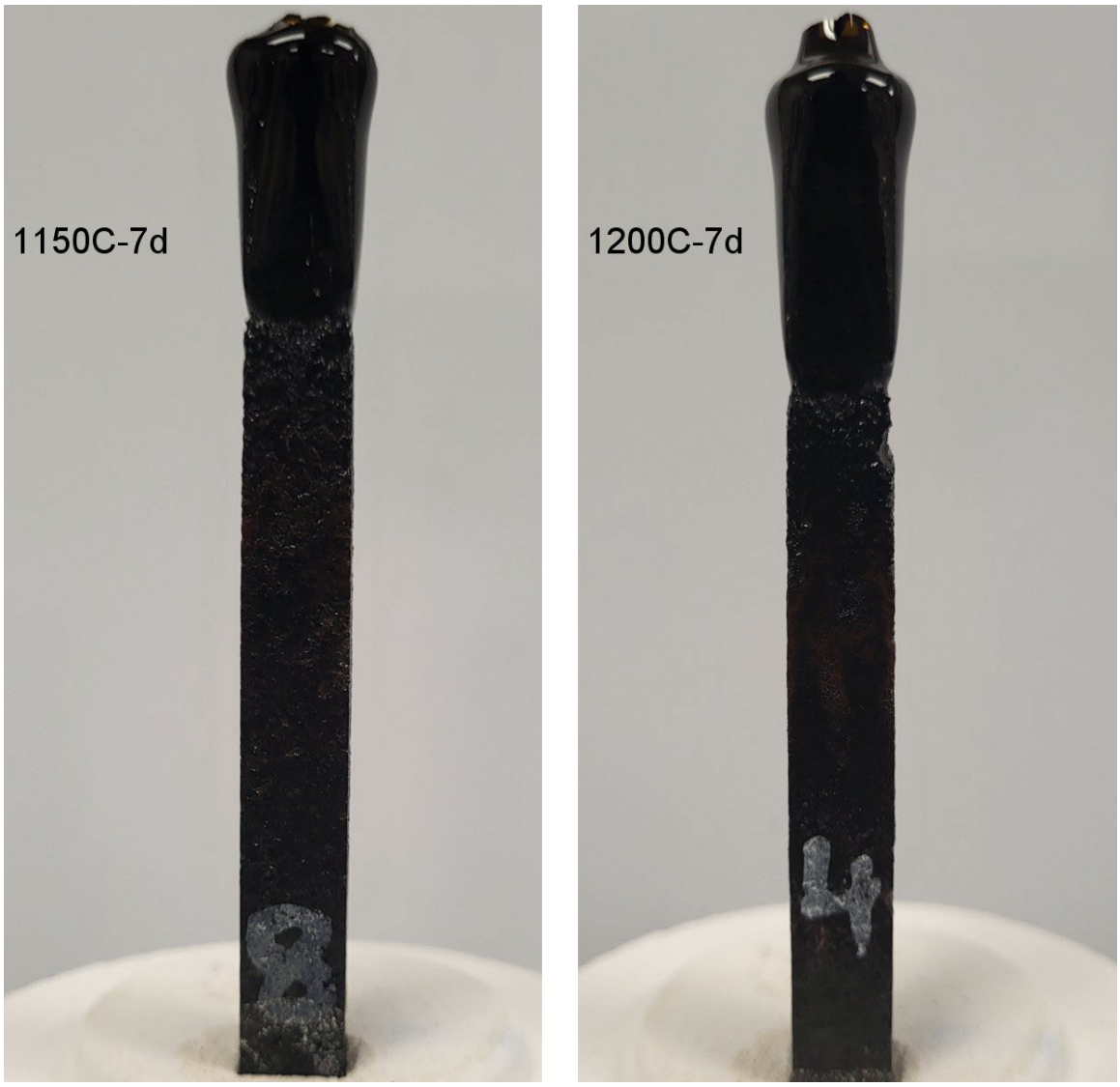

Figure A.4. K-3 coupons after refractory corrosion test, HAL24M2-04.

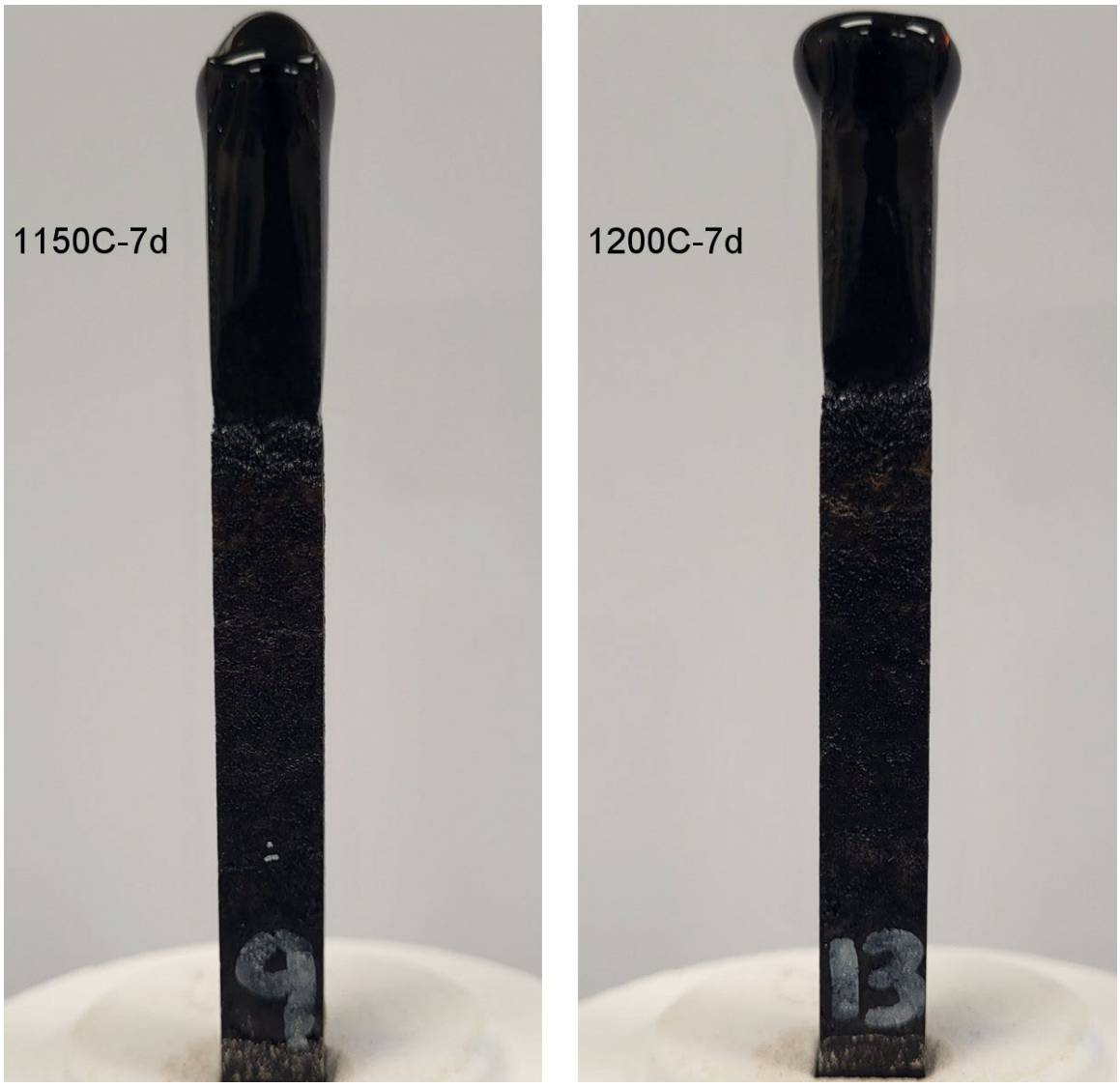

Figure A.5. K-3 coupons after refractory corrosion test, HAL24M2-05-1.

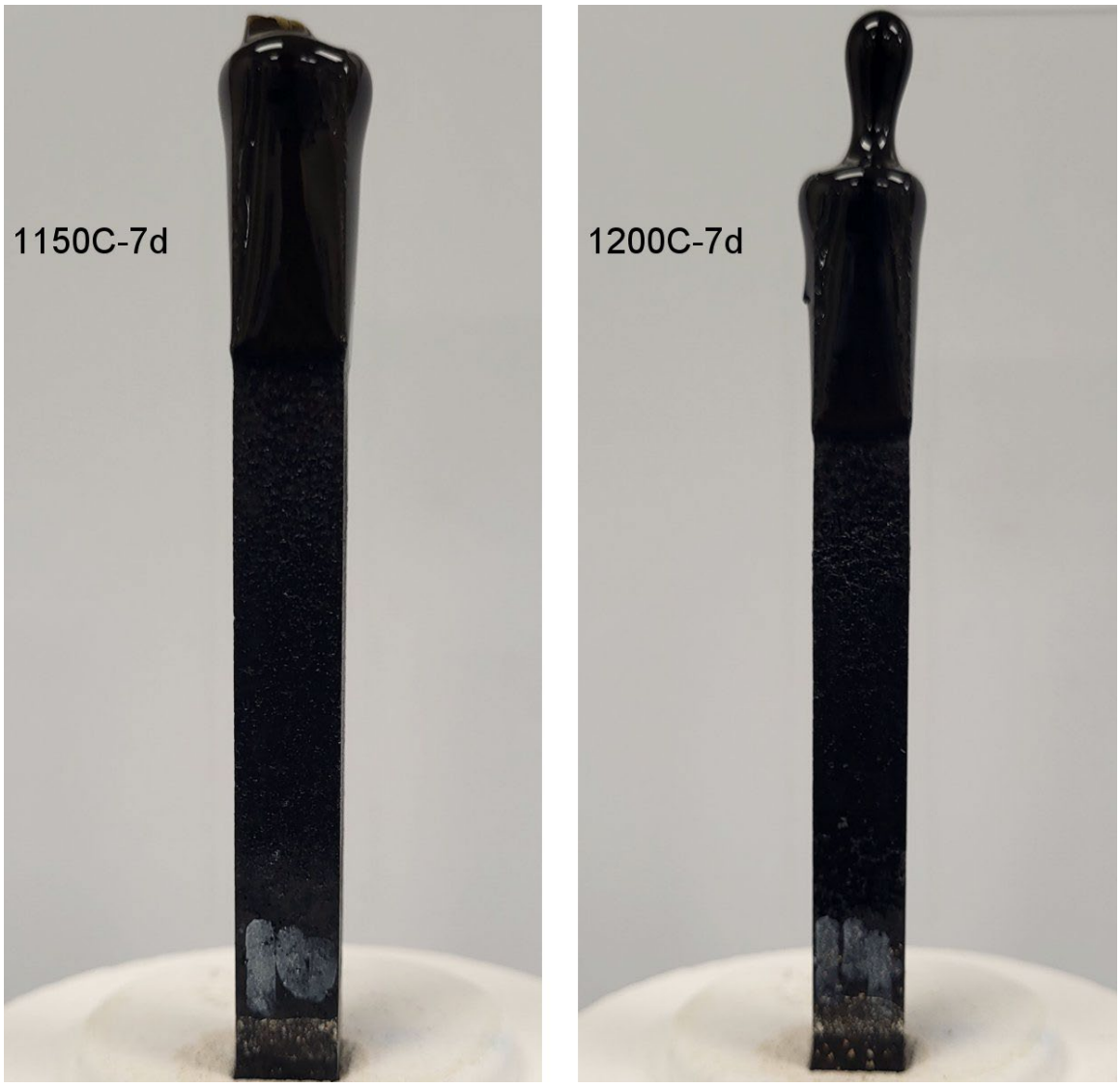

Figure A.6. K-3 coupons after refractory corrosion test, HAL24M2-06-1.

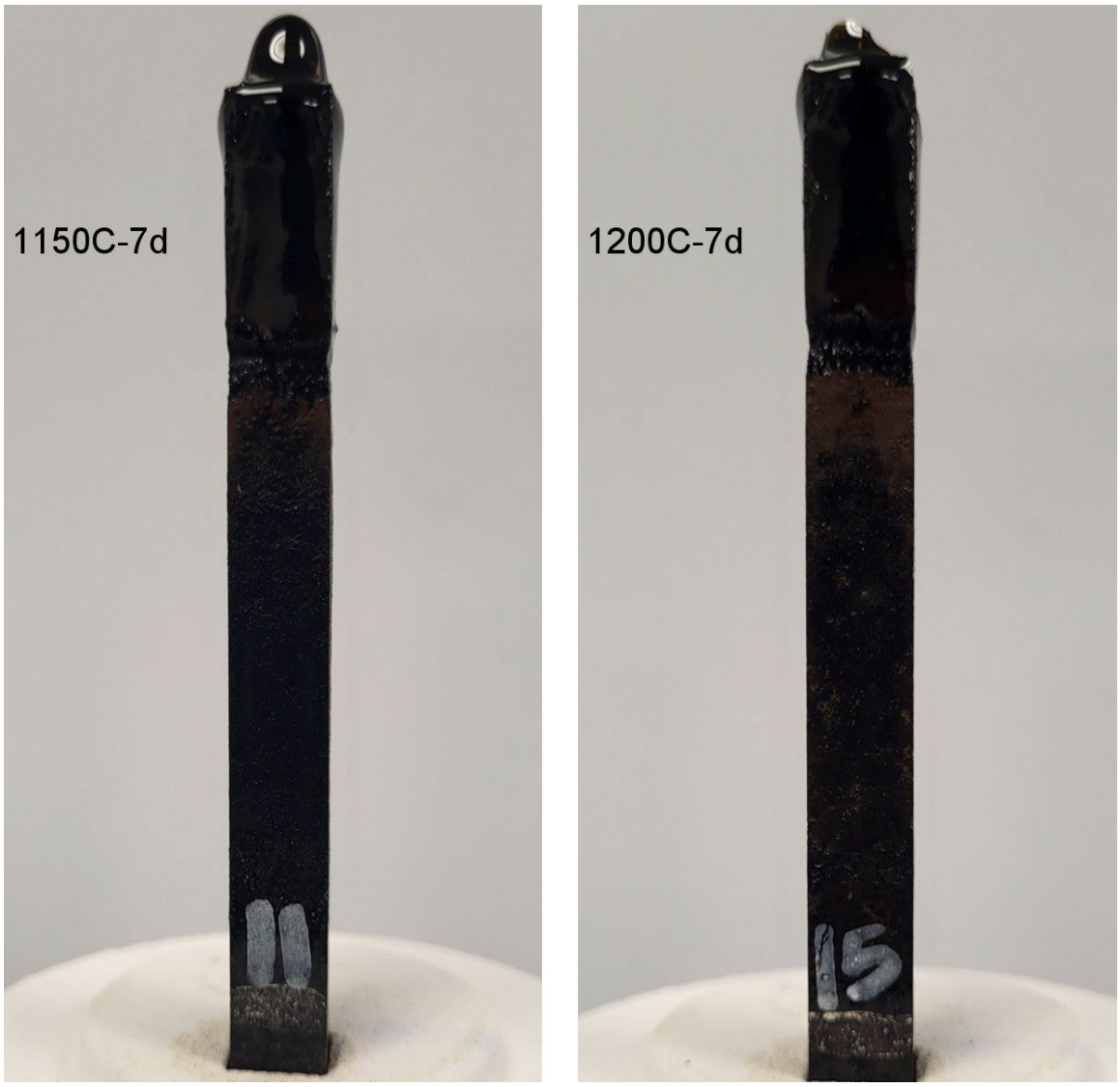

Figure A.7. K-3 coupons after refractory corrosion test, HAL24M2-07.

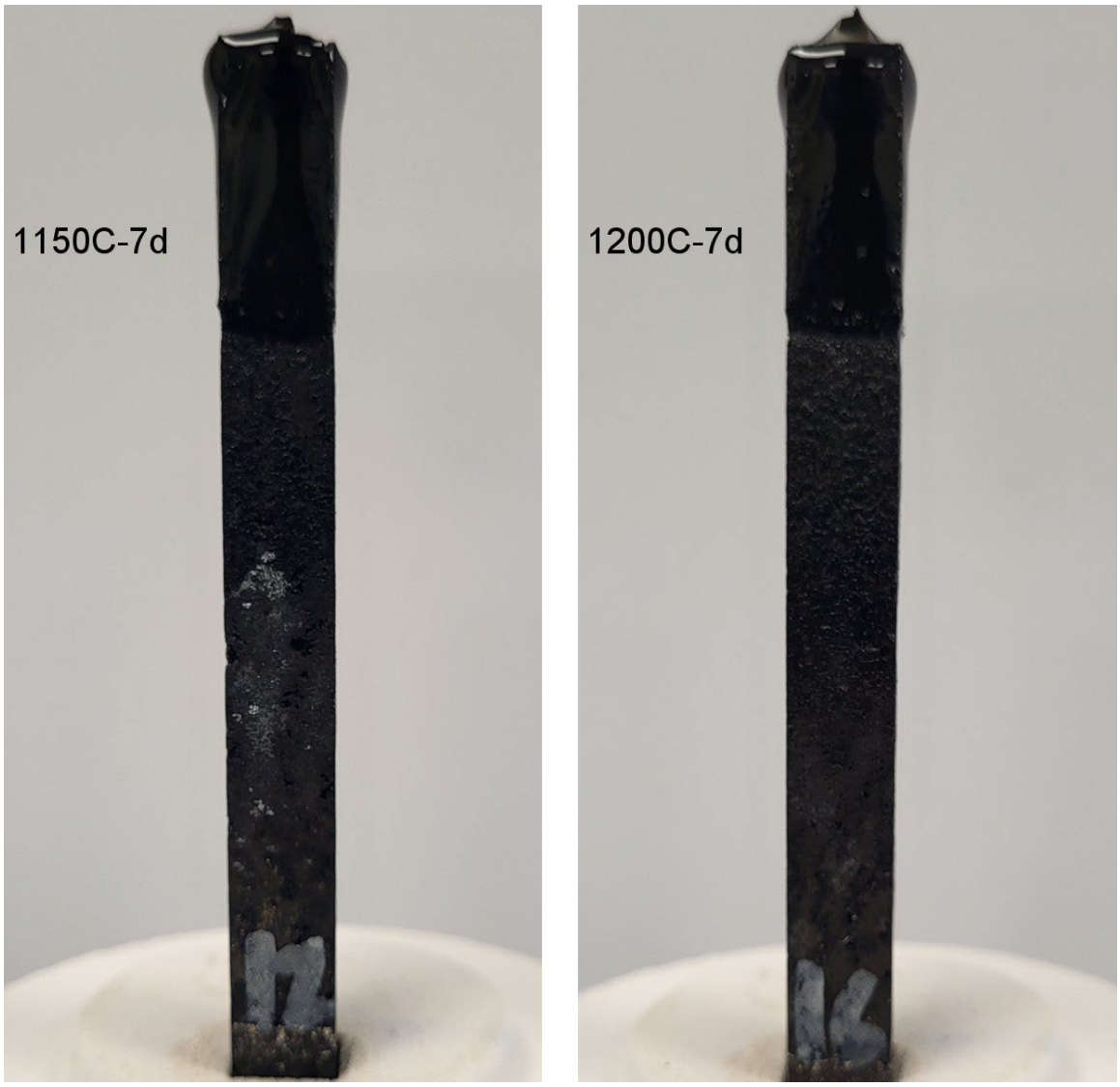

Figure A.8. K-3 coupons after refractory corrosion test, HAL24M2-08.

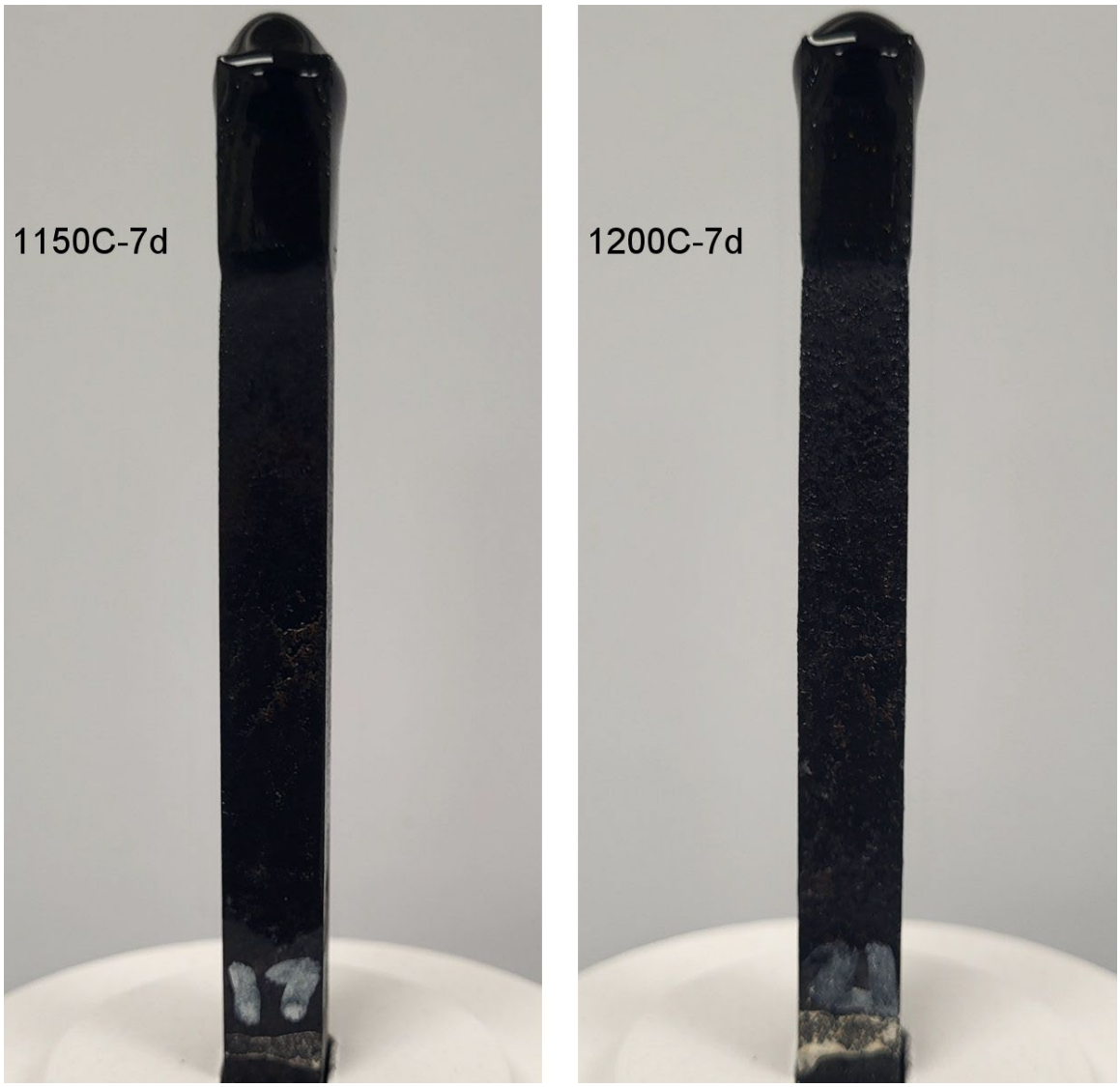

Figure A.9. K-3 coupons after refractory corrosion test, HAL24M2-09.

Figure A.10. K-3 coupons after refractory corrosion test, HAL24M2-10.

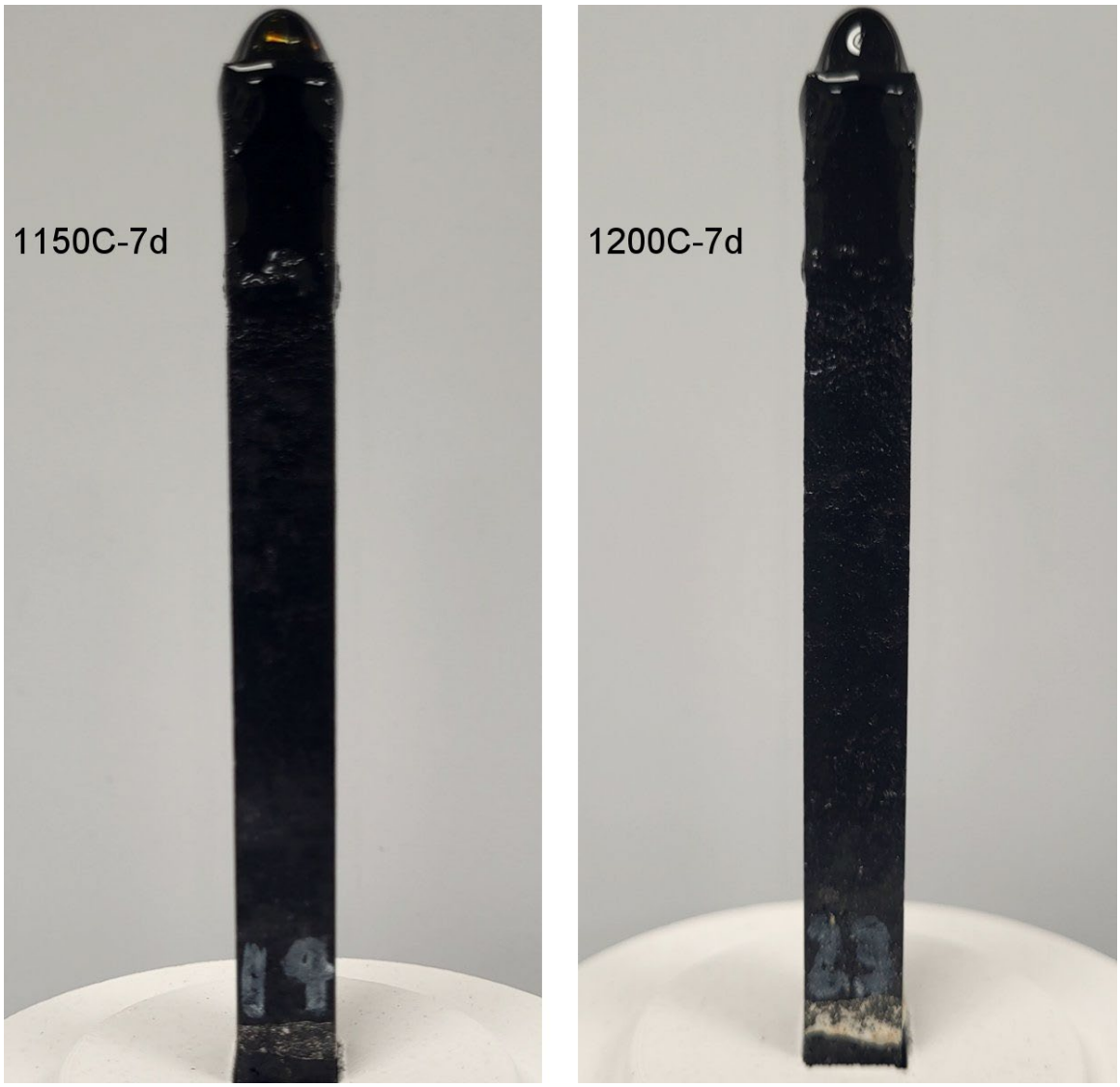

Figure A.11. K-3 coupons after refractory corrosion test, HAL24M2-11.

Figure A.12. K-3 coupons after refractory corrosion test, HAL24M2-12.

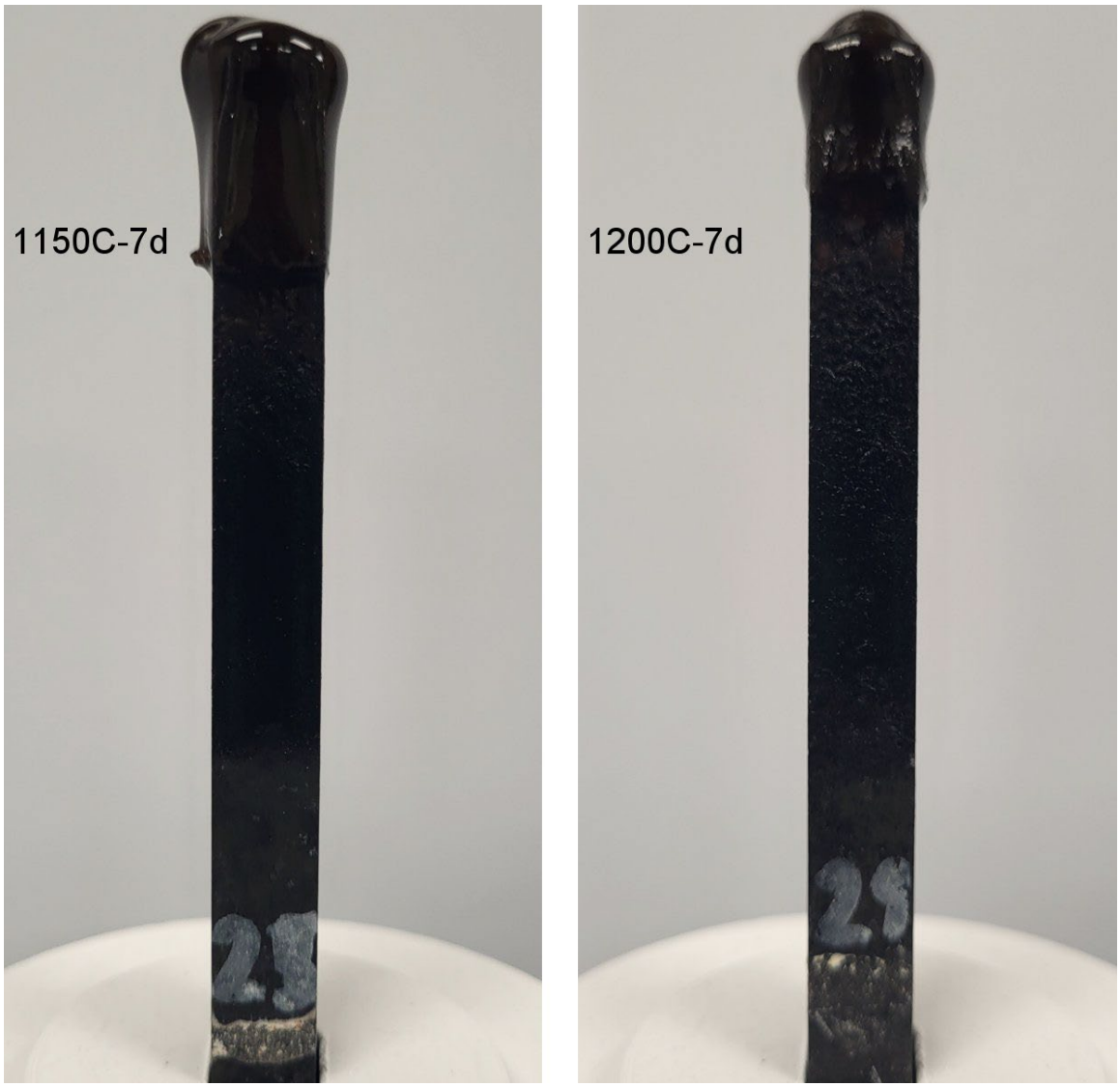

Figure A.13. K-3 coupons after refractory corrosion test, HAL24M2-13.

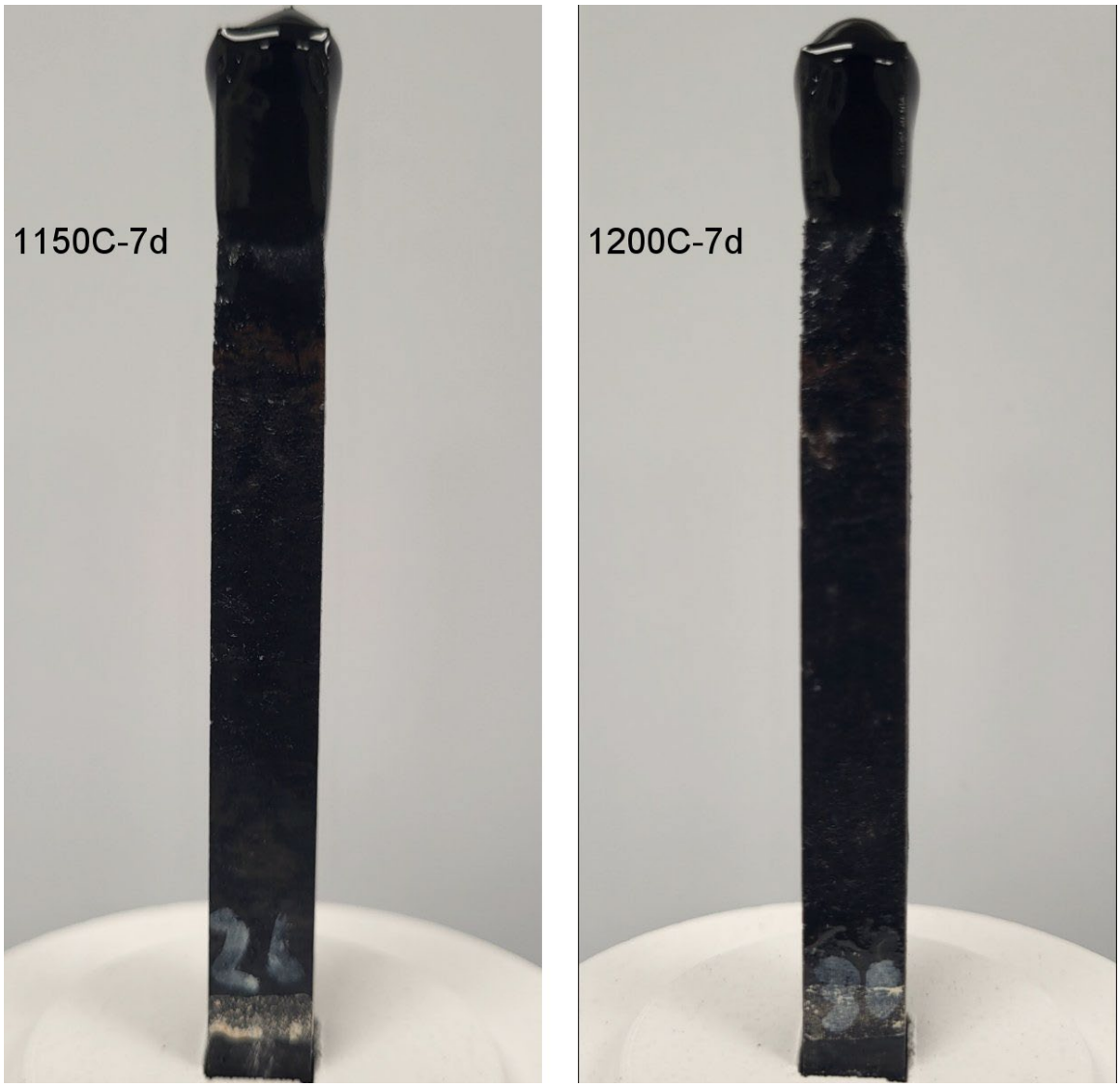

Figure A.14. K-3 coupons after refractory corrosion test, HAL24M2-14.

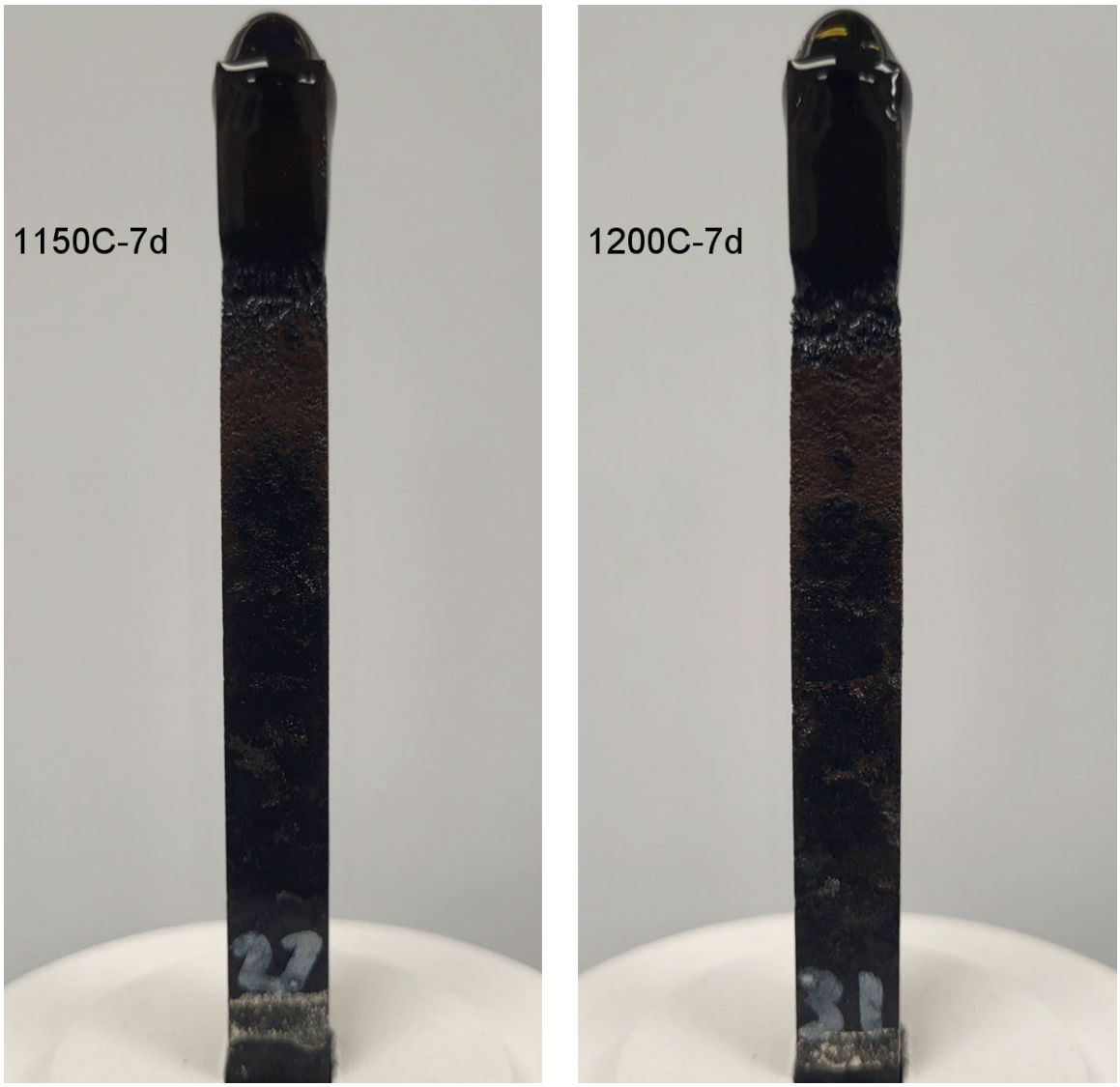

Figure A.15. K-3 coupons after refractory corrosion test, HAL24M2-15.

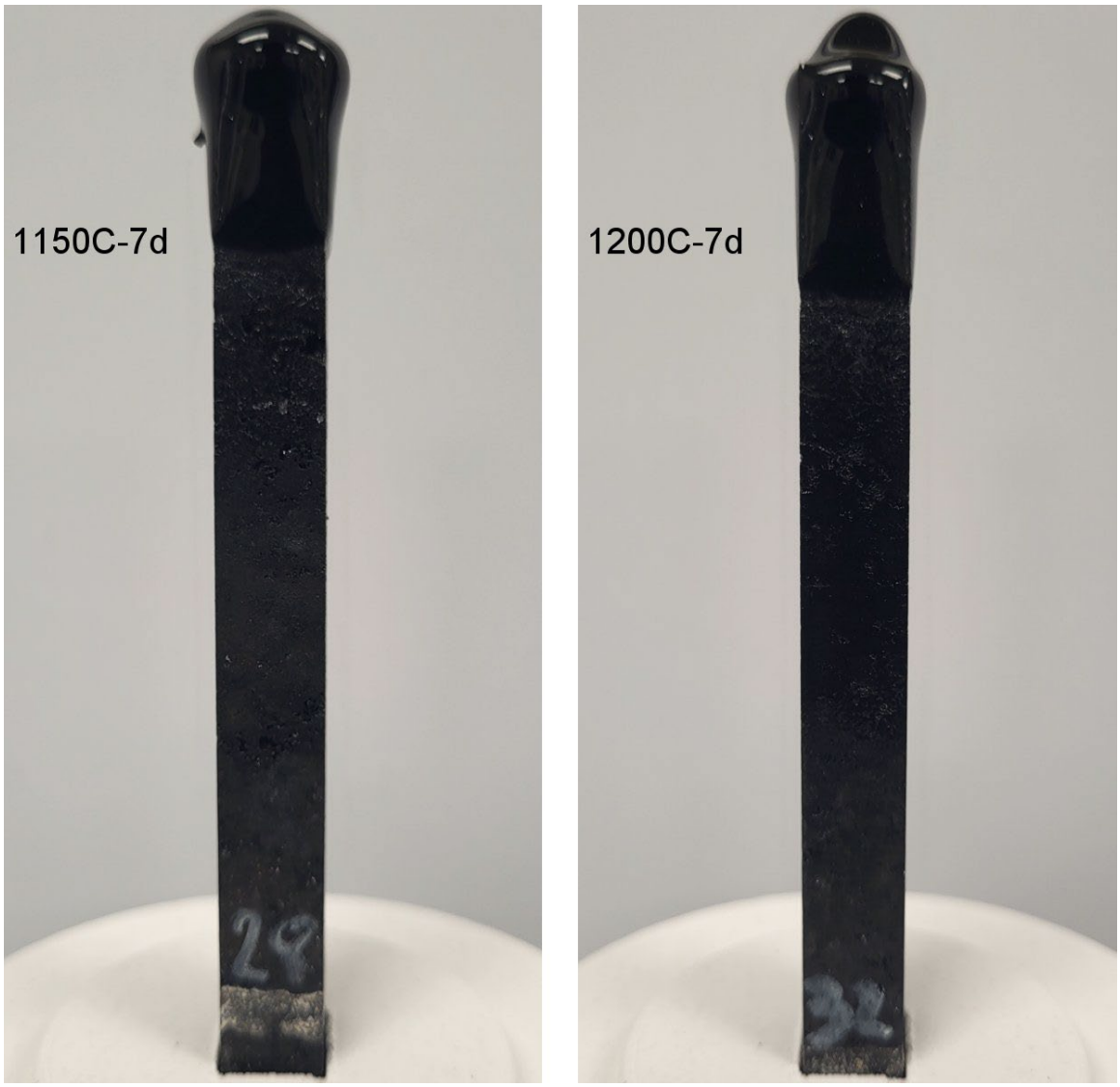

Figure A.16. K-3 coupons after refractory corrosion test, HAL24M2-16.

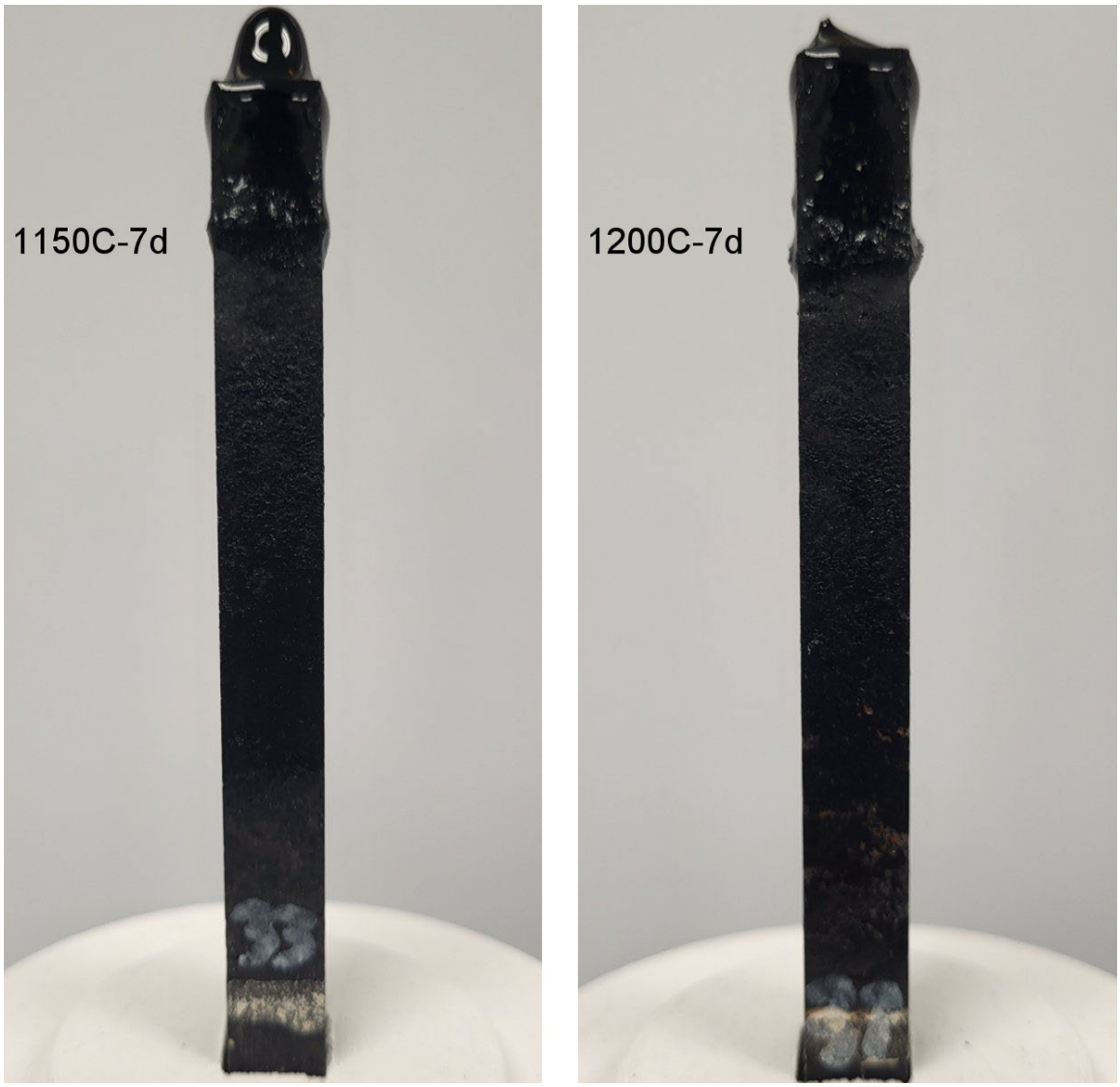

Figure A.17. K-3 coupons after refractory corrosion test, HAL24M2-17.

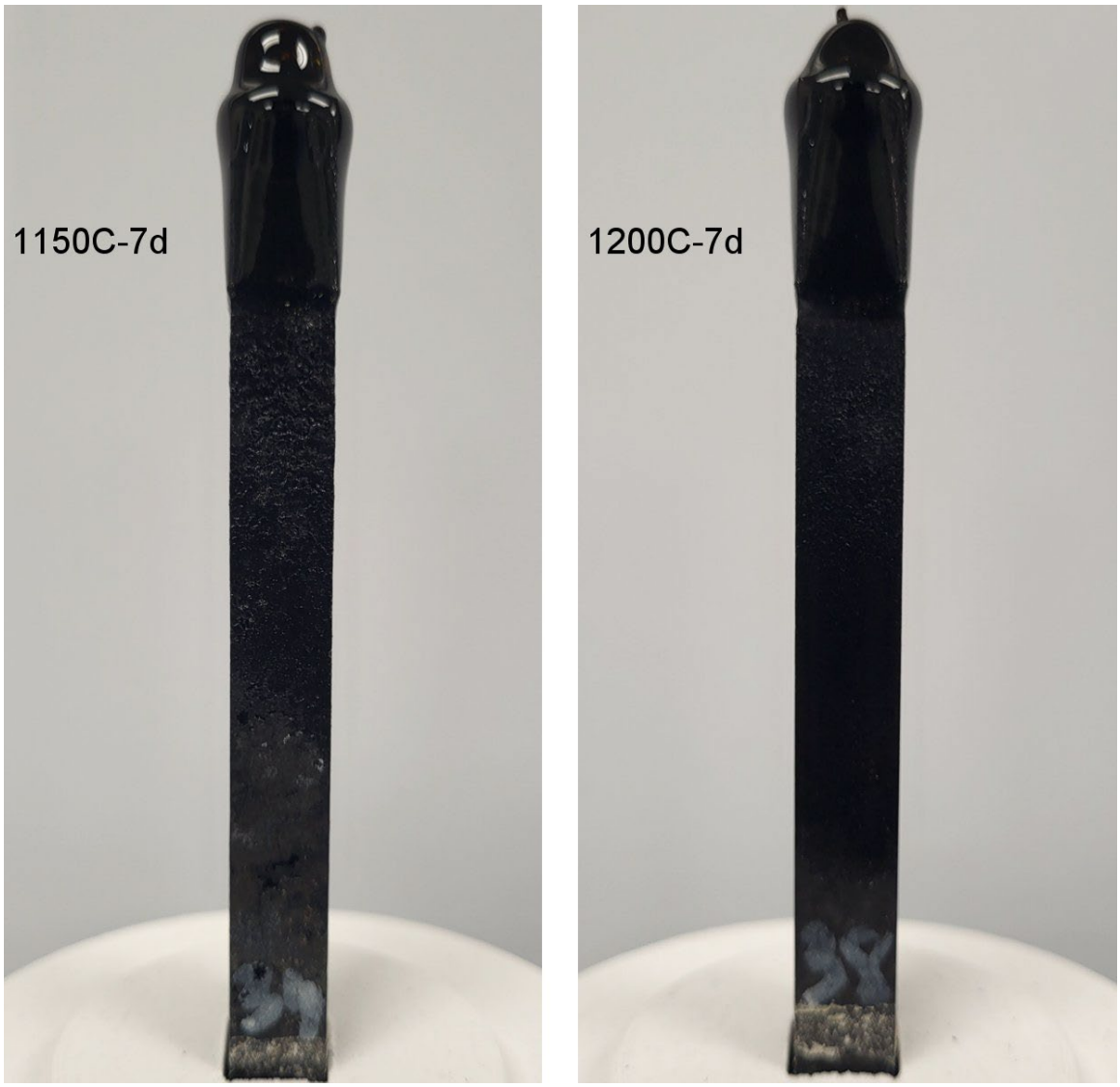

Figure A.18. K-3 coupons after refractory corrosion test, HAL24M2-18.

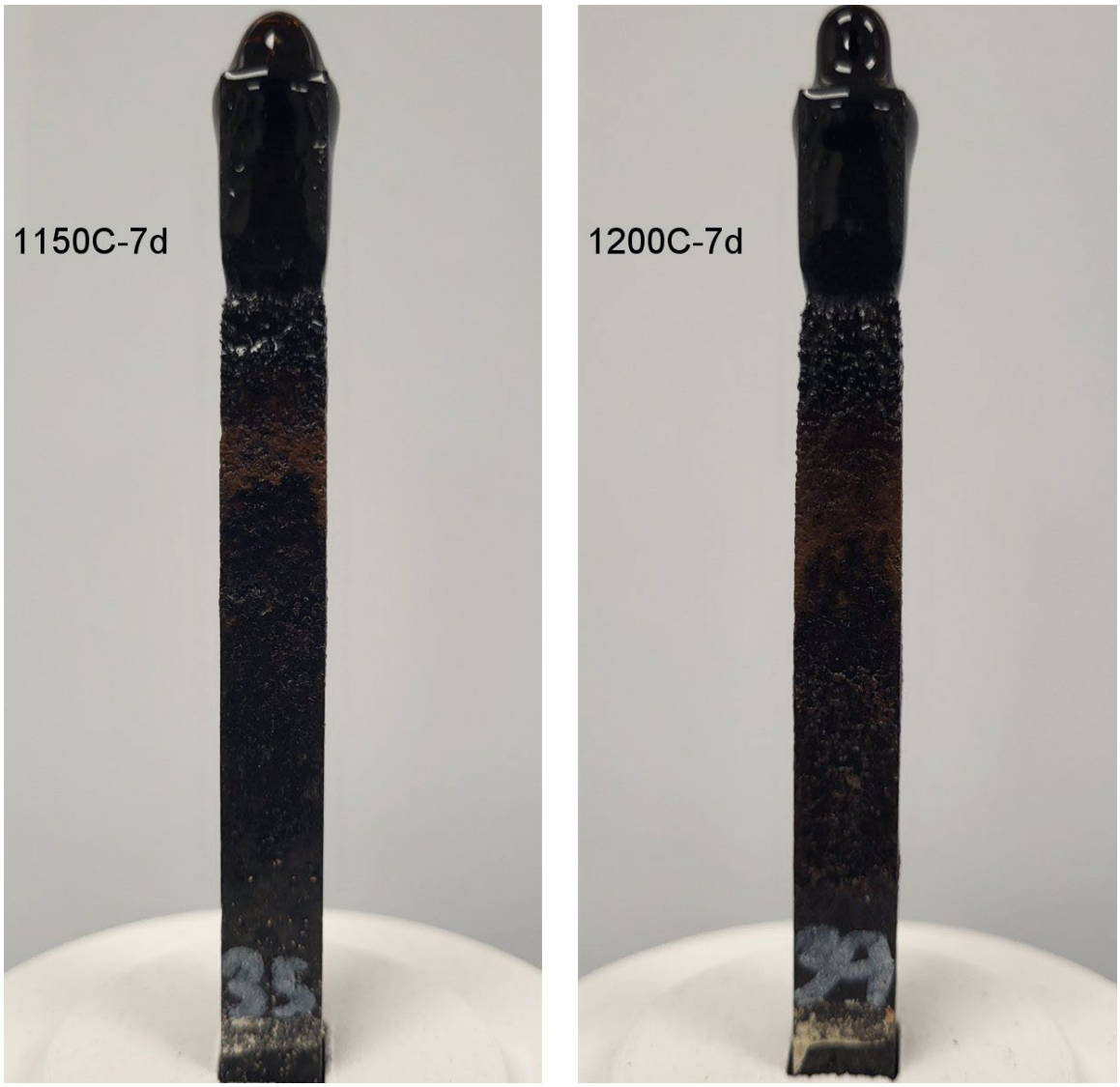

Figure A.19. K-3 coupons after refractory corrosion test, HAL24M2-19.

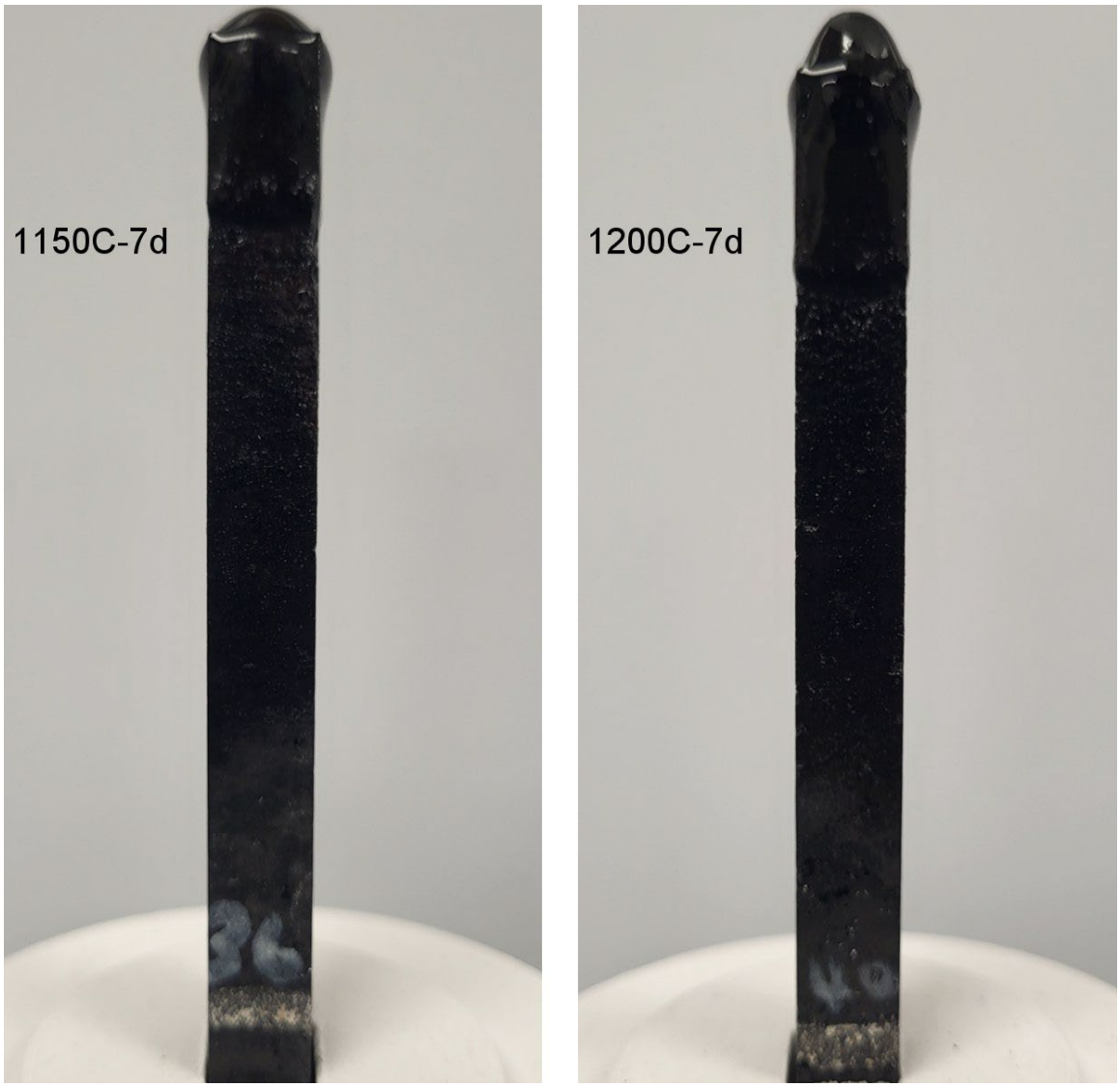

Figure A.20. K-3 coupons after refractory corrosion test, HAL24M2-20.

Appendix B – Micro-CT Results of K-3 Refractory Corrosion Test

This appendix presents the micro-CT images used for the dimension measurements of the K-3 refractory coupons tested for corrosion with the HAL24M2 glasses. Each figure shows the results of one test coupon, including cross-section view images, top-view images with outlines and bounding rectangles, and a plot of corrosion depth measured based on the bounding rectangles. For each figure, (a) shows the cross-section view of the post-test coupon at the center from both the A-A and B-B directions with the neck marked by red arrows. A plot of corrosion depth along the coupon is also shown. The neck is expected in the region of 20 to 35 mm from the bottom of the coupon, which is highlighted in the neck plot. In each figure, (b) shows the top-view slices at the neck location with the pre-test image outlined in cyan and post-test image outlined in red. For the same coupon, neck corrosion depth and neck locations measured from the A-A and B-B directions are not exactly the same because, since the K-3 is not homogeneous, the pores and uneven distribution of the different phases can affect the corrosion damage on different faces.

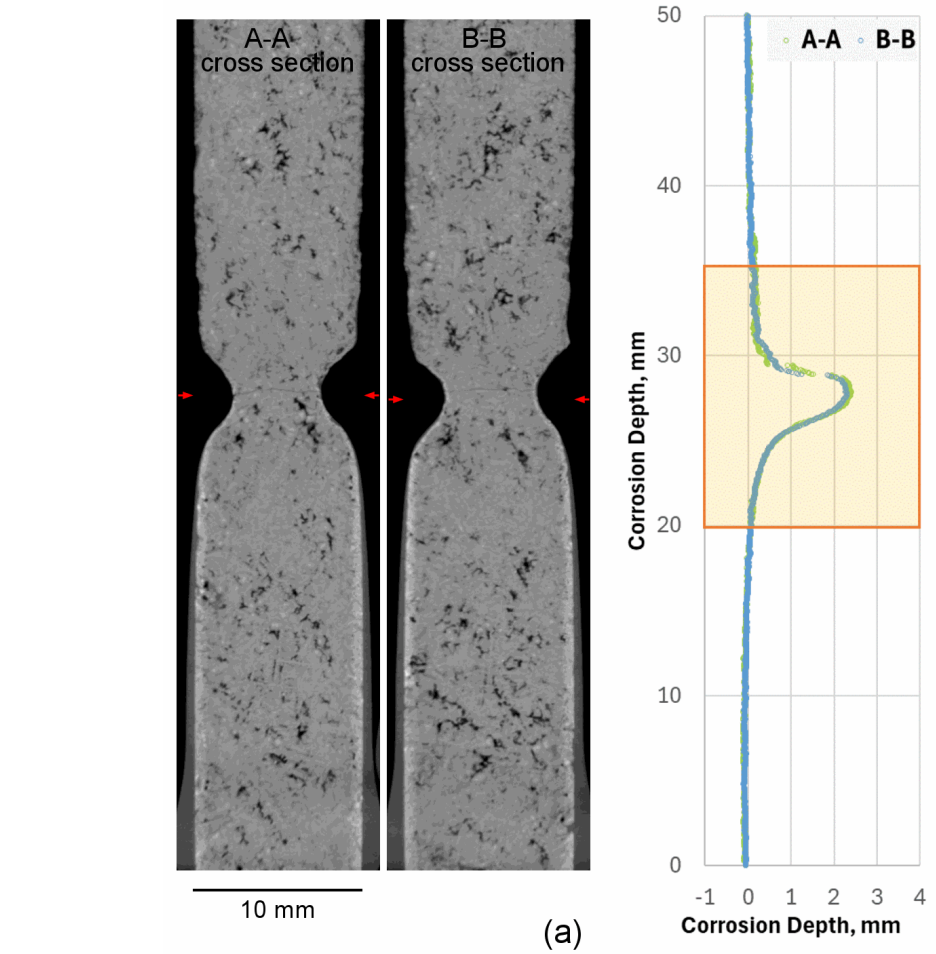

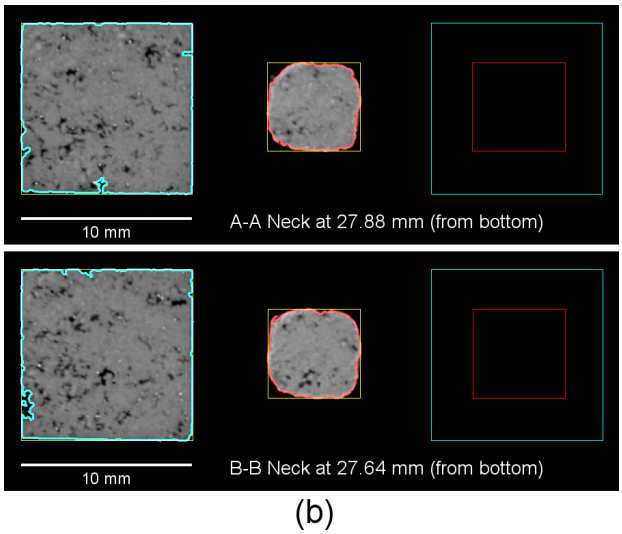

Neck Depth, mm	
A-A	2.42
B-B	2.32
Average	2.37
Standard deviation	0.071
Note: coupon broke at the neck; the crack did not affect measurement	

Figure B.1. Micro-CT results of K-3 refractory corrosion test, HAL24M2-01 - 1150 °C - 7day. (a) cross section at center. (b) top view slice at neck location.

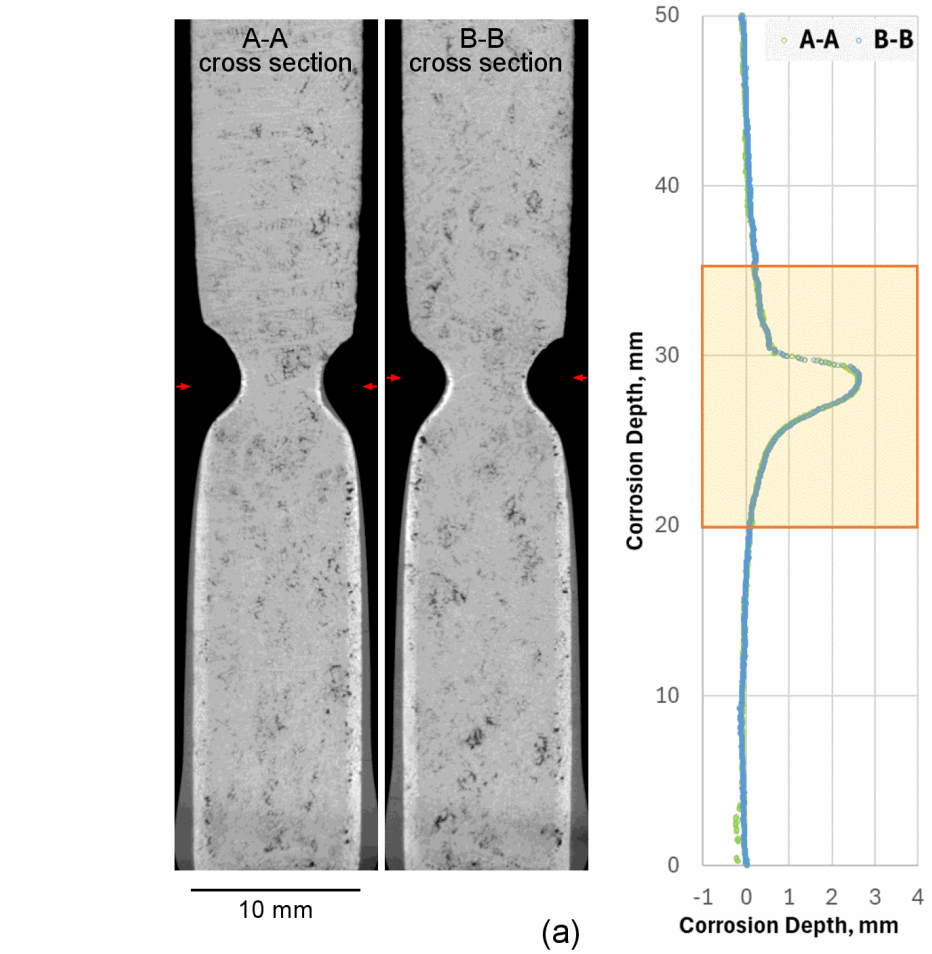

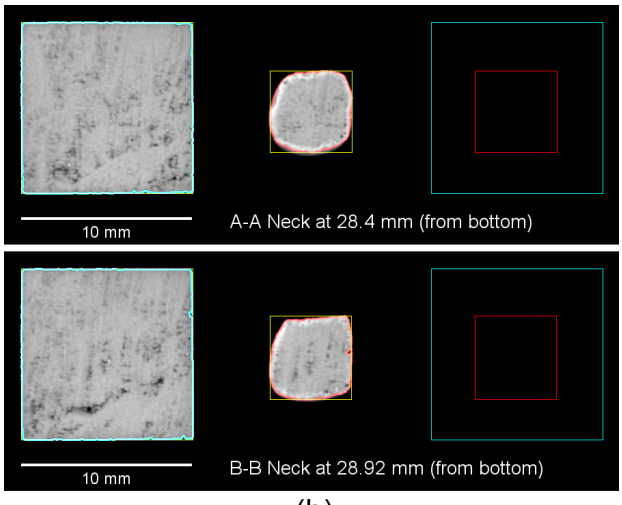

Neck Depth, mm	
A-A	2.62
B-B	2.64
Average	2.63
Standard deviation	0.014

Figure B.2. Micro-CT results of K-3 refractory corrosion test, HAL24M2-01 - 1200 °C - 7day. (a) cross section at center. (b) top view slice at neck location.

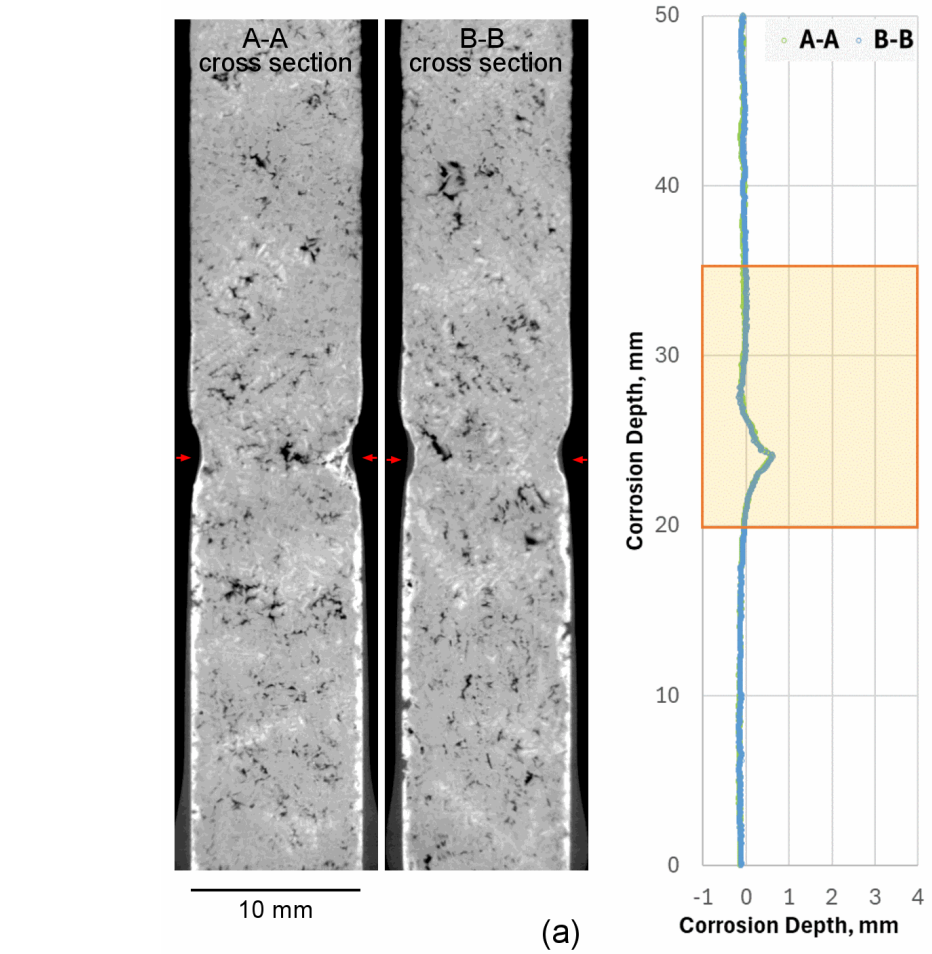

Neck Depth, mm	
A-A	0.62
B-B	0.64
Average	0.63
Standard deviation	0.014

Figure B.3. Micro-CT results of K-3 refractory corrosion test, HAL24M2-02 - 1150 °C - 7day. (a) cross section at center. (b) top view slice at neck location.

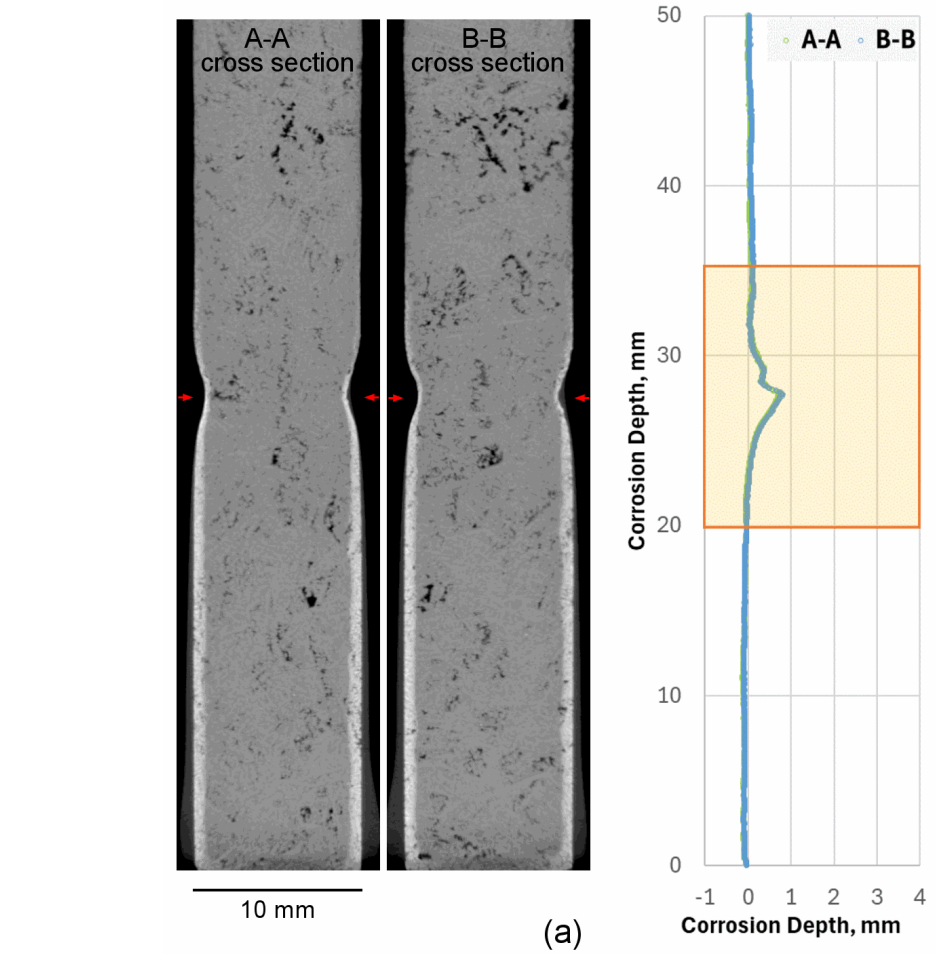

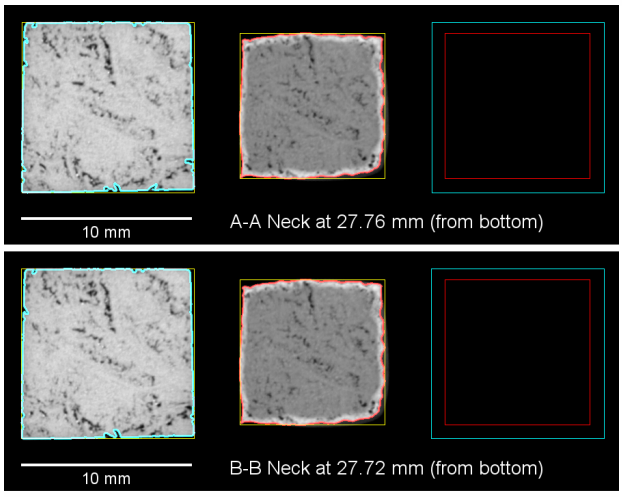

Neck Depth, mm	
A-A	0.74
B-B	0.82
Average	0.78
Standard deviation	0.057

Figure B.4. Micro-CT results of K-3 refractory corrosion test, HAL24M2-02 - 1200 °C - 7day. (a) cross section at center. (b) top view slice at neck location.

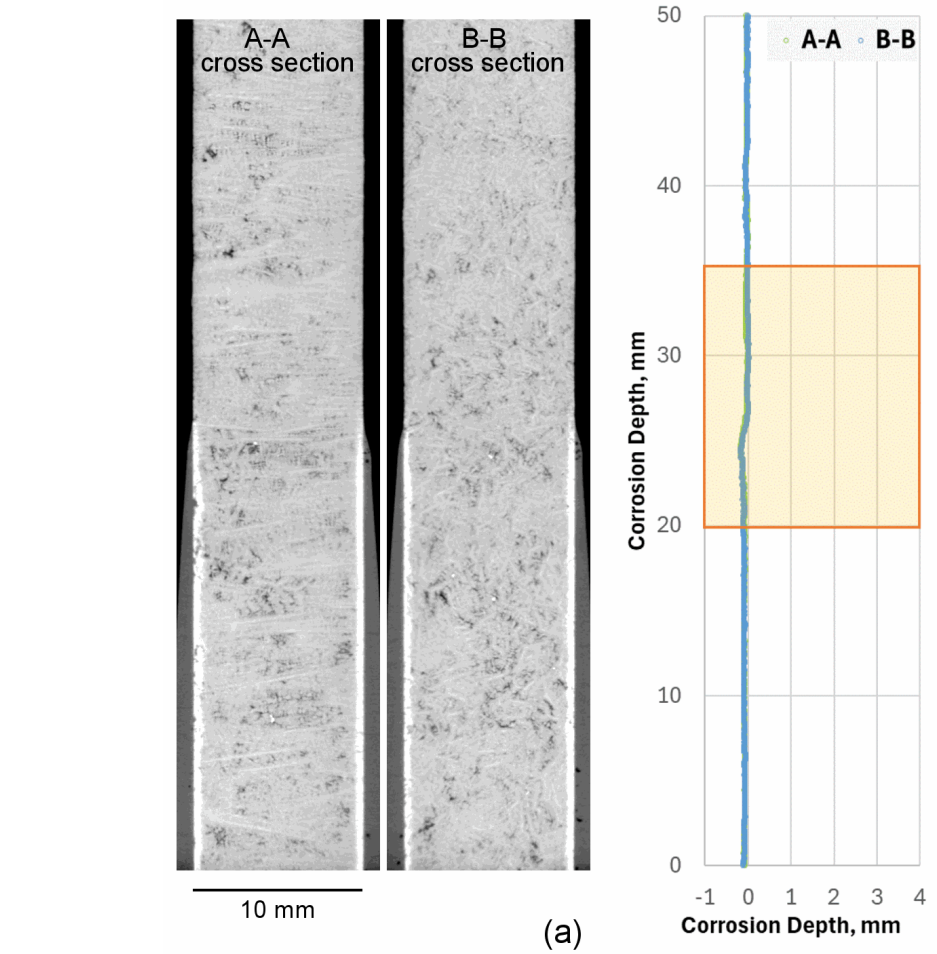

Neck Depth, mm	
A-A	0.02
B-B	0.04
Average	0.03
Standard deviation	0.014
Note: no clear neck. Heights of the x-y slices in (b) are random.	

Figure B.5. Micro-CT results of K-3 refractory corrosion test, HAL24M2-03 - 1150 °C - 7day. (a) cross section at center. (b) top view slice at neck location.

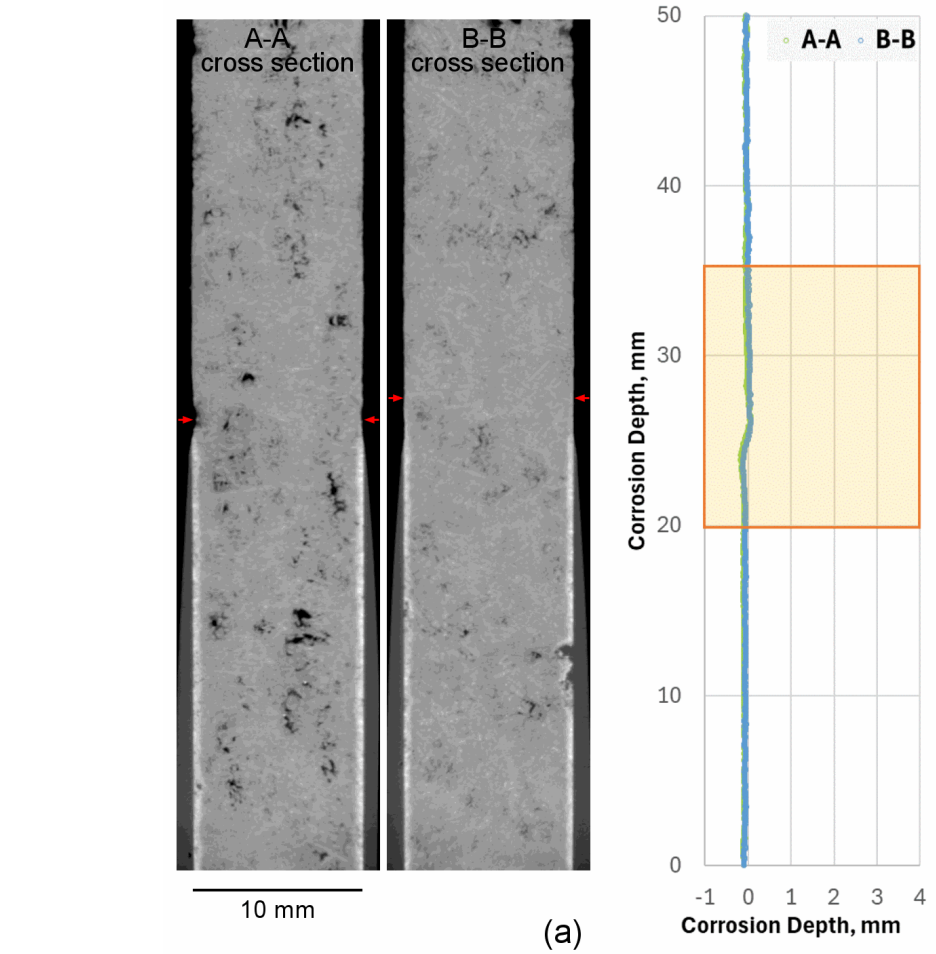

Neck Depth, mm	
A-A	0.08
B-B	0.08
Average	0.08
Standard deviation	0.000

Figure B.6. Micro-CT results of K-3 refractory corrosion test, HAL24M2-03 - 1200 °C - 7day. (a) cross section at center. (b) top view slice at neck location.

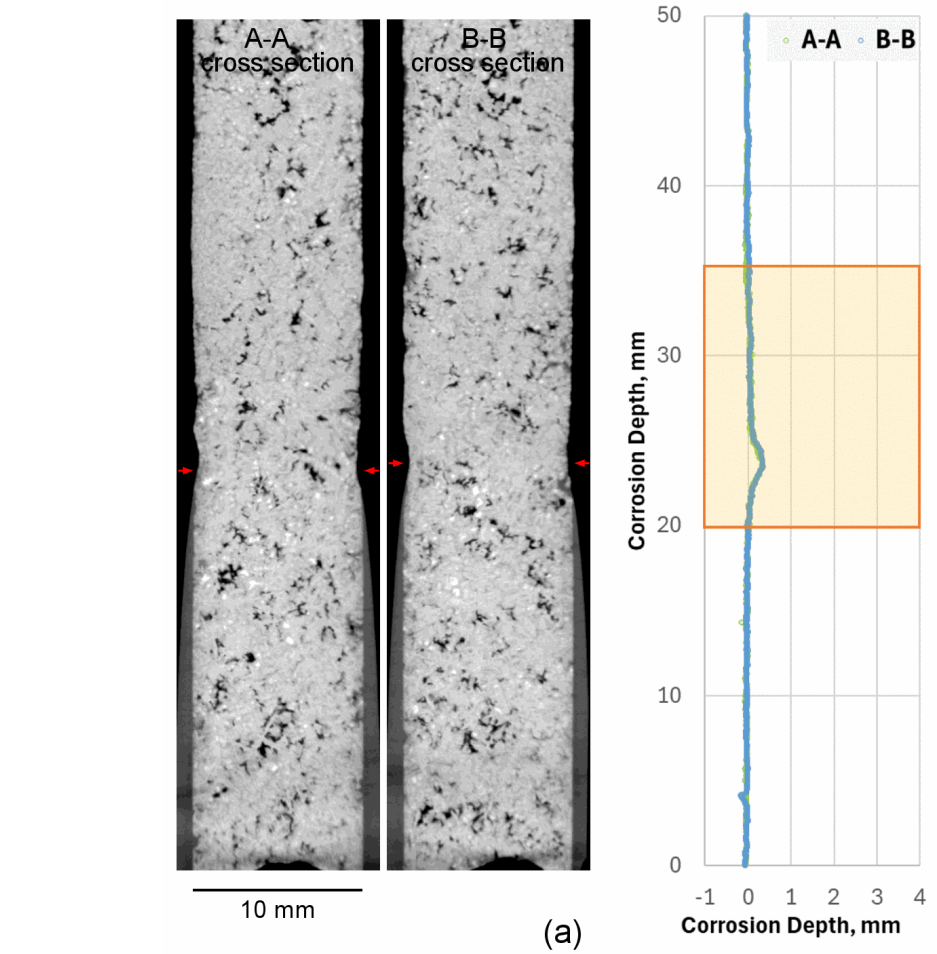

Neck Depth, mm	
A-A	0.36
B-B	0.34
Average	0.35
Standard deviation	0.014

Figure B.7. Micro-CT results of K-3 refractory corrosion test, HAL24M2-04 - 1150 °C - 7day. (a) cross section at center. (b) top view slice at neck location.

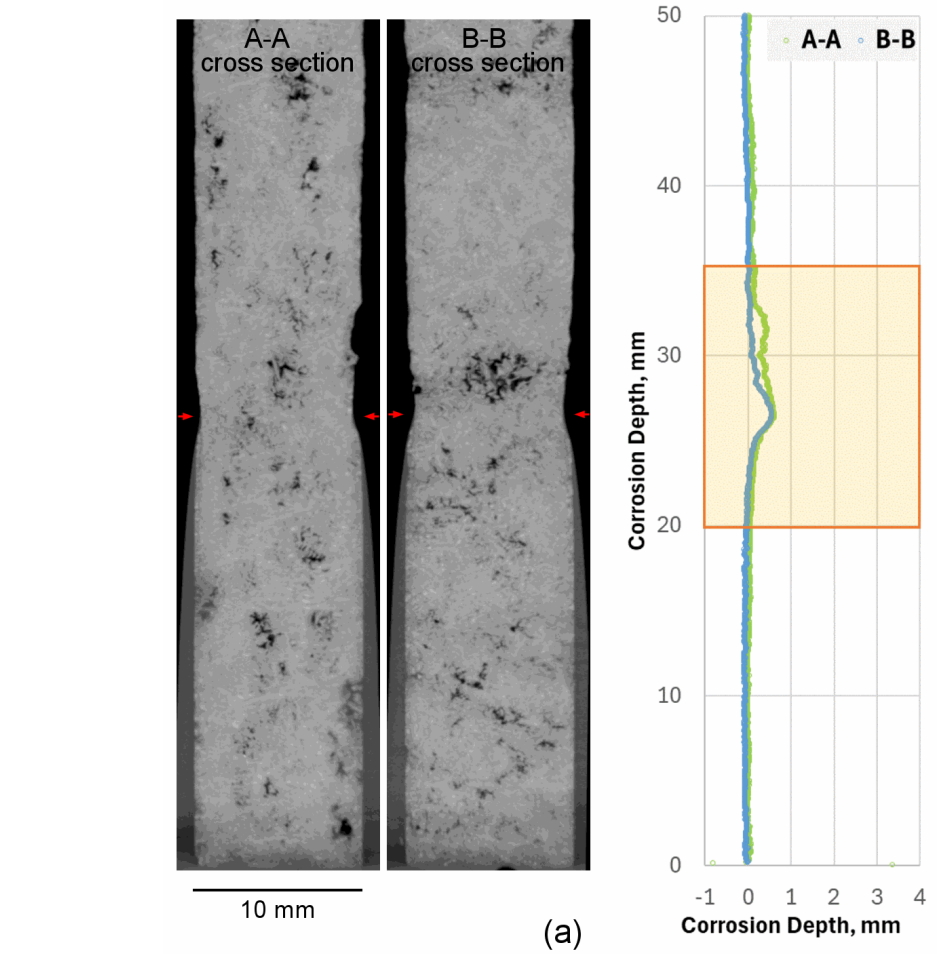

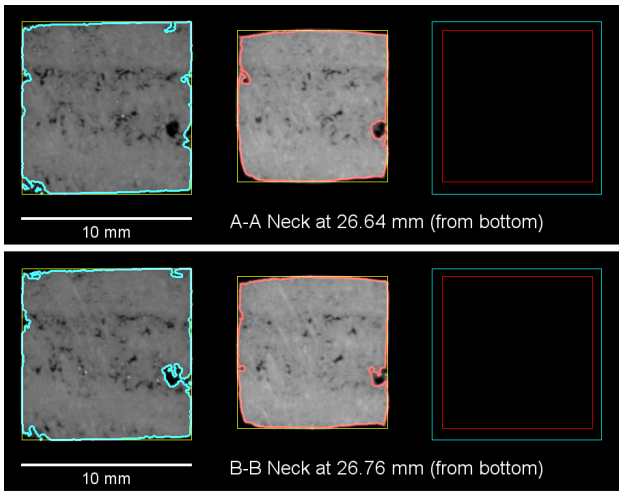

Neck Depth, mm	
A-A	0.62
B-B	0.56
Average	0.59
Standard deviation	0.042

Figure B.8. Micro-CT results of K-3 refractory corrosion test, HAL24M2-04 - 1200 °C - 7day. (a) cross section at center. (b) top view slice at neck location.

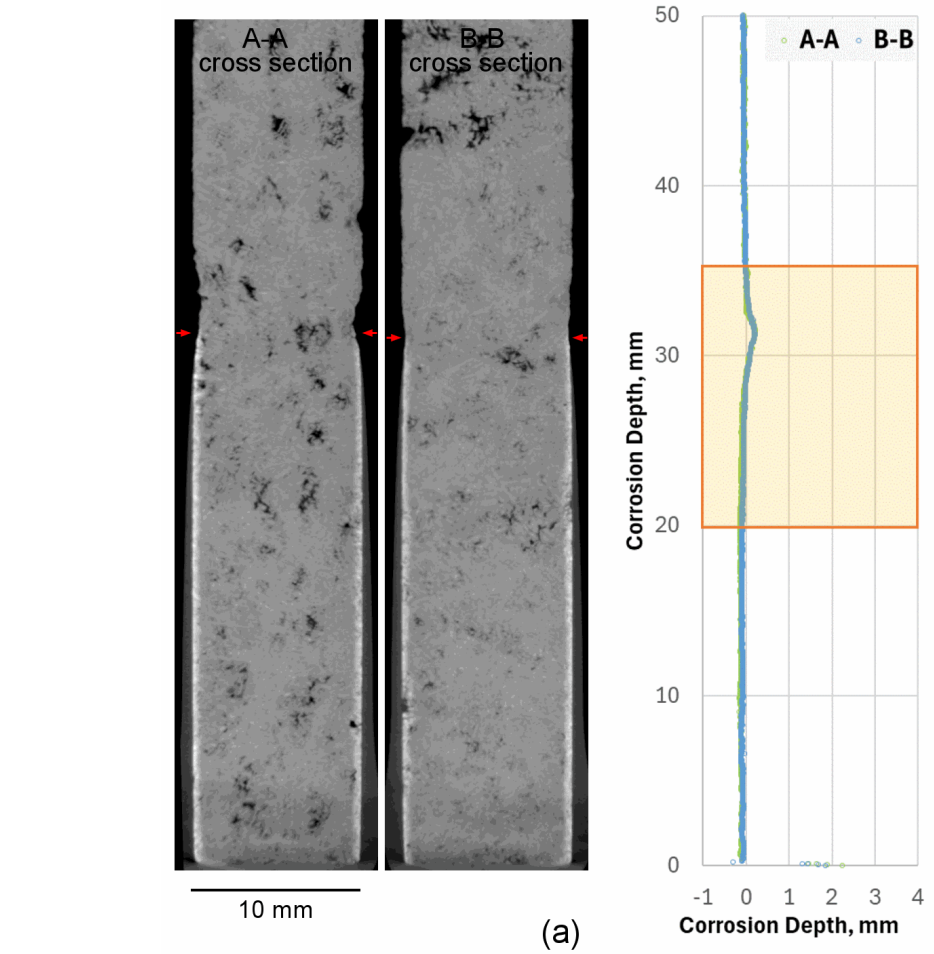

Neck Depth, mm	
A-A	0.22
B-B	0.22
Average	0.22
Standard deviation	0.000

Figure B.9. Micro-CT results of K-3 refractory corrosion test, HAL24M2-05 - 1150 °C - 7day. (a) cross section at center. (b) top view slice at neck location.

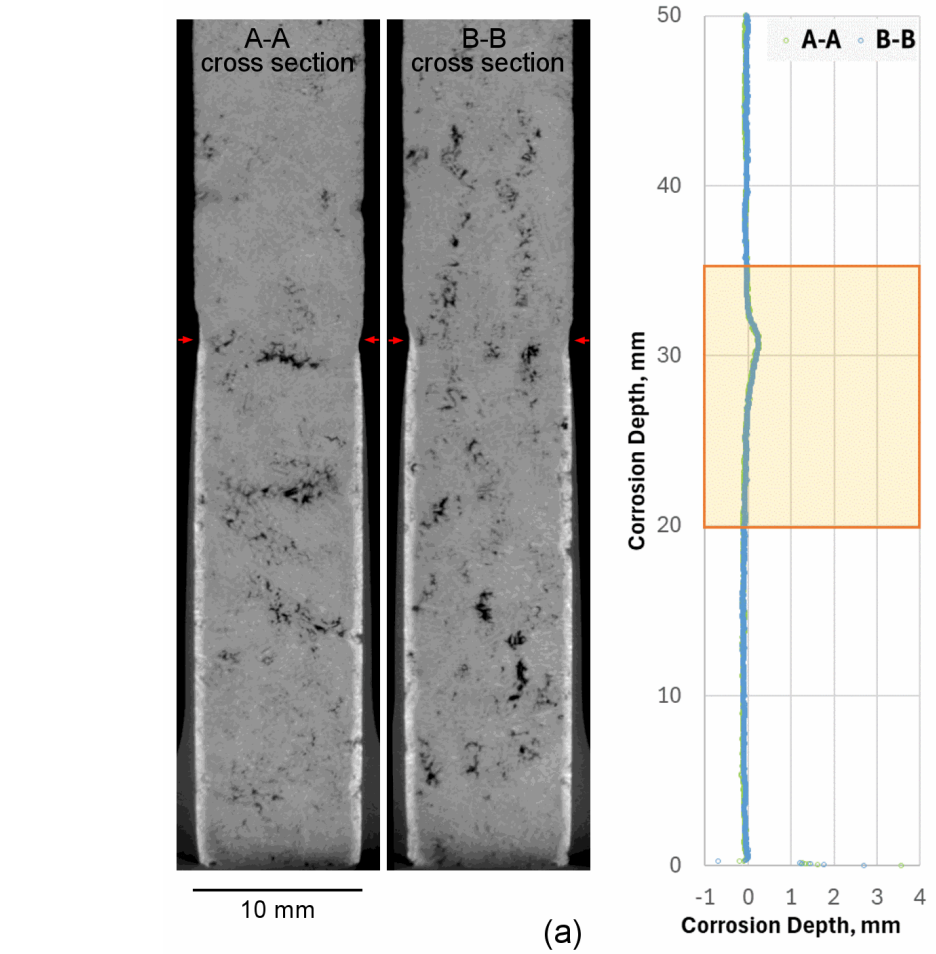

Neck Depth, mm	
A-A	0.26
B-B	0.24
Average	0.25
Standard deviation	0.014

Figure B.10. Micro-CT results of K-3 refractory corrosion test, HAL24M2-05 - 1200 °C - 7day. (a) cross section at center. (b) top view slice at neck location.

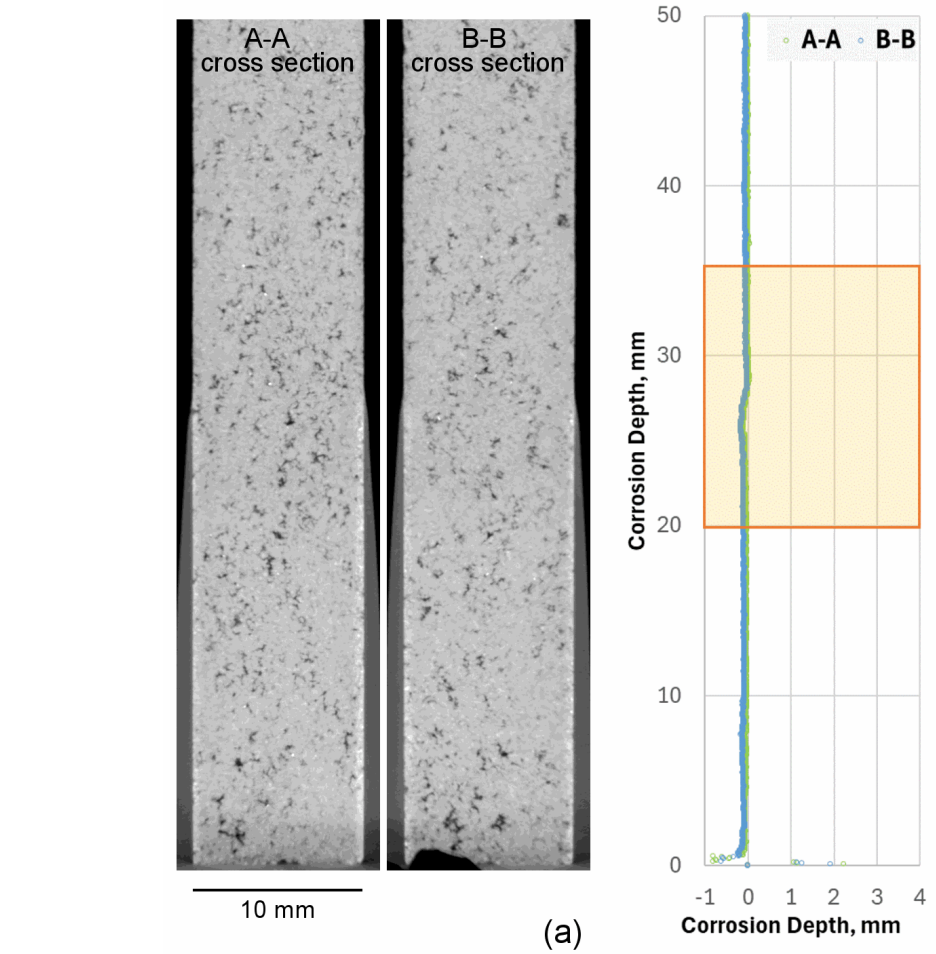

Neck Depth, mm	
A-A	0.04
B-B	0
Average	0.02
Standard deviation	0.028
Note: no clear neck. Heights of the x-y slices in (b) are random.	

Figure B.11. Micro-CT results of K-3 refractory corrosion test, HAL24M2-06 - 1150 °C - 7day. (a) cross section at center. (b) top view slice at neck location.

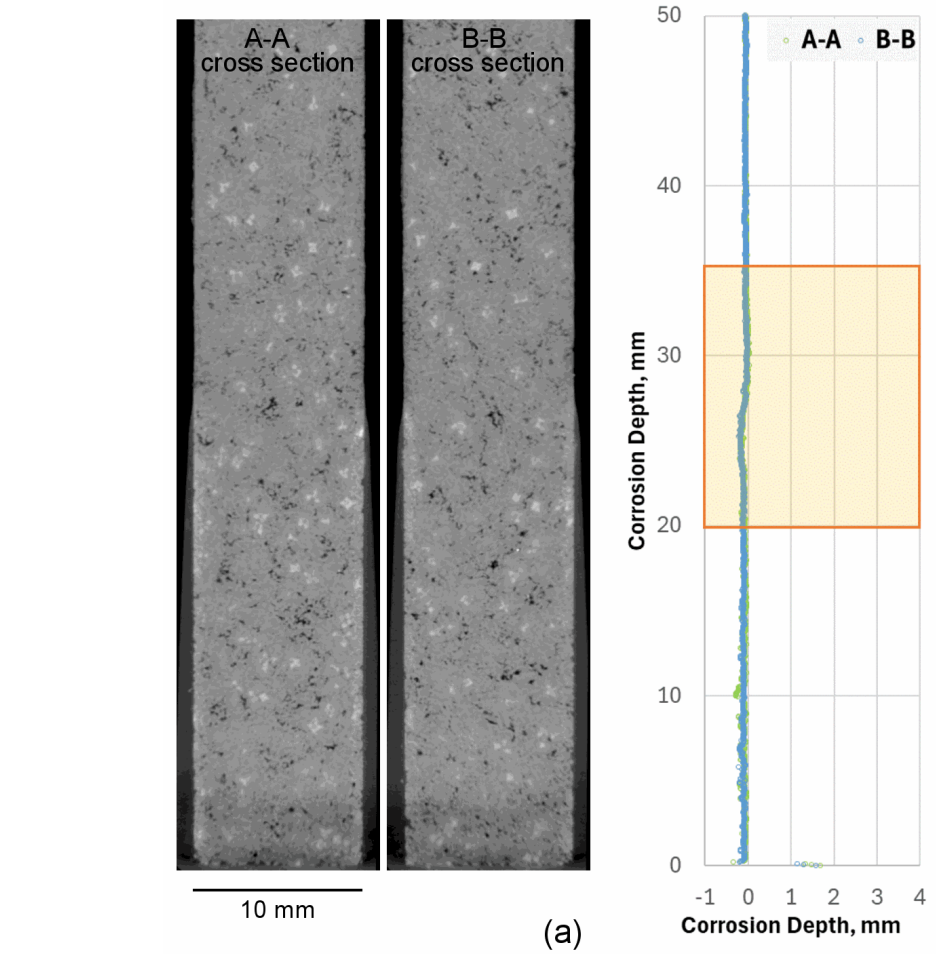

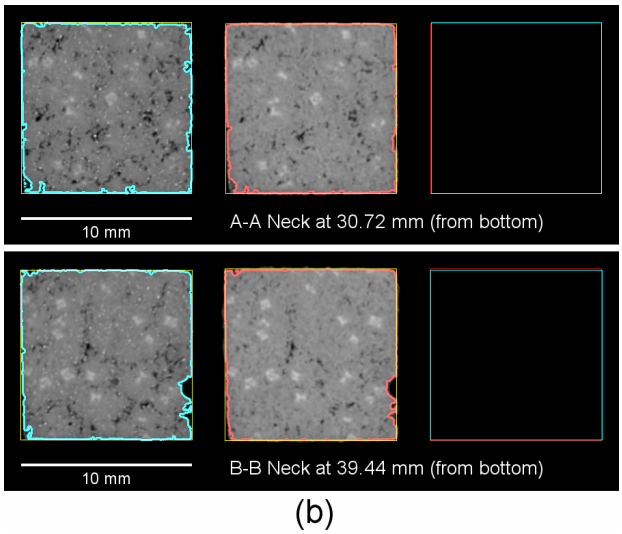

Neck Depth, mm	
A-A	0.04
B-B	0
Average	0.02
Standard deviation	0.028
Note: no clear neck. Heights of the x-y slices in (b) are random.	

Figure B.12. Micro-CT results of K-3 refractory corrosion test, HAL24M2-06 - 1200 °C - 7day. (a) cross section at center. (b) top view slice at neck location.

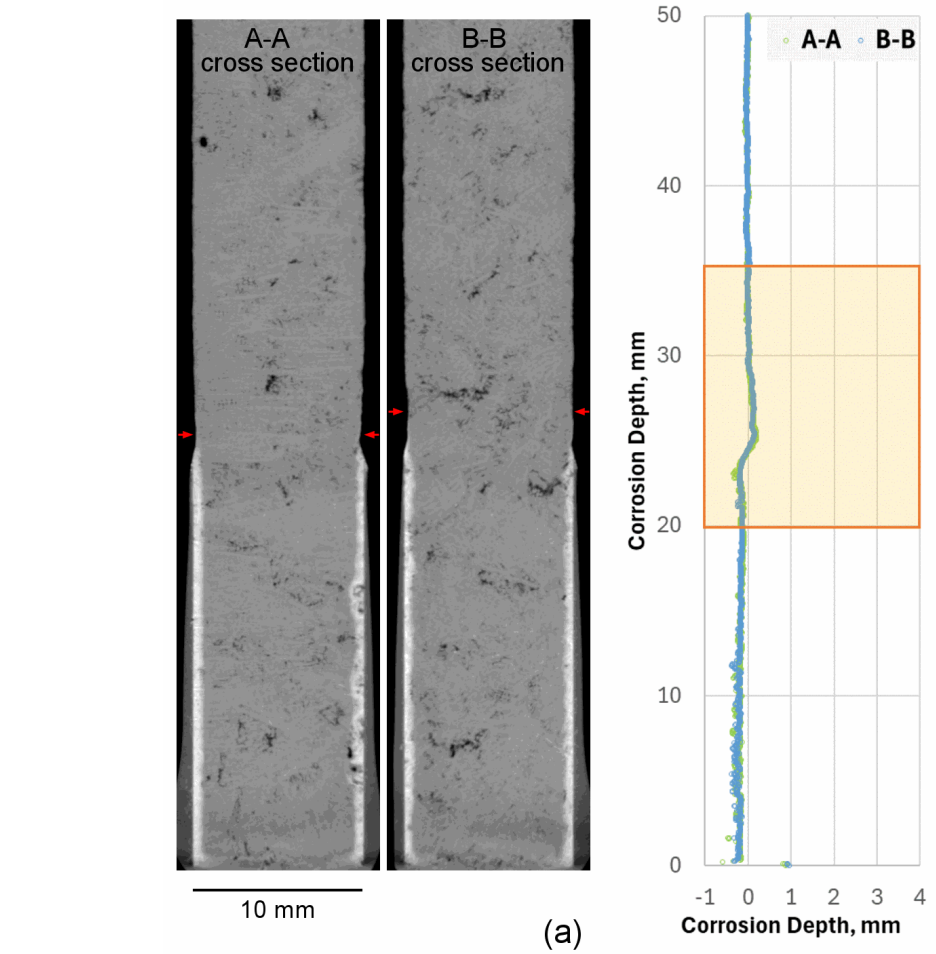

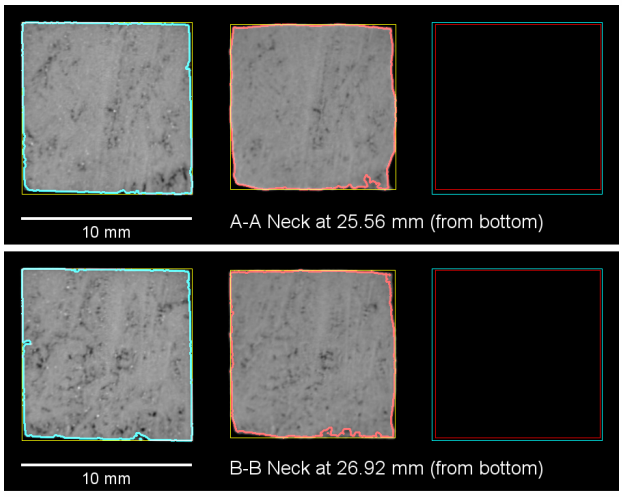

Neck Depth, mm	
A-A	0.2
B-B	0.16
Average	0.18
Standard deviation	0.028

Figure B.13. Micro-CT results of K-3 refractory corrosion test, HAL24M2-07 - 1150 °C - 7day. (a) cross section at center. (b) top view slice at neck location.

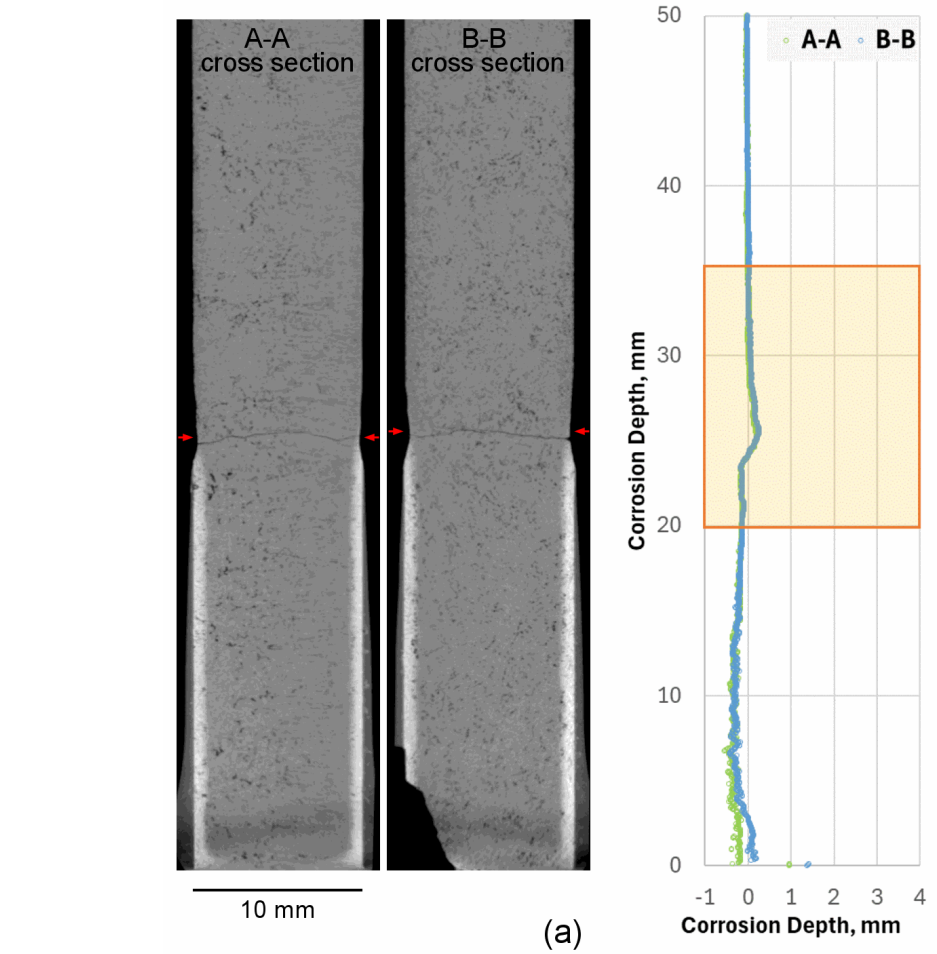

Neck Depth, mm	
A-A	0.22
B-B	0.26
Average	0.24
Standard deviation	0.028
Note: coupon broke at the neck; the crack did not affect measurement	

Figure B.14. Micro-CT results of K-3 refractory corrosion test, HAL24M2-07 - 1200 °C - 7day. (a) cross section at center. (b) top view slice at neck location.

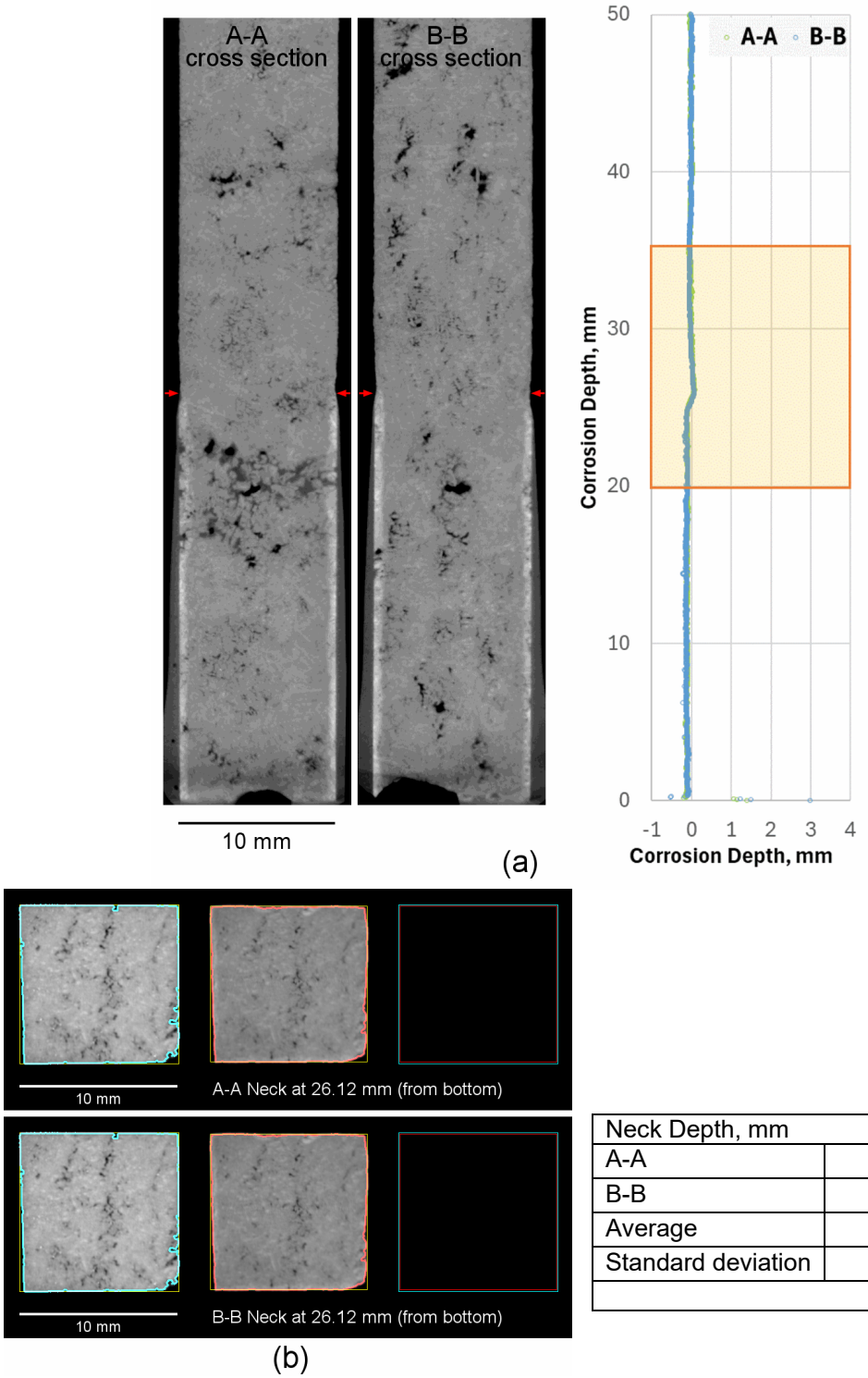

Neck Depth, mm	
A-A	0.1
B-B	0.08
Average	0.09
Standard deviation	0.014

Figure B.15. Micro-CT results of K-3 refractory corrosion test, HAL24M2-08 - 1150 °C - 7day. (a) cross section at center. (b) top view slice at neck location.

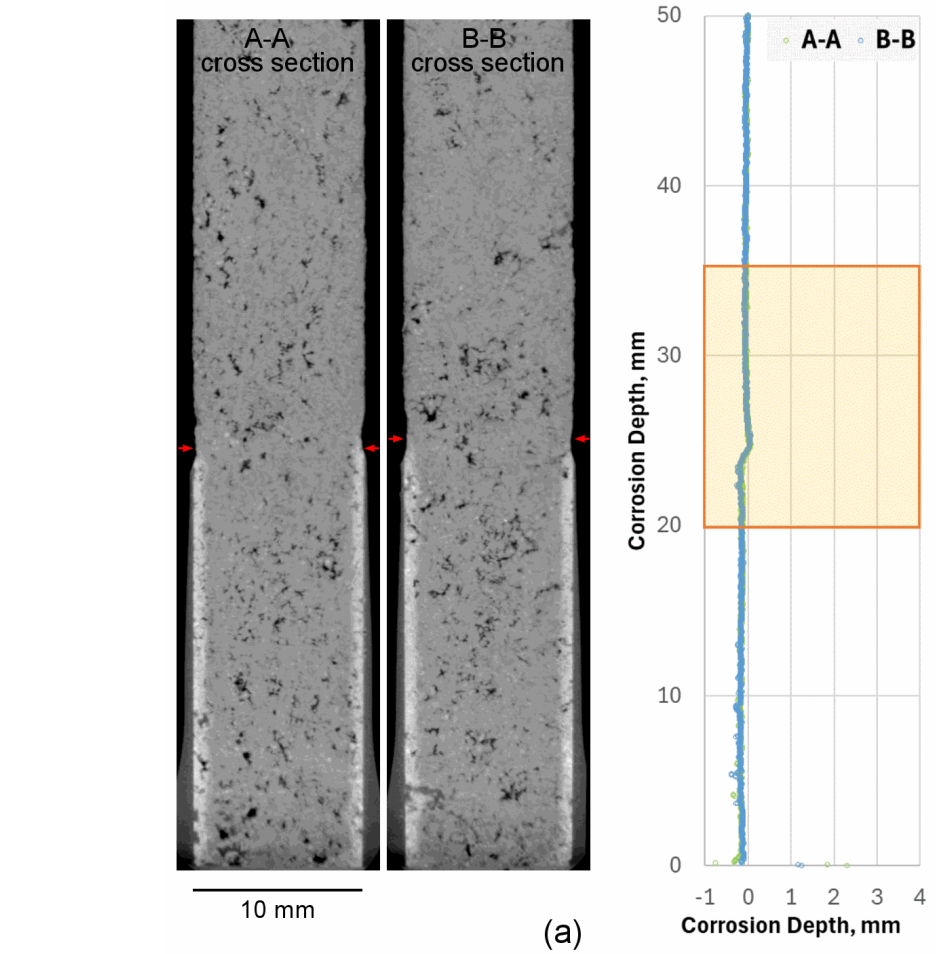

Neck Depth, mm	
A-A	0.08
B-B	0.08
Average	0.08
Standard deviation	0.000

Figure B.16. Micro-CT results of K-3 refractory corrosion test, HAL24M2-08 - 1200 °C - 7day. (a) cross section at center. (b) top view slice at neck location.

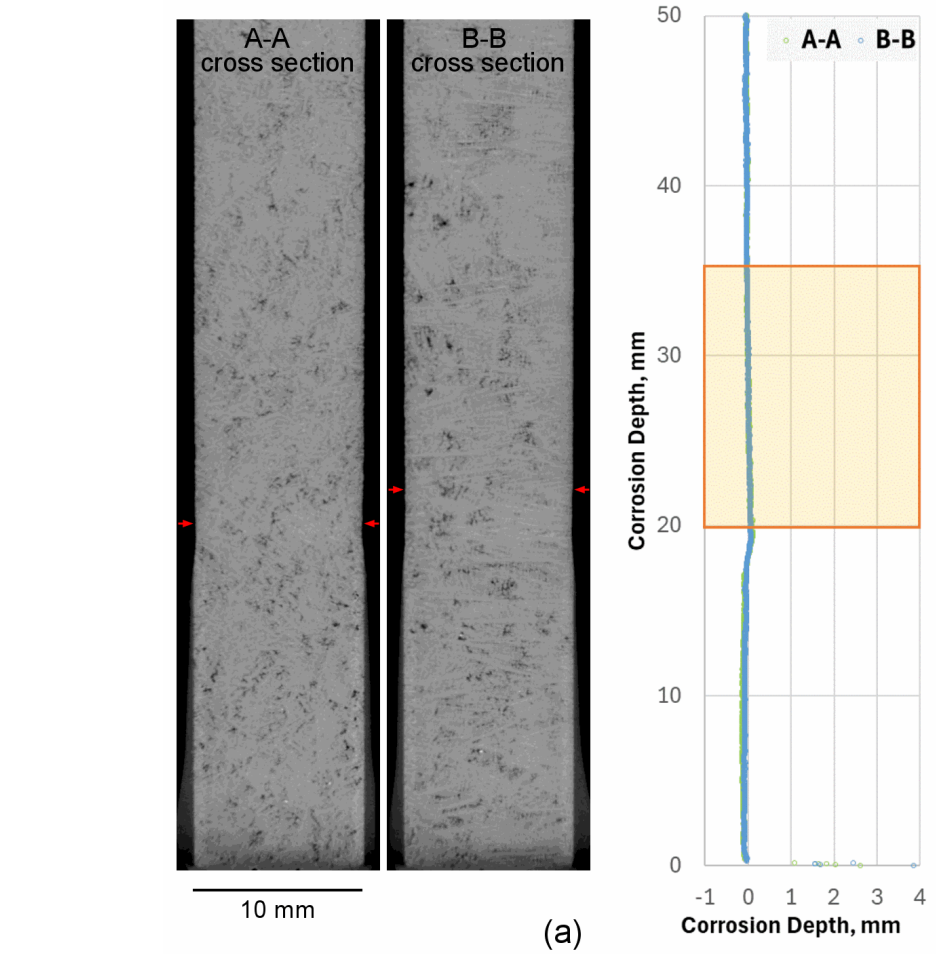

Neck Depth, mm	
A-A	0.12
B-B	0.08
Average	0.1
Standard deviation	0.028

Figure B.17. Micro-CT results of K-3 refractory corrosion test, HAL24M2-09 - 1150 °C - 7day. (a) cross section at center. (b) top view slice at neck location.

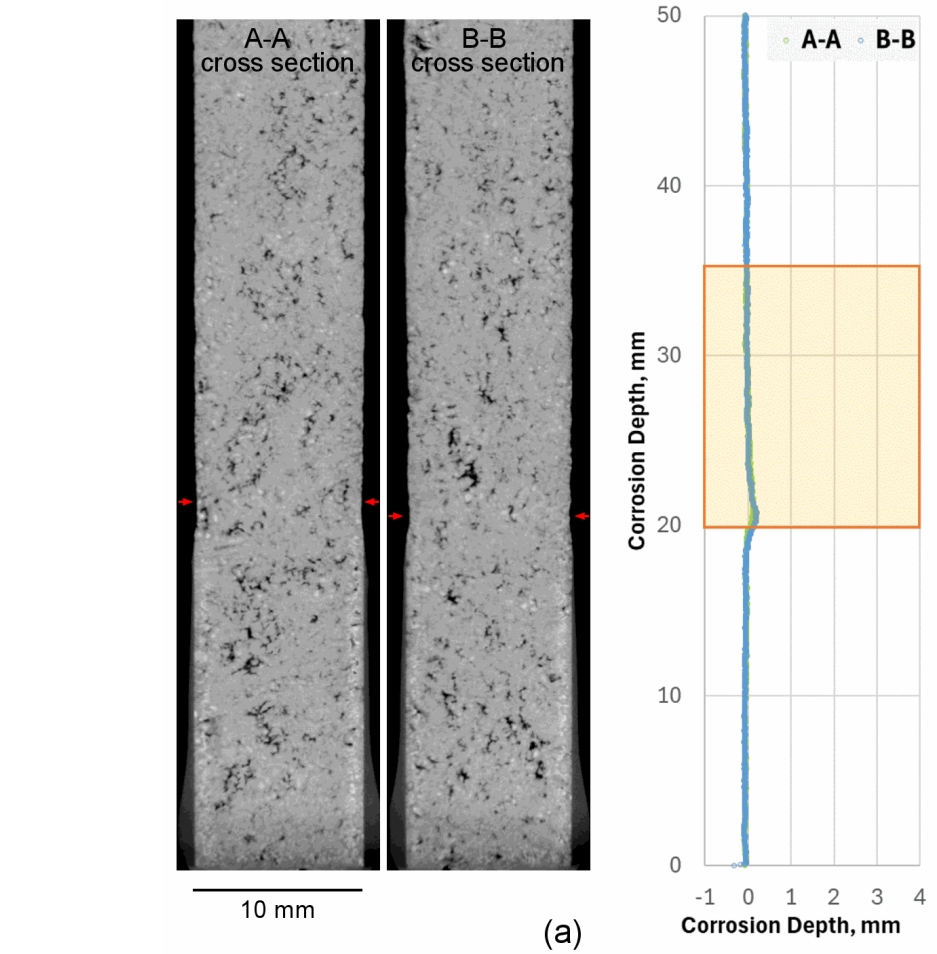

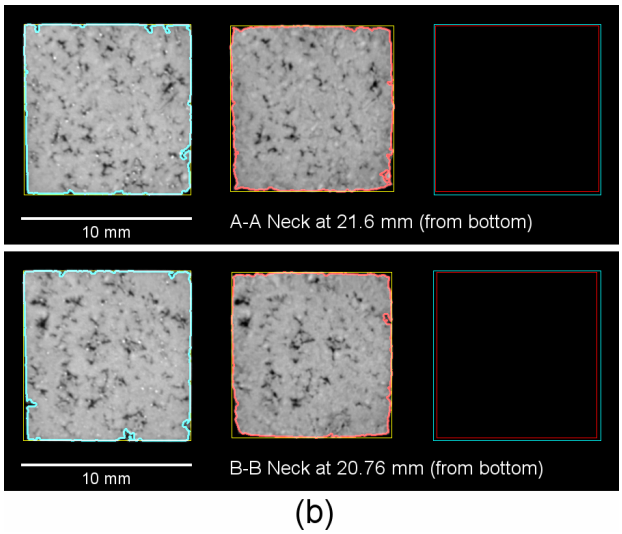

Neck Depth, mm	
A-A	0.14
B-B	0.22
Average	0.18
Standard deviation	0.057

Figure B.18. Micro-CT results of K-3 refractory corrosion test, HAL24M2-09 - 1200 °C - 7day. (a) cross section at center. (b) top view slice at neck location.

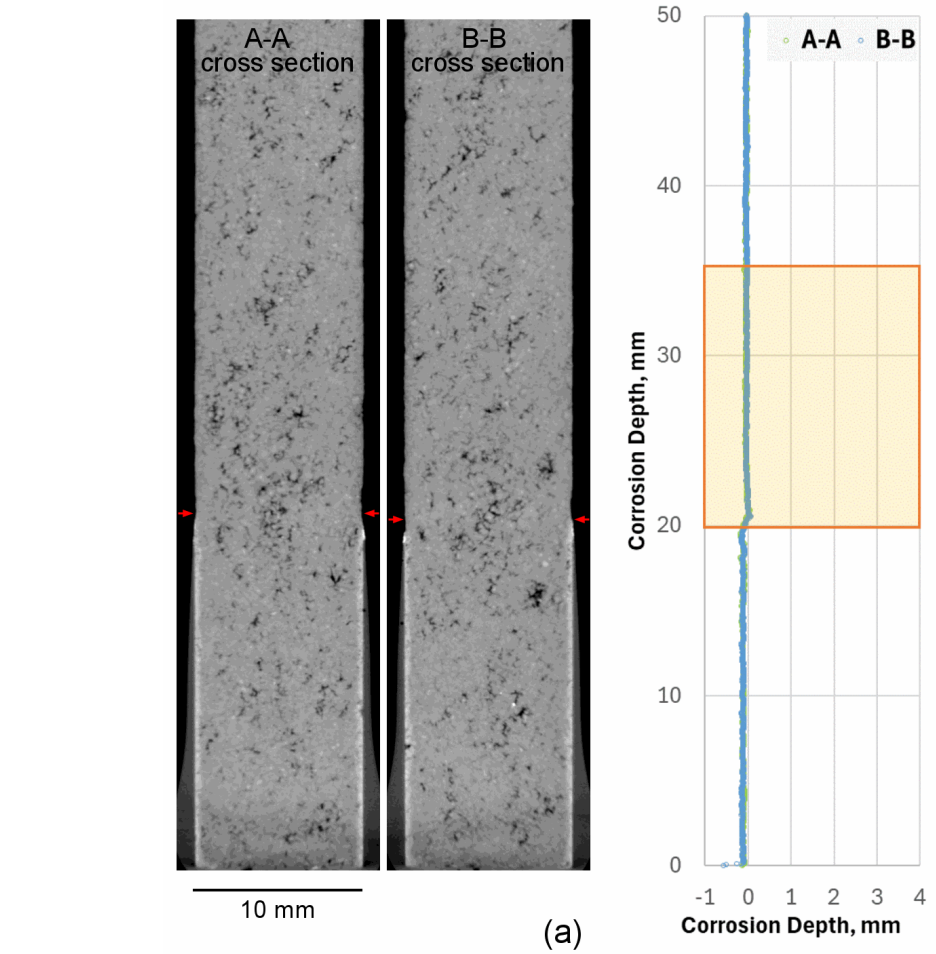

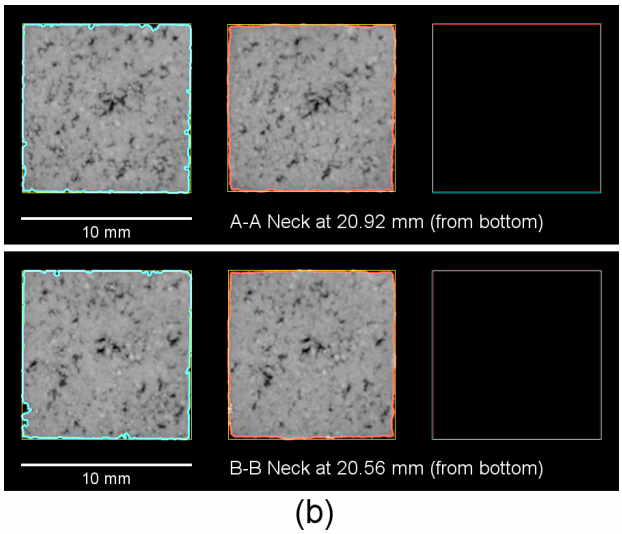

Neck Depth, mm	
A-A	0.06
B-B	0.08
Average	0.07
Standard deviation	0.014

Figure B.19. Micro-CT results of K-3 refractory corrosion test, HAL24M2-10 - 1150 °C - 7day. (a) cross section at center. (b) top view slice at neck location.

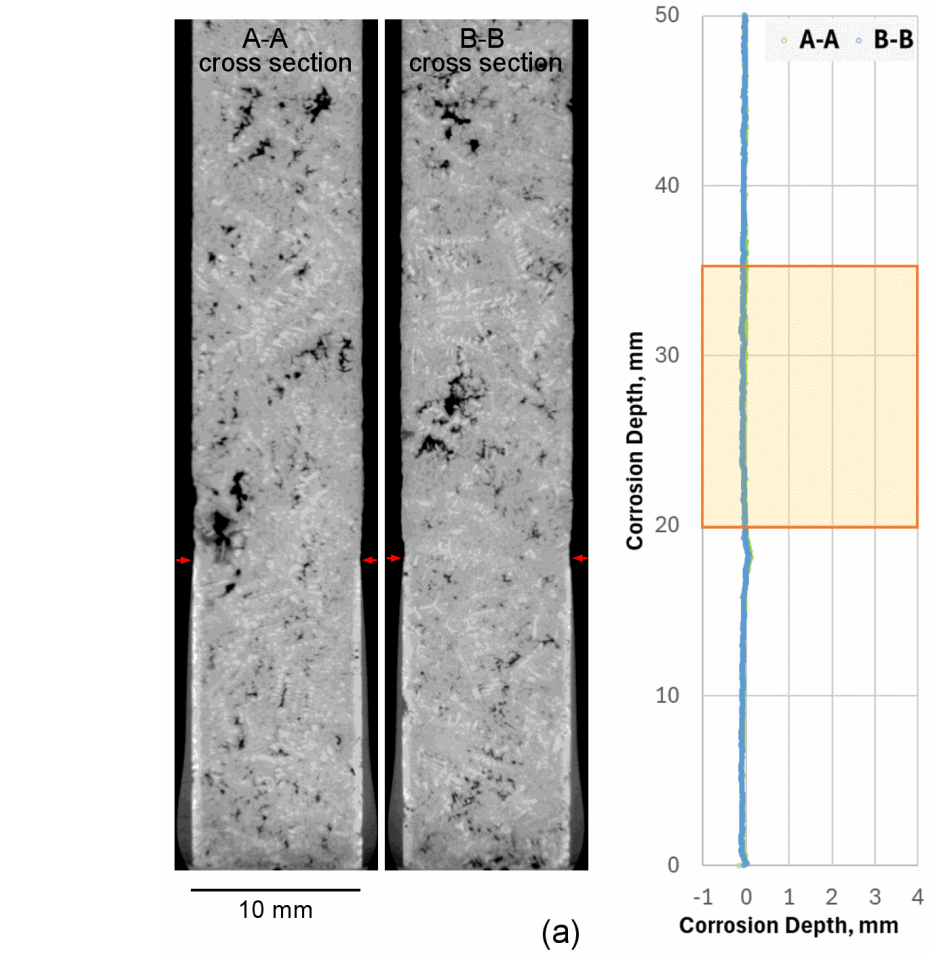

Neck Depth, mm	
A-A	0.12
B-B	0.08
Average	0.1
Standard deviation	0.028

Figure B.20. Micro-CT results of K-3 refractory corrosion test, HAL24M2-10 - 1200 °C - 7day. (a) cross section at center. (b) top view slice at neck location.

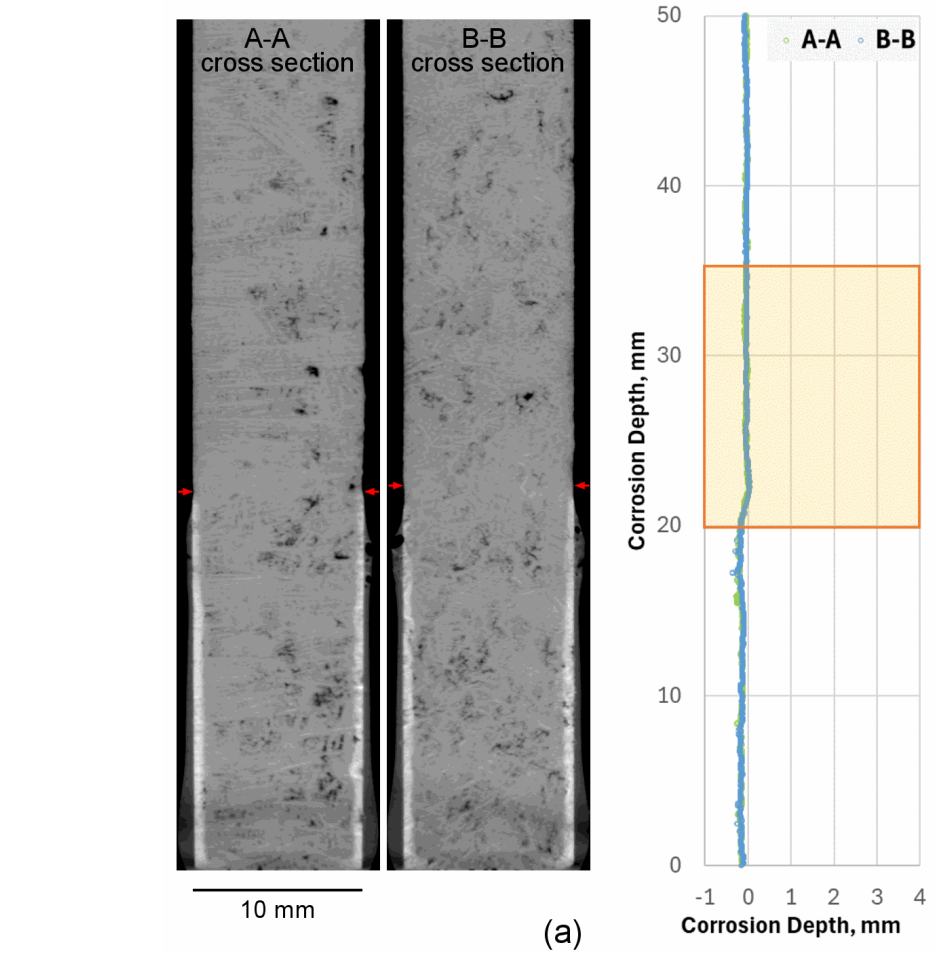

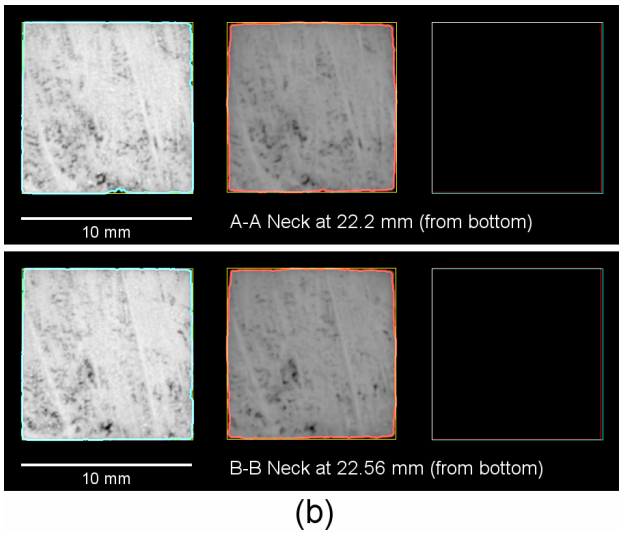

Neck Depth, mm	
A-A	0.04
B-B	0.06
Average	0.05
Standard deviation	0.014

Figure B.21. Micro-CT results of K-3 refractory corrosion test, HAL24M2-11 - 1150 °C - 7day. (a) cross section at center. (b) top view slice at neck location.

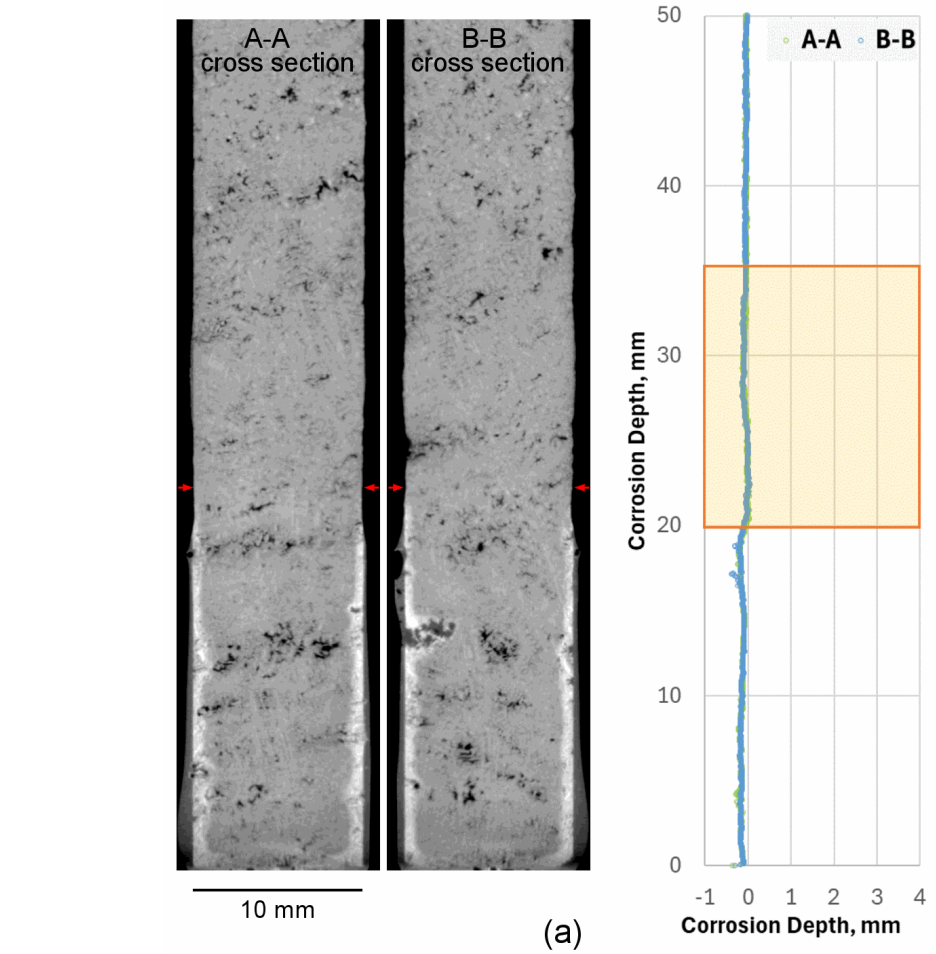

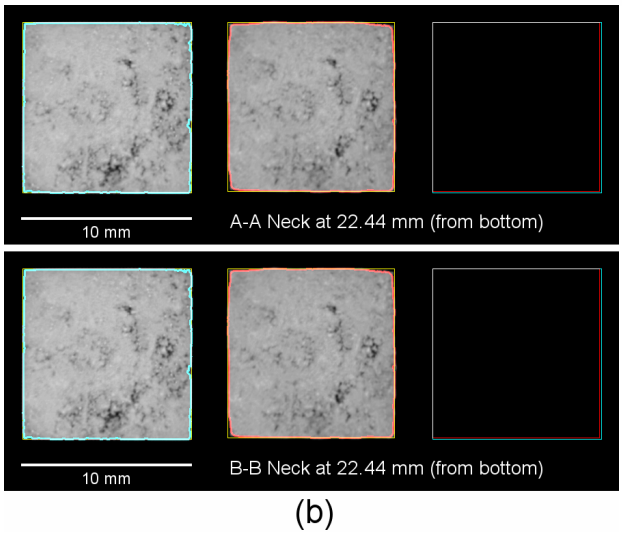

Neck Depth, mm	
A-A	0.04
B-B	0.06
Average	0.05
Standard deviation	0.014

Figure B.22. Micro-CT results of K-3 refractory corrosion test, HAL24M2-11 - 1200 °C - 7day. (a) cross section at center. (b) top view slice at neck location.

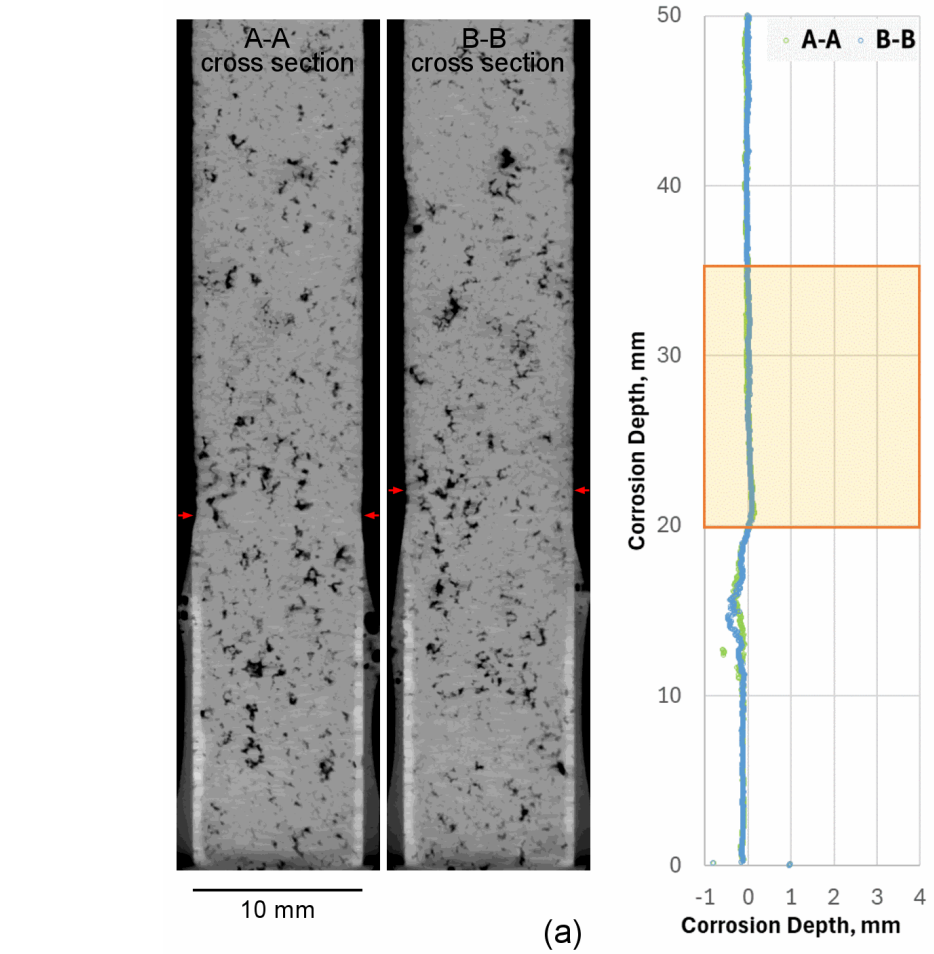

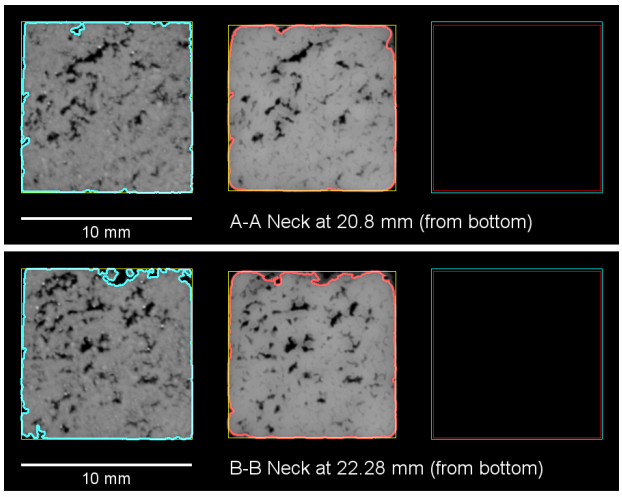

Neck Depth, mm	
A-A	0.16
B-B	0.1
Average	0.13
Standard deviation	0.042

Figure B.23. Micro-CT results of K-3 refractory corrosion test, HAL24M2-12 - 1150 °C - 7day. (a) cross section at center. (b) top view slice at neck location.

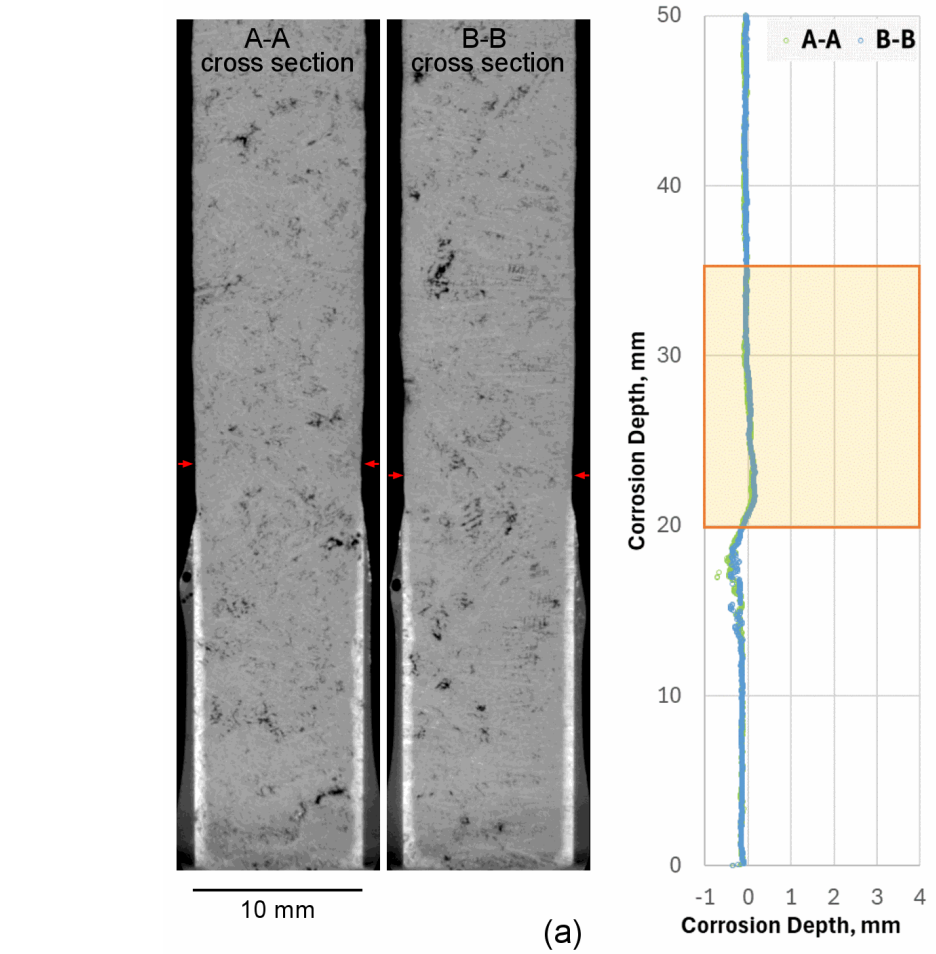

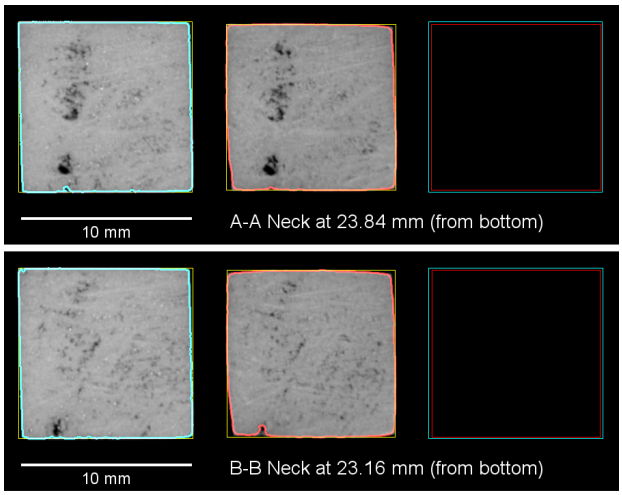

Neck Depth, mm	
A-A	0.14
B-B	0.18
Average	0.16
Standard deviation	0.028

Figure B.24. Micro-CT results of K-3 refractory corrosion test, HAL24M2-12 - 1200 °C - 7day. (a) cross section at center. (b) top view slice at neck location.

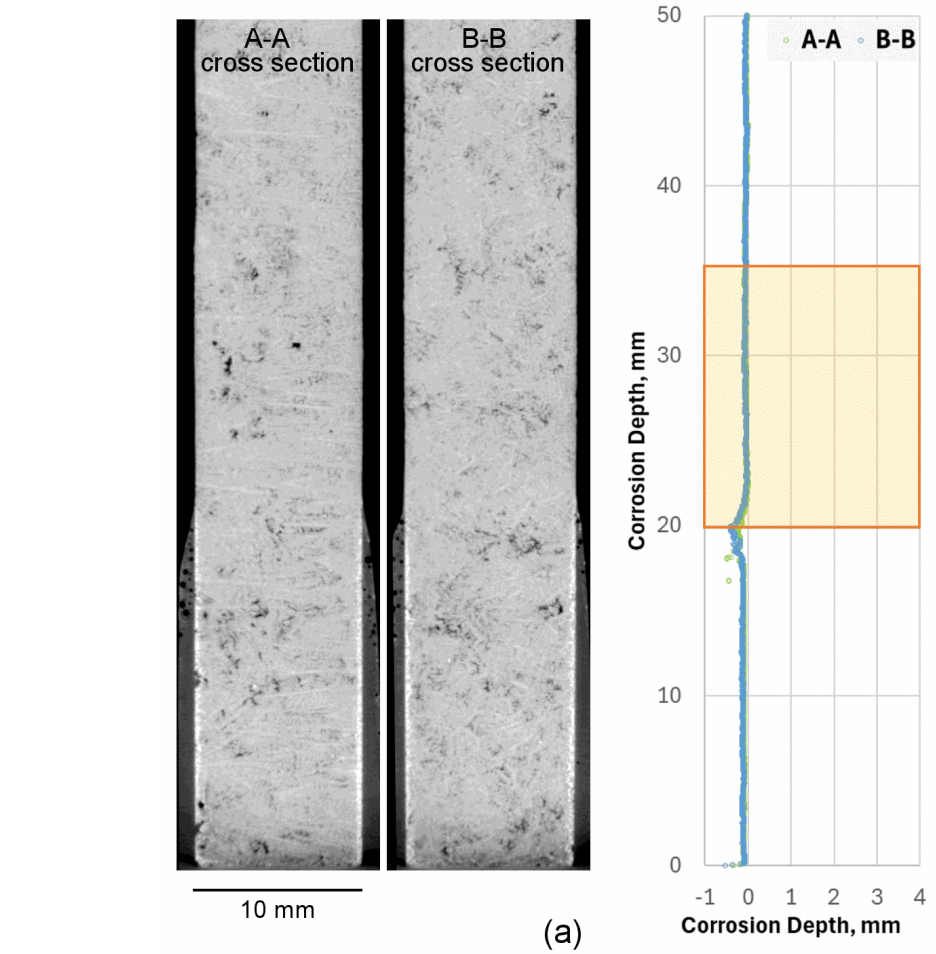

Neck Depth, mm	
A-A	0.02
B-B	0
Average	0.01
Standard deviation	0.014
Note: no clear neck. Heights of the x-y slices in (b) are random.	

Figure B.25. Micro-CT results of K-3 refractory corrosion test, HAL24M2-13 - 1150 °C - 7day. (a) cross section at center. (b) top view slice at neck location.

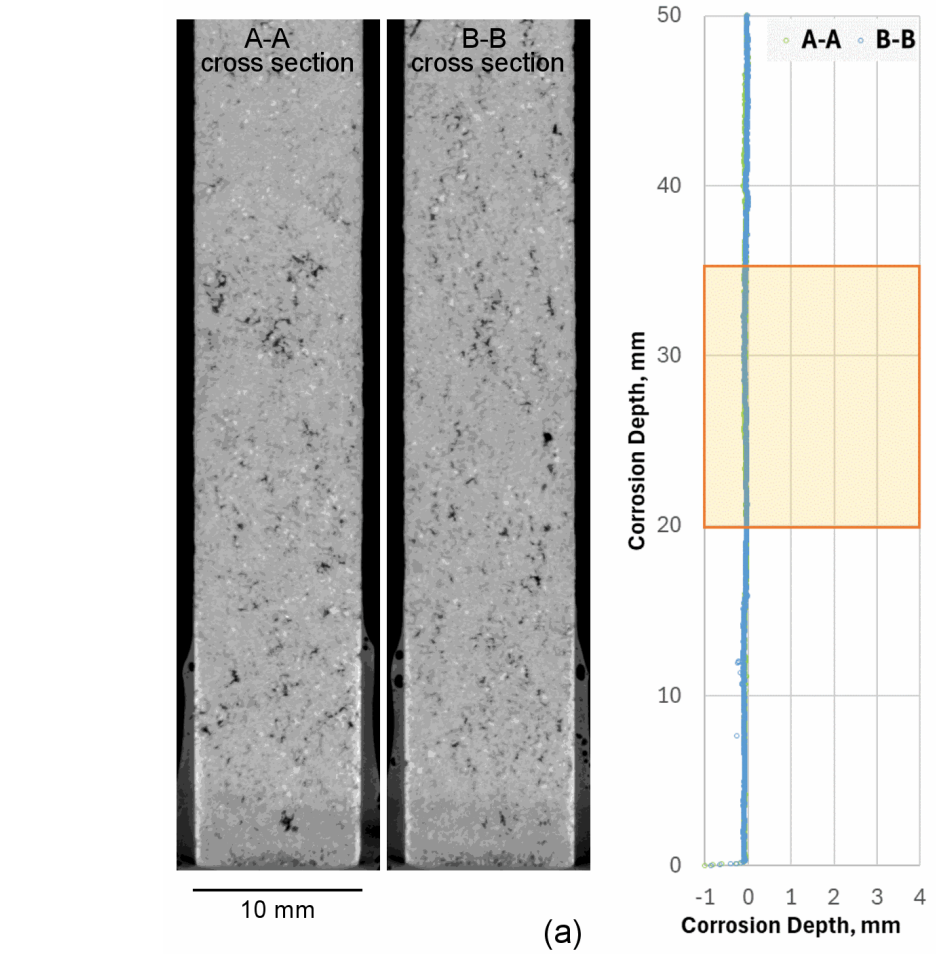

Neck Depth, mm	
A-A	-0.02
B-B	0.02
Average	0
Standard deviation	0.028
Note: no clear neck. Heights of the x-y slices in (b) are random.	

Figure B.26. Micro-CT results of K-3 refractory corrosion test, HAL24M2-13 - 1200 °C - 7day. (a) cross section at center. (b) top view slice at neck location.

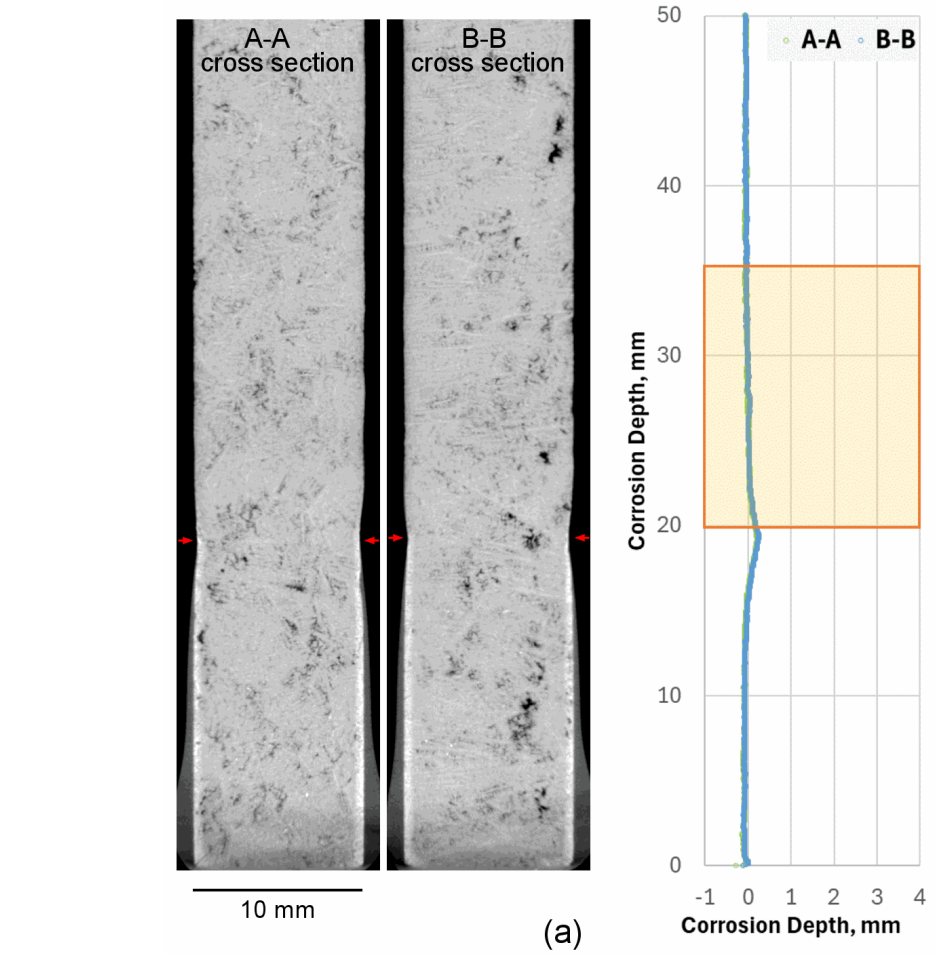

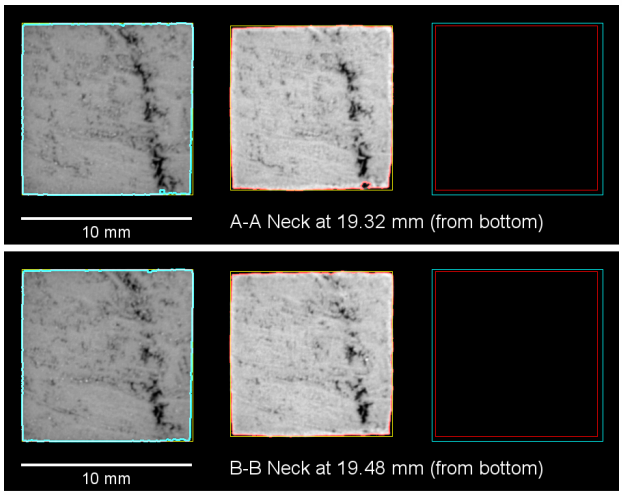

Neck Depth, mm	
A-A	0.22
B-B	0.26
Average	0.24
Standard deviation	0.028

Figure B.27. Micro-CT results of K-3 refractory corrosion test, HAL24M2-14 - 1150 °C - 7day. (a) cross section at center. (b) top view slice at neck location.

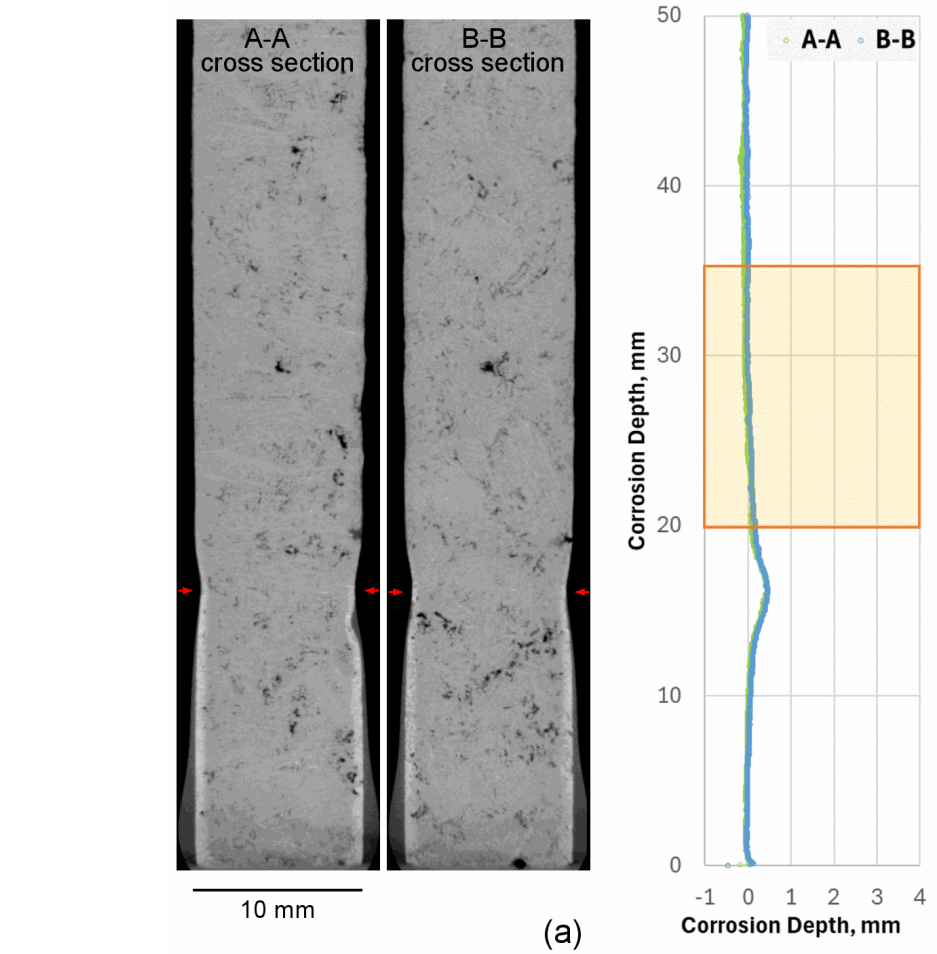

Neck Depth, mm	
A-A	0.48
B-B	0.48
Average	0.48
Standard deviation	0.000
Note: the neck is lower, out of the 20-35 mm range, which should be caused by glass amount and crucible shape.	

Figure B.28. Micro-CT results of K-3 refractory corrosion test, HAL24M2-14 - 1200 °C - 7day. (a) cross section at center. (b) top view slice at neck location.

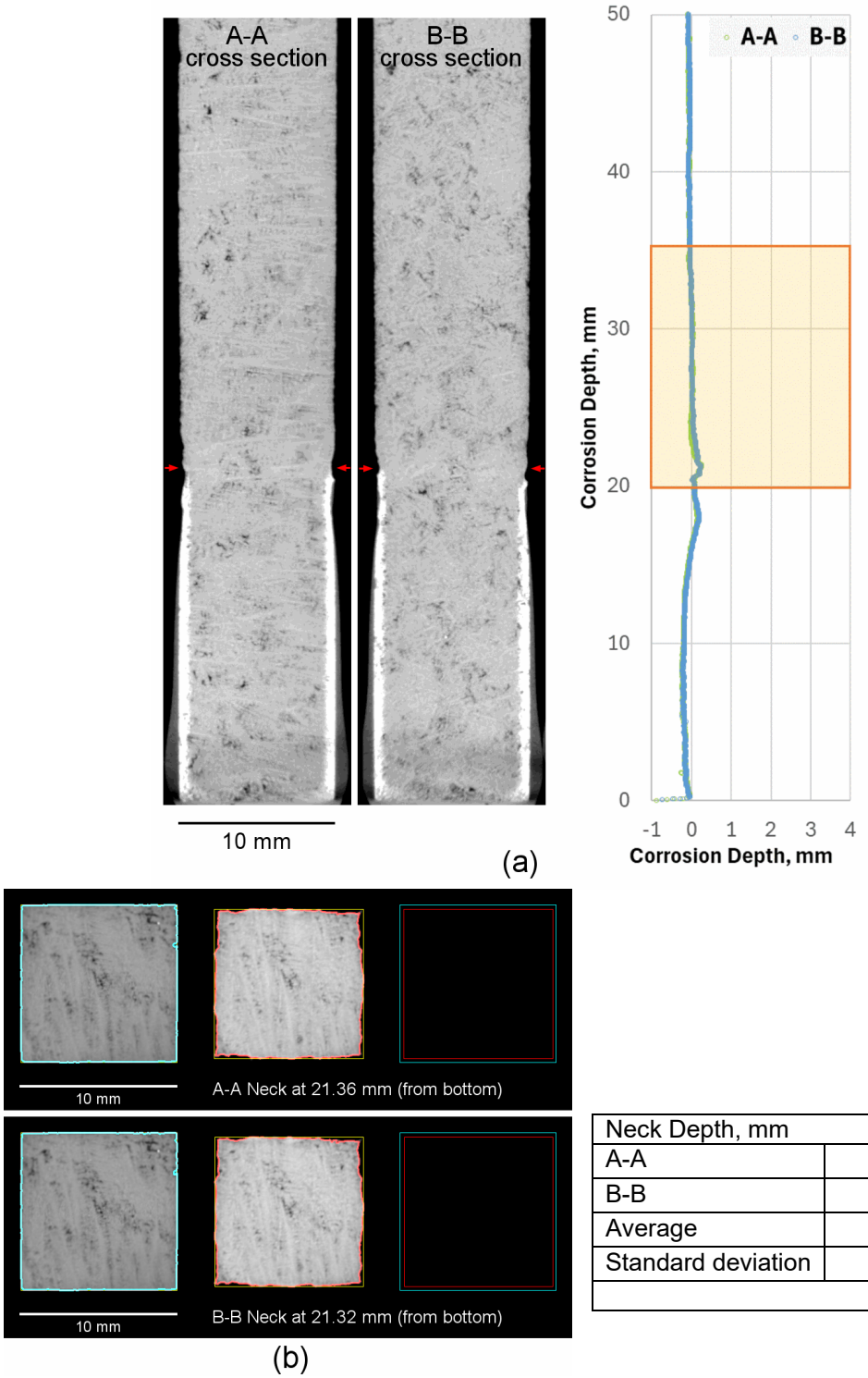

Neck Depth, mm	
A-A	0.26
B-B	0.24
Average	0.25
Standard deviation	0.014

Figure B.29. Micro-CT results of K-3 refractory corrosion test, HAL24M2-15 - 1150 °C - 7day. (a) cross section at center. (b) top view slice at neck location.

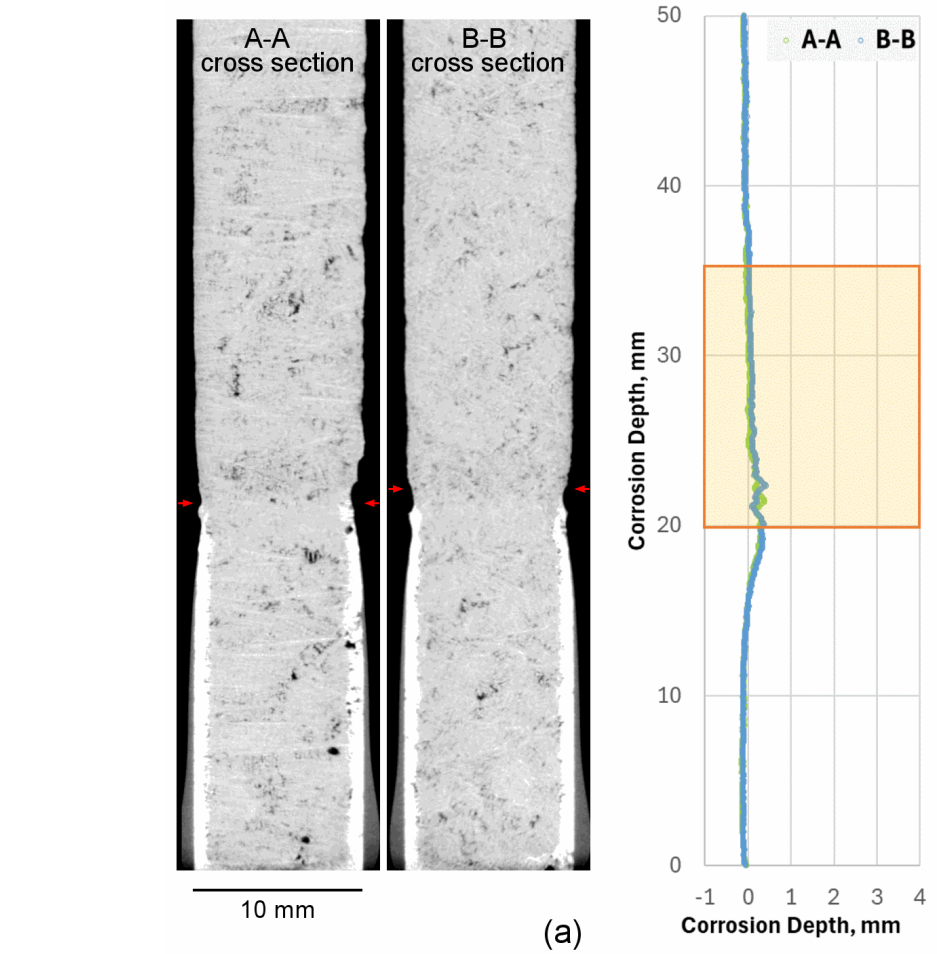

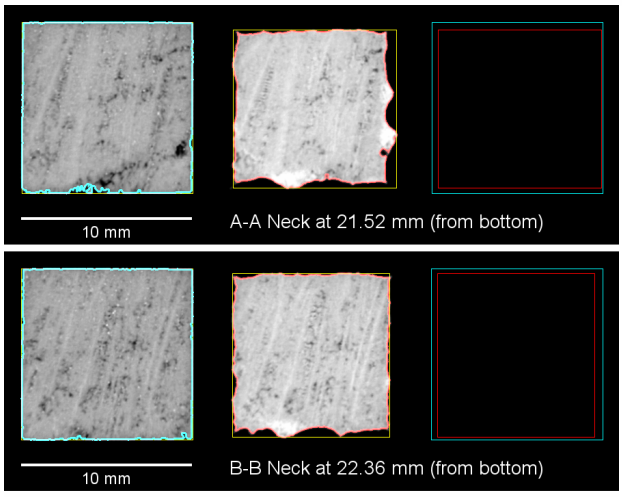

Neck Depth, mm	
A-A	0.38
B-B	0.42
Average	0.4
Standard deviation	0.028

Figure B.30. Micro-CT results of K-3 refractory corrosion test, HAL24M2-15 - 1200 °C - 7day. (a) cross section at center. (b) top view slice at neck location.

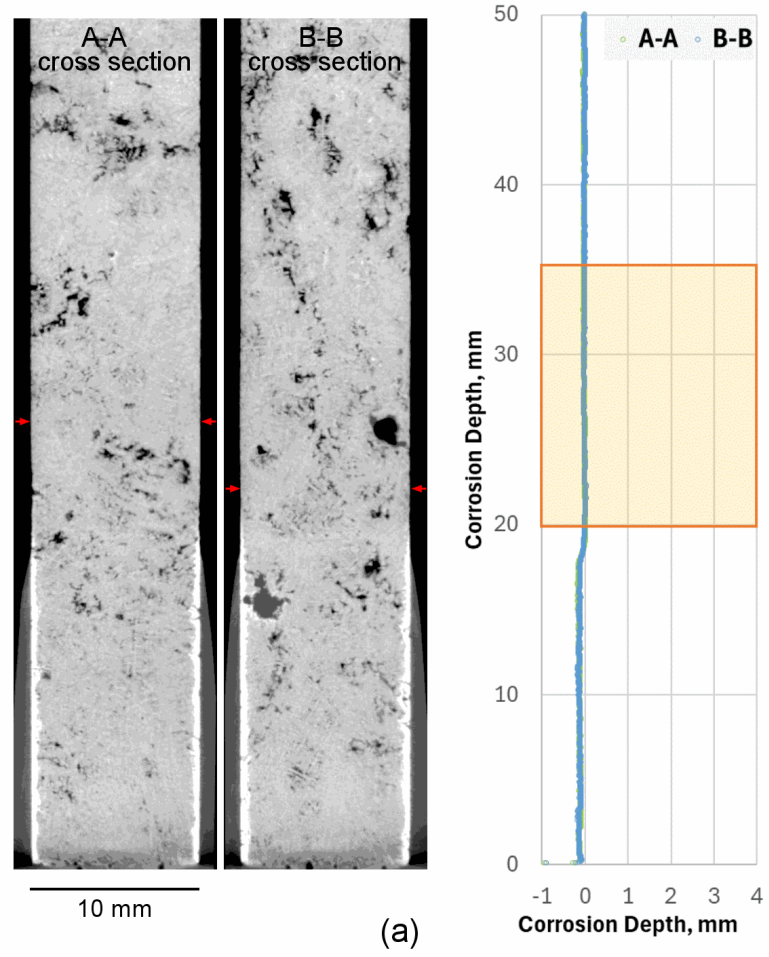

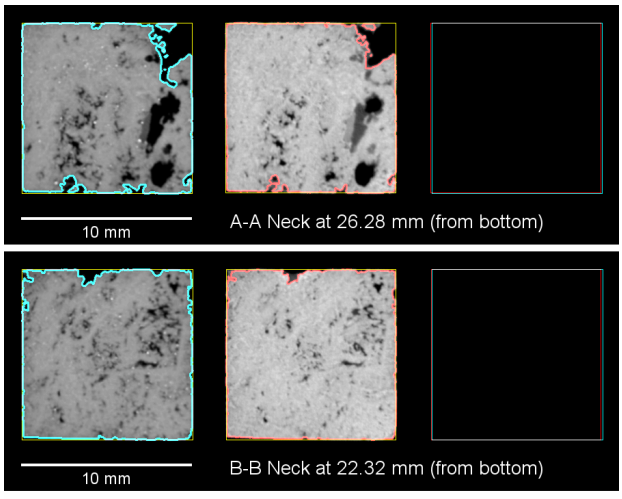

Neck Depth, mm	
A-A	0.02
B-B	0.04
Average	0.03
Standard deviation	0.014

Figure B.31. Micro-CT results of K-3 refractory corrosion test, HAL24M2-16 - 1150 °C - 7day. (a) cross section at center. (b) top view slice at neck location.

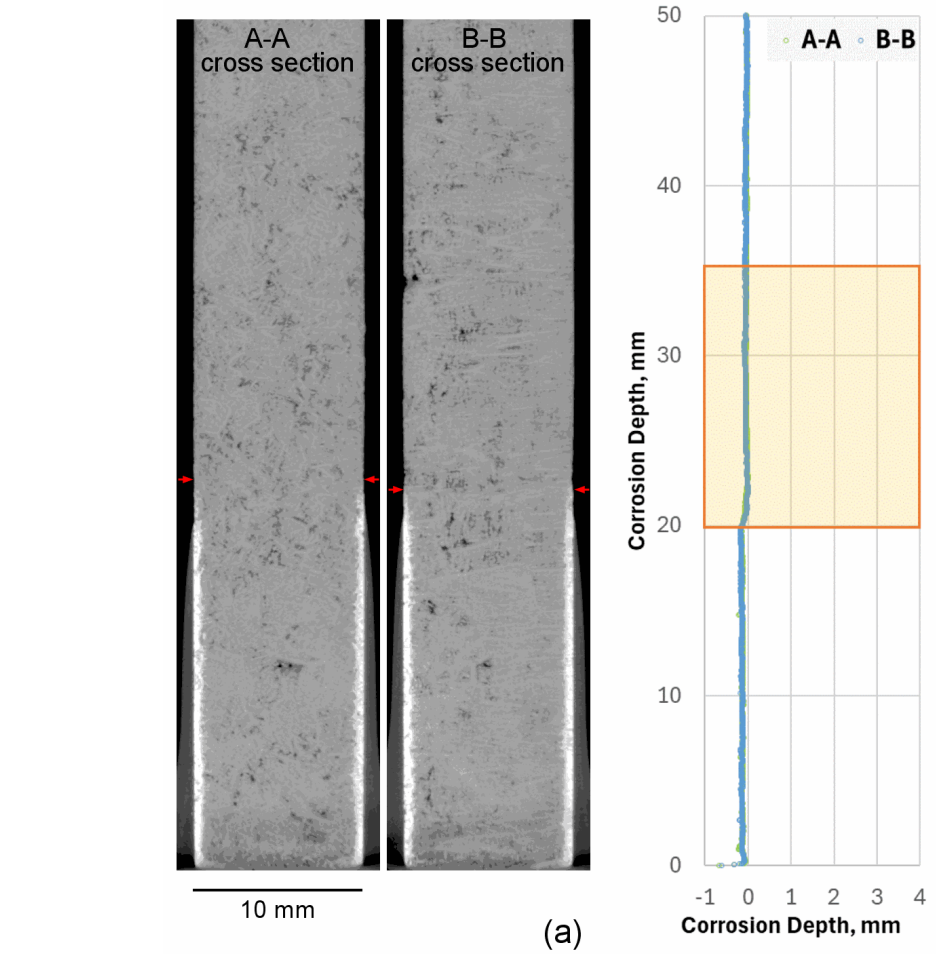

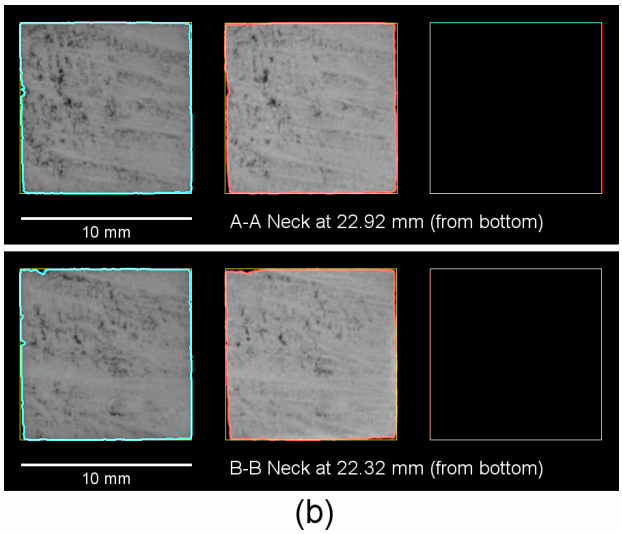

Neck Depth, mm	
A-A	0.02
B-B	0.02
Average	0.02
Standard deviation	0.000

Figure B.32. Micro-CT results of K-3 refractory corrosion test, HAL24M2-16 - 1200 °C - 7day. (a) cross section at center. (b) top view slice at neck location.

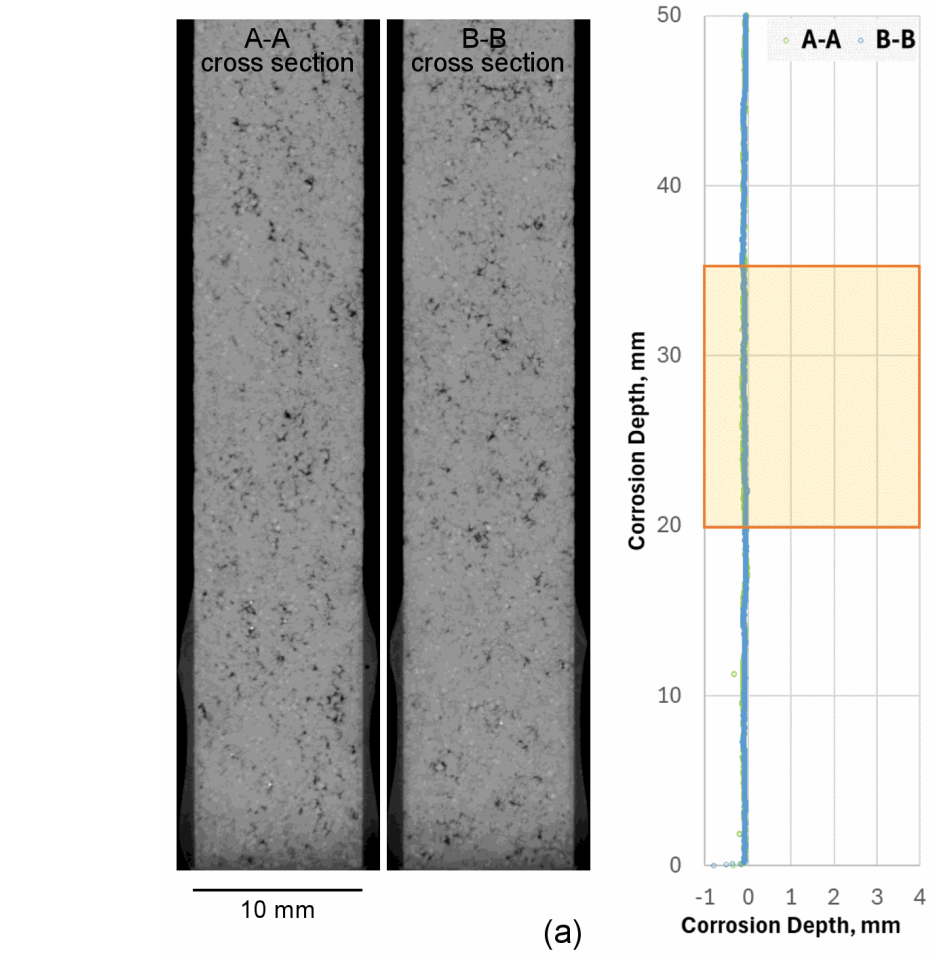

Neck Depth, mm	
A-A	0
B-B	0
Average	0
Standard deviation	0.000
Note: no clear neck. Heights of the x-y slices in (b) are random.	

Figure B.33. Micro-CT results of K-3 refractory corrosion test, HAL24M2-17 - 1150 °C - 7day. (a) cross section at center. (b) top view slice at neck location.

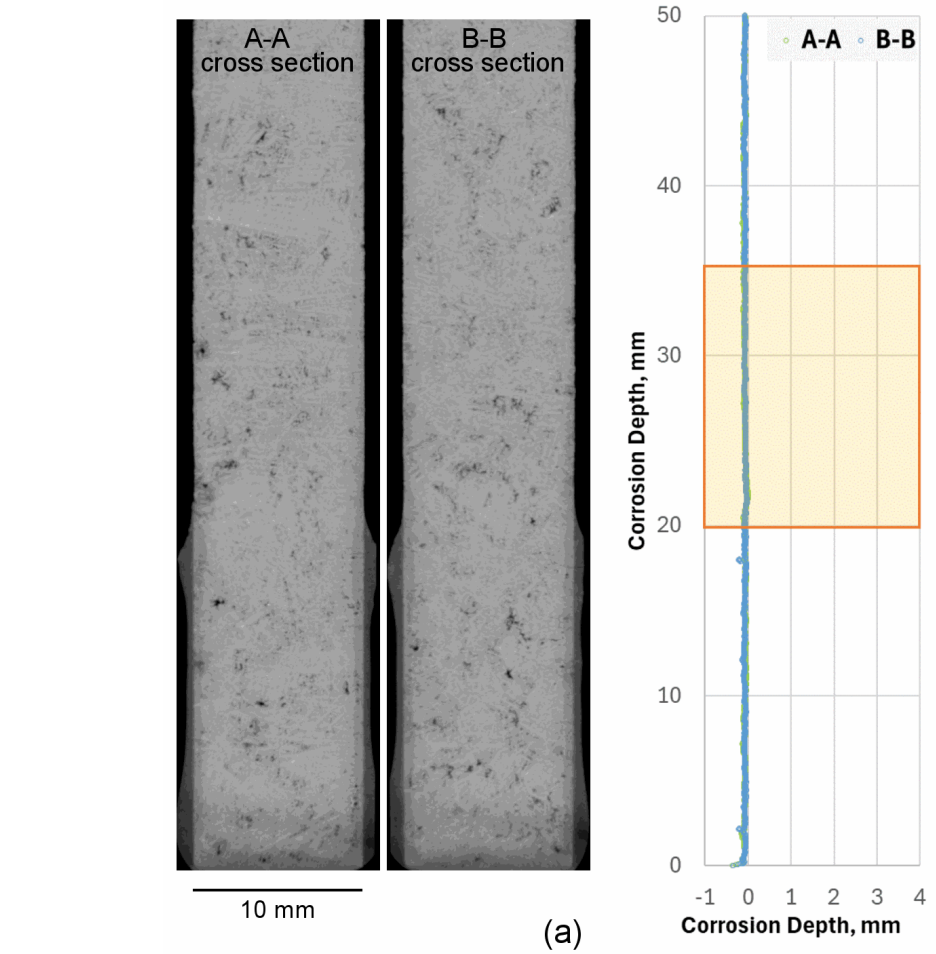

Neck Depth, mm	
A-A	0.02
B-B	0
Average	0.01
Standard deviation	0.014
Note: no clear neck. Heights of the x-y slices in (b) are random.	

Figure B.34. Micro-CT results of K-3 refractory corrosion test, HAL24M2-17 - 1200 °C - 7day. (a) cross section at center. (b) top view slice at neck location.

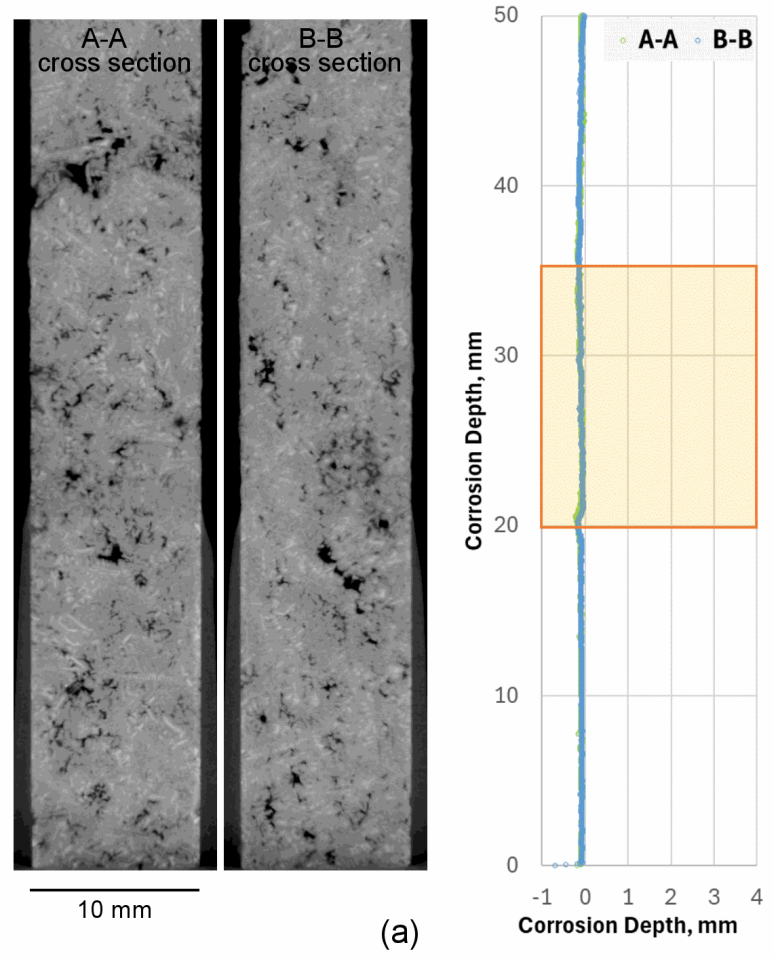

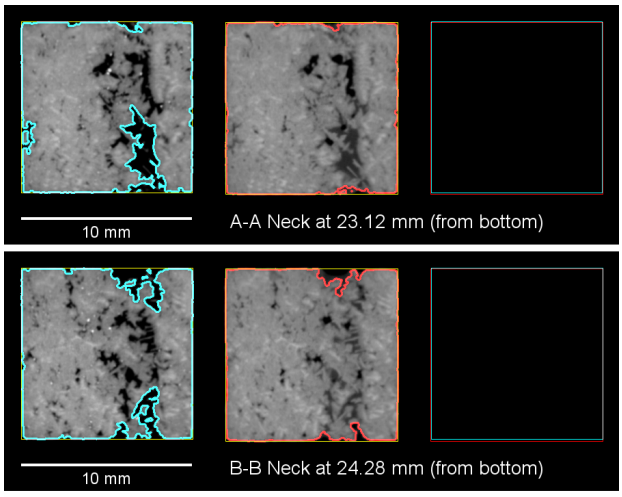

Neck Depth, mm	
A-A	-0.02
B-B	-0.02
Average	-0.02
Standard deviation	0.000
Note: no clear neck. Heights of the x-y slices in (b) are random.	

Figure B.35. Micro-CT results of K-3 refractory corrosion test, HAL24M2-18 - 1150 °C - 7day. (a) cross section at center. (b) top view slice at neck location.

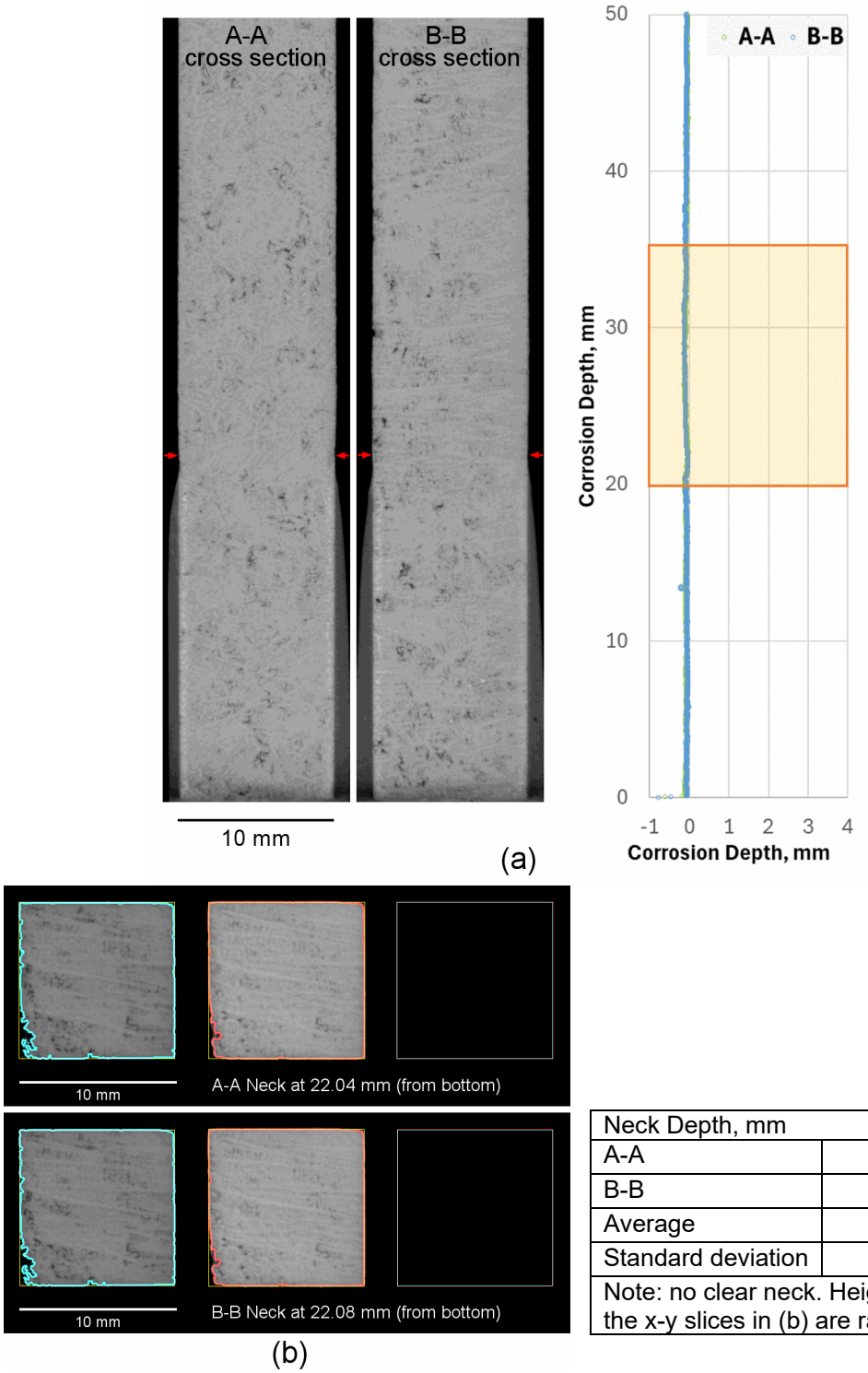

Neck Depth, mm	
A-A	0
B-B	-0.02
Average	-0.01
Standard deviation	0.014
Note: no clear neck. Heights of the x-y slices in (b) are random.	

Figure B.36. Micro-CT results of K-3 refractory corrosion test, HAL24M2-18 - 1200 °C - 7day. (a) cross section at center. (b) top view slice at neck location.

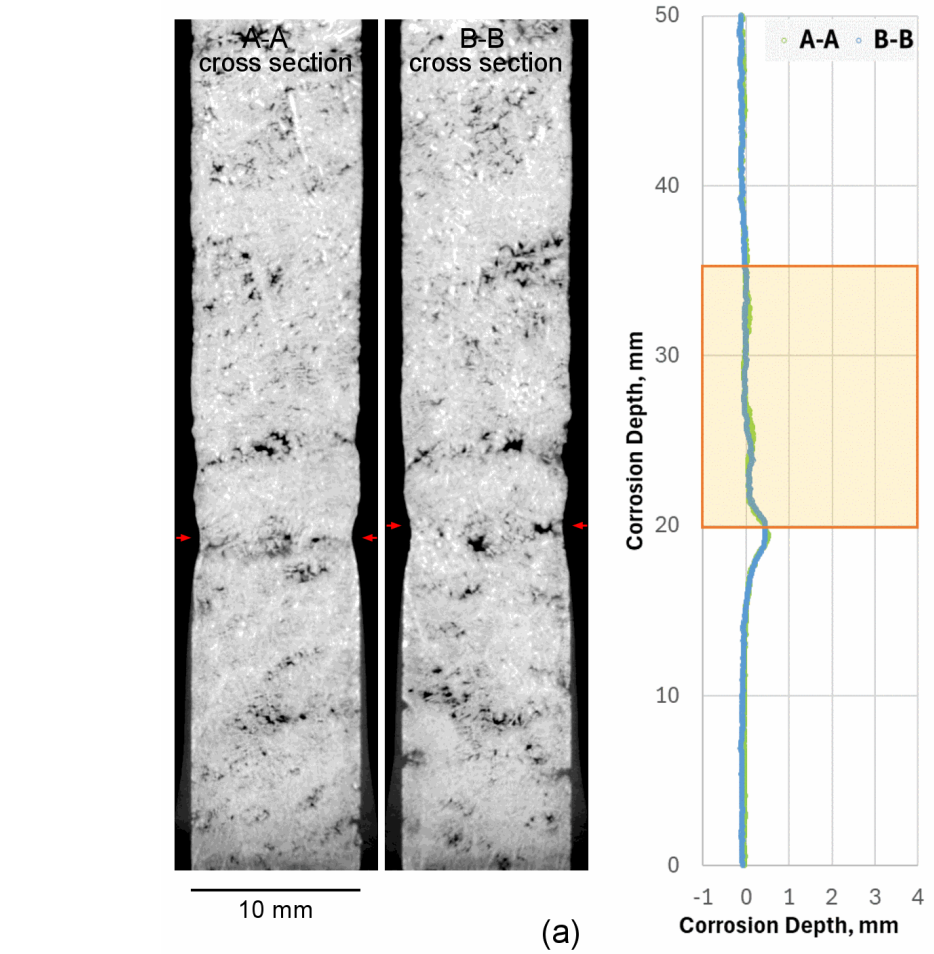

Neck Depth, mm	
A-A	0.54
B-B	0.46
Average	0.5
Standard deviation	0.057

Figure B.37. Micro-CT results of K-3 refractory corrosion test, HAL24M2-19 - 1150 °C - 7day. (a) cross section at center. (b) top view slice at neck location.

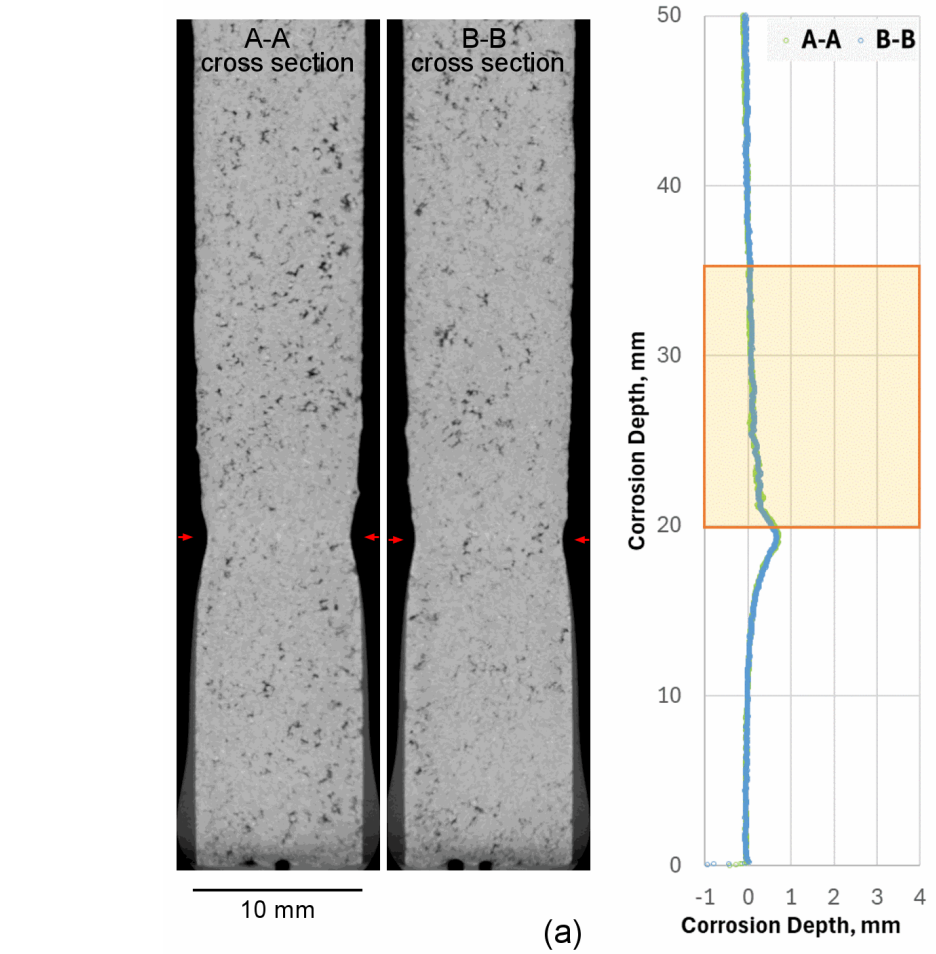

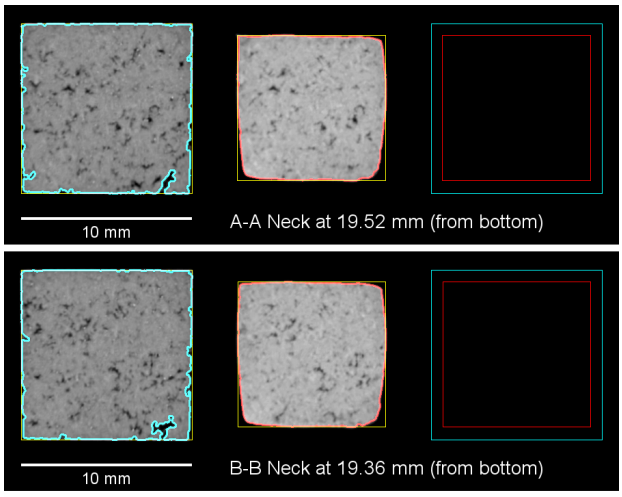

Neck Depth, mm	
A-A	0.72
B-B	0.68
Average	0.7
Standard deviation	0.028

Figure B.38. Micro-CT results of K-3 refractory corrosion test, HAL24M2-19 - 1200 °C - 7day. (a) cross section at center. (b) top view slice at neck location.

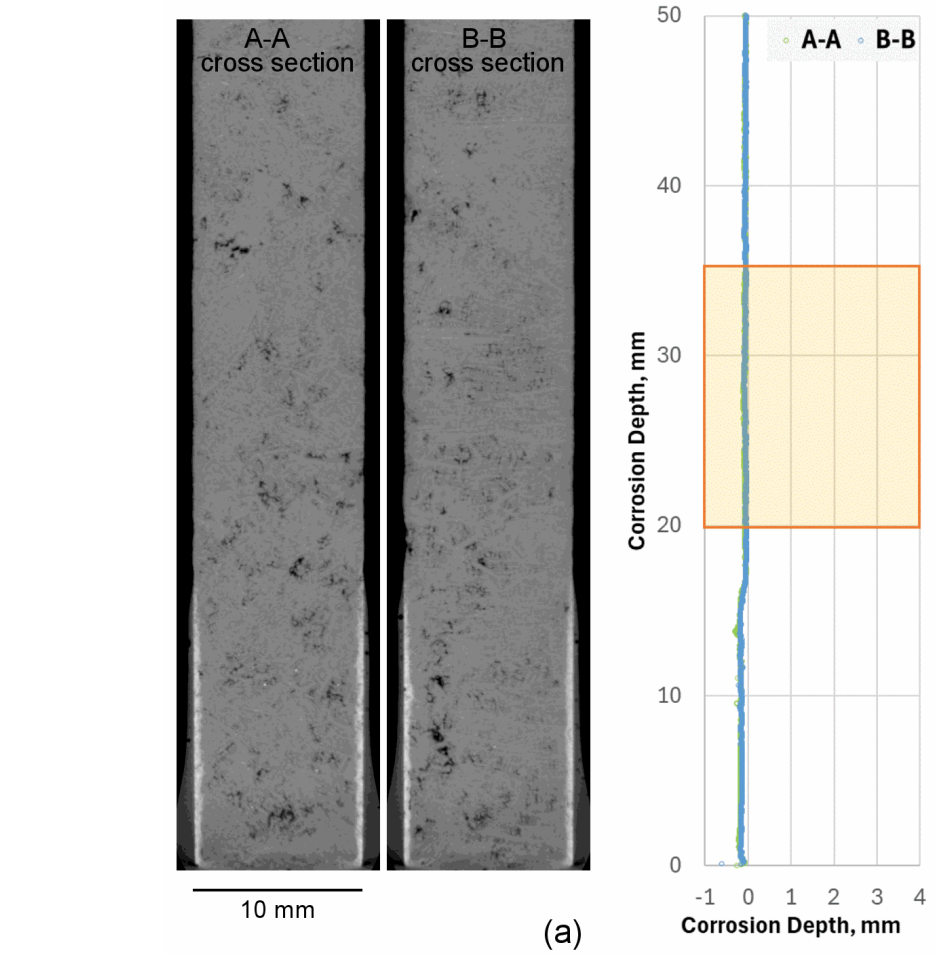

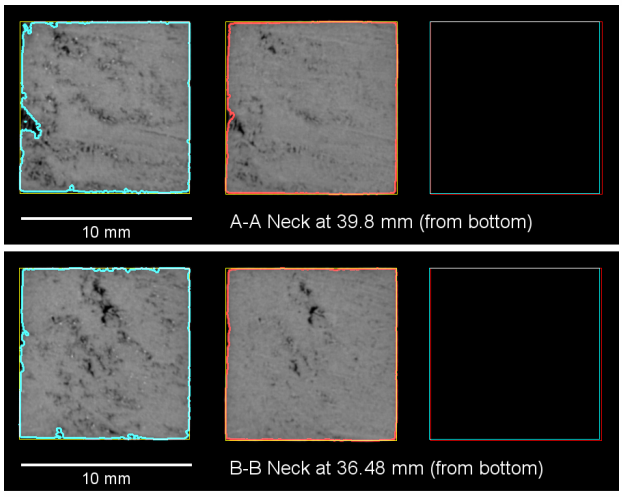

Neck Depth, mm	
A-A	-0.02
B-B	-0.02
Average	-0.02
Standard deviation	0.000
Note: no clear neck. Heights of the x-y slices in (b) are random.	

Figure B.39. Micro-CT results of K-3 refractory corrosion test, HAL24M2-20 - 1150 °C - 7day. (a) cross section at center. (b) top view slice at neck location.

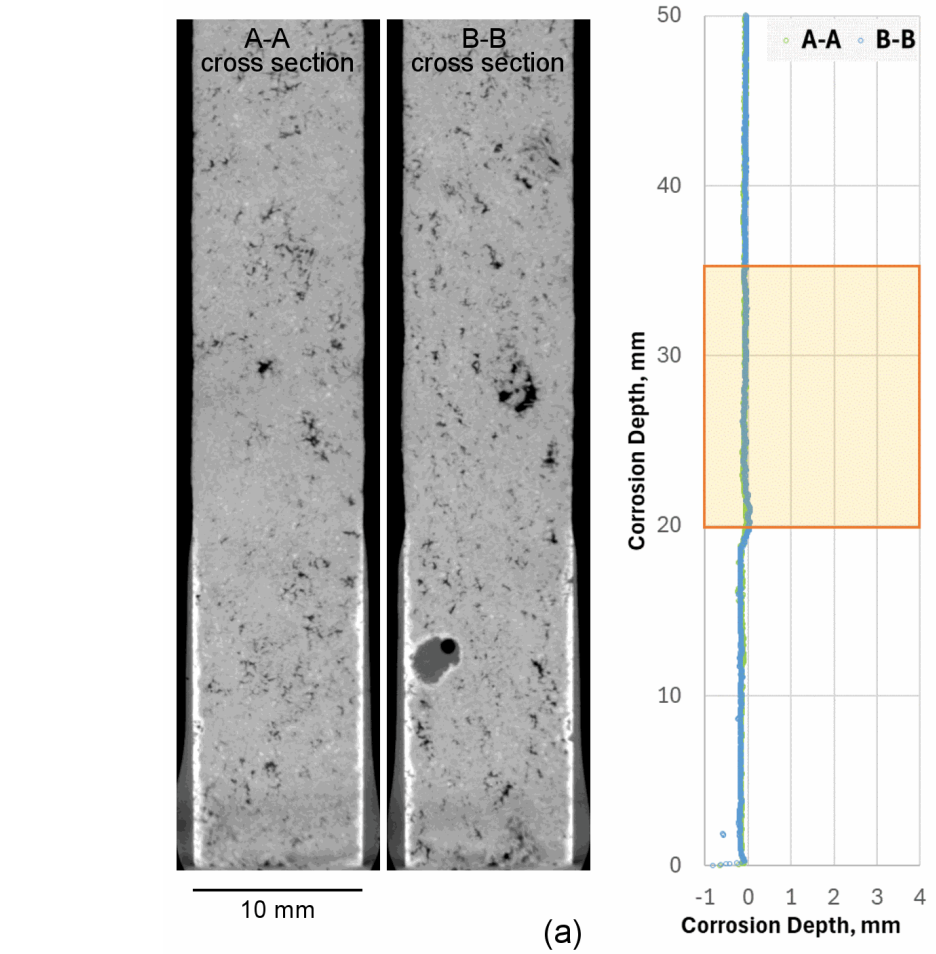

Neck Depth, mm	
A-A	-0.02
B-B	0.06
Average	0.02
Standard deviation	0.057
Note: no clear neck. Heights of the x-y slices in (b) are random.	

Figure B.40. Micro-CT results of K-3 refractory corrosion test, HAL24M2-20 - 1200 °C - 7day. (a) cross section at center. (b) top view slice at neck location.

Pacific Northwest National Laboratory

902 Battelle Boulevard
P.O. Box 999
Richland, WA 99354
1-888-375-PNNL (7665)

www.pnnl.gov